www.csiro.au

# Assessment of regional-scale effects on groundwater balance and quality linked to increased inter-aquifer leakage

**Saskia Noorduijn, Jim McCallum, Rebecca Doble, Bailin Wu, Dirk Mallants**

This report was commissioned by the Department of the Environment and Energy and was prepared by CSIRO.

**2018**

## Citation

This report should be cited as:

Saskia Noorduijn, McCallum J, Doble R, Wu B, Mallants D (2018). Assessment of regional-scale effects on groundwater balance linked to increased inter-aquifer leakage, prepared by the Commonwealth Scientific and Industrial Research Organisation (CSIRO), Canberra, in collaboration with Flinders University of South Australia.

## Acknowledgements

This report was subject to peer review during its development. We specifically acknowledge Professor Jim Underschultz (University of Queensland), Professor Craig Simmons (Flinders University of South Australia), Dr. Luk Peeters (CSIRO Land and Water), Dr. Ludovic Ricard (CSIRO Energy), and Dr. Rod Dann (Department of the Environment and Energy) for their contributions to the review.

## Table of Contents

## List of Figures

## List of Tables

# Executive summary

The project “Bore and well induced inter-aquifer groundwater connectivity: Consequence modelling and experimental design” focuses on identifying the potential consequences on groundwater balance and water quality due to preferential pathways generated by failed or open bore holes in regions where coal seam gas development occurs. The project aims to develop methodologies and techniques that will identify and potentially quantify the potential risks associated with well and bore-induced inter-aquifer connectivity. The project has two components: i) a critical literature review and local-scale assessments using groundwater modelling to identify the types of compromised bore integrity that may be measureable in coal seam gas-bearing basins, and ii) regional groundwater modelling to assess the consequences of well and bore hole-induced inter-aquifer connectivity and the number of required connective pathways to create a range of noticeable impacts.

This report documents the regional-scale assessments that were undertaken to explore whether or not there could be noticeable consequences on the groundwater balance (i.e. groundwater heads) from enhanced inter-aquifer connectivity owing to leakage pathways linked to hydrocarbon wells, degraded groundwater bores, and poorly decommissioned coal exploration bores. The regional-scale assessments are building on the outcomes of the previous pathway conceptualisation work and local-scale assessments of potential consequences on the groundwater balance linked to individual leaky wells or bores. This report also explores the potential effects on groundwater quality as a result of enhanced groundwater exchange between aquifers due to anthropogenically induced leakage pathways.

A three-dimensional groundwater flow model for a case study area in the Gunnedah Basin, NSW, was build that included five distinctly different model layers (from top to bottom): an aquifer, aquitard, coal seam gas reservoir, aquitard, and coal seam gas reservoir. Realistic depressurisation conditions were imposed on the two coal seam target formations to generate groundwater flow conditions typical of a coal seam gas well during and after gas production. Leakage pathways were considered to exist either due to leaky coal seam gas wells or an open coal exploration borehole. Leakage was assumed to exist only after the active gas production phase and across 425 hypothetical well locations. The simulations considered hypothetical failure rates from 0 (all wells intact) to 100 % (all wells provide leakage pathways). Groundwater leakage if it occurs is most likely to be through the micro-annulus of the well casing and was conceptualised as flow through an open pipe with an effective hydraulic conductivity conservatively taken to be one order of magnitude lager than the upper end of a distribution of field measurements previously reported. For the open borehole, groundwater flow was also conceptualised as flow through an open pipe, but with a much higher effective hydraulic conductivity than the leaky well. Because the number of deep and open decommissioned coal exploration boreholes in the study area is likely very small, the maximum failure rate tested was limited to 5% of the hypothetical well locations.

Numerical simulations across all failure rates (0-100 % for coal seam gas wells) demonstrated inter-aquifer connectivity does not appear to be materially enhanced by the presence of leaky coal seam gas wells in a coal seam gas well field. There was a negligible additional head decrease in the aquifer compared to the head decrease owing to flow across the bulk of the aquitards following depressurisation of the target coal seam formation.

Numerical simulations with open coal exploration bores that have no restriction to groundwater flow demonstrated the influence on regional scale inter-aquifer leakage is observable by comparison to

the leaky well scenarios. The most impacted area (maximum drawdown of approximately 10 m) is primarily situated immediately above the gas extraction area. At 10 km beyond the boundary of the gas extraction area the maximum drawdown is about 5 m, whereas at 20 km the drawdown is virtually zero. The area affected by the 5% failure rate is approximately 7,500 $km^2$, based on a minimum additional drawdown of 0.1 m. At such locations, the additional head drawdown in the groundwater aquifer due to enhanced inter-aquifer leakage is at most 2 m for a 5% failure rate for an open borehole. For smaller failure rates the impact is smaller, mainly because of the larger number of clustered bores for a 5% failure rate creating a larger cumulative effect.

Using a three-dimensional analytical solution to the convection-dispersion equation the effect of leaky wells on groundwater quality was shown to be limited to 10 m downstream the well with increases in concentration that were never higher than 4% of the solute source. For an open borehole, an increase up to 12% of the source concentration was observed at a maximum distance of approximately 100 m.

A final discussion is devoted to possible tools and technologies for monitoring well integrity failure, including an outline of a proposed experimental program for monitoring inter-aquifer leakage in a coal seam gas field. The proposed approach involves continued monitoring throughout the entire lifecycle of a well and after well decommissioning.

## Abbreviations

| General abbreviations | Description |
|---|---|
| AHD | Australian datum |
| CHB | constant head boundary |
| CLN | Continuous linear network package from MODFLOW-USG |
| CSG | Coal seam gas |
| CSIRO | Commonwealth Scientific and Industrial Research Organisation |
| MODFLOW-USG | MODFLOW-Unstructured Grid |
| MODHMS-FWL4 | MODHMS fracture well package |
| US EPA | United States Environmental Protection Agency |

## Glossary

| Term | Description |
|---|---|
| Abandoning | To cease efforts to produce fluids from a well and to plug the well without adversely affecting the environment. |
| Annulus | The gap between tubing and casing or between two casing strings or between the casing and the wellbore. The annulus between the tubing and casing is the primary path for producing gas from coal seam gas wells. |
| Bore | A narrow, artificially constructed hole or cavity used to intercept, collect or store water from an aquifer, or to passively observe or collect groundwater information. Also known as a borehole, drill holes or piezometer. This report uses the term 'bore' in reference to the extraction, exploration or monitoring or water. |
| Borehole | A hole drilled for purposes other than production of oil, gas or water (e.g. a mineral exploration borehole). |
| Coal seam gas | A form of natural gas (generally 95 to 97% pure methane, $CH_4$) typically extracted from permeable coal seams at depths of 300 to 1000 m. Also called coal seam methane (CSM) or coalbed methane (CBM). |
| Decommissioning | The process to remove a well from service. |
| Formation pore pressure | The pressure in the porous rock around the well. |
| Fracture gradient | The pressure required to induce fractures in rock at a given depth. |
| Hydraulic fracturing | Also known as 'fracking', 'fraccing', 'fracture simulation' or 'fluid-driven fractures', is the process by which hydrocarbon (oil and gas) bearing geological formations are 'stimulated' to enhance the flow of hydrocarbons and other fluids towards the well. The process involves the injection of fluids, gas, proppant and other additives under high pressure into a geological formation to create a fracture connecting the well to the reservoir. The fracture acts as a high conductivity channel through which the gas, and any associated water, can flow. |
| Hydrostatic pressure | The theoretical pore pressure that would be expected purely from the weight of water in a column running from the depth of interest to the surface. |
| Open well | As used in this report: A completed well or wellbore that has continuity through the well column and open communication with the aquifer. Examples include an abandoned exploration wellbore that has not been through a process of decommissioning or a production well that has |

| Term | Description |
|---|---|
| | been repurposed for water extraction. |
| Offset wellbores | An existing wellbore close to a proposed well that provides information for planning the proposed well. |
| Well | As used in this report: a completed structure, following drilling of a wellbore, used for production of oil or gas and typically including casing, cement, and tubing strings. |
| Well failure | Well failure or loss of well integrity may result from a well breach (or number of well breaches). Well failure can take the form of a hydrological (fluid movement between different geological units) or environmental (fluid leaks from the well at surface or contamination of water resources) breach. |
| Wellbore | The hole initially produced by drilling and intended to be cased and cemented to create a well for production of oil or gas. |

## Symbols

| Symbol | Short description, units |
|---|---|
| $A$ | Cross-section flow area [$m^2$] |
| $A_{ref}$ | Area of the reference aquitard [$m^2$] |
| $A_{well,\ i}$ | Cross sectional area of each leaky well [$m^2$] |
| $d$ | Cylinder length [m] |
| $D$ | Hydraulic diameter of conduit [m] |
| $G$ | Acceleration of gravity [$m^{-2}$] |
| $h$ | Hydraulic head [m] |
| $h_f$ | Head loss due to friction [m] |
| $k$ | Permeability [$m^2$] |
| $K_h$ | Horizontal hydraulic conductivity [$m.d^{-1}$] |
| $K_{eq}$ | Equivalent hydraulic conductivity of the combined aquitard and the leaky wells [m/d] |
| $K_{ref}$ | Background hydraulic conductivity for aquitards [$m.d^{-1}$] |
| $K_v$ | Vertical hydraulic conductivity [$m.d^{-1}$] |
| $K_{eff}$ | Effective hydraulic conductivity of the well [$m.d^{-1}$] |
| $L$ | Length of flow path [m] |
| $Q$ | Volumetric fluid flux [$m^3.d^{-1}$] |
| $r_w$ | Well radius [m] |
| $\rho$ | Density of failed wells [-] |
| $S_y$ | Specific yield [-] |
| $S_s$ | specific storage [$m^{-1}$] |
| $T_1, T_2$ | Transmissivity for Aquifer-1, -2 [$m^2/d$] |
| $z$ | Thickness of the aquitard [m] |

# 1 Introduction

## 1.1 Terms of reference

Subsurface resources such as minerals, water and hydrocarbons are routinely exploited within Australia for industrial or agricultural uses. In such cases the resources are defined and/ or obtained via the exploration and/ or construction of bore holes and wells within the subsurface rock strata. In many cases these activities intersect various rock assemblages of different composition or quality. Such rock assemblages can contain desirable resources such as groundwater; however, in the case of coal seam gas they may represent additional challenges to safe abstraction of underlying resources. To ensure efficient and environmentally sustainable utilisation of either groundwater or coal seam gas resources, bore holes or wells which penetrate multiple rock strata must be constructed to a high standard (National Water Commission 2012). Such standards ensure best practice while minimising the risk of bore integrity issues, such as the movement of gasses or liquids between two or more separate hydrostratigraphic units.

Recommendations from previous work by the Office of Water Science (Commonwealth of Australia 2014) have identified that a better understanding of the consequence of bore failure should be attempted. As such this scope of work aims to address this knowledge gap.

This project aims to determine the consequence of inter-aquifer connectivity caused by the degradation or substandard construction of bore holes and wells. Declines in bore integrity promote potential hydraulic communication, which can alter the hydrological regime present in layered aquifer systems. This project expands on previous work by using analytical and numerical groundwater models to predict the consequence of inter-aquifer leakage through failed bore holes. The project will attempt to use:

- previously constructed numerical groundwater models to determine the regional-scale magnitudes of aquifer connectivity via open bore hole conduits required to cause inter-aquifer leakage
- analytical models to determine the local-scale magnitudes of aquifer connectivity via open bore hole conduits.

The modelling will assess the consequences of well and bore hole connectivity, including the number of required connective pathways required to create a range of noticeable impacts. Impacts will be assessed by changes in:

- aquifer potentiometric surface change or groundwater flux;
- aquifer hydraulic gradient change; and
- changes in temperature or salinity within aquifers where possible.

In conjunction with both modelling approaches, propose possible experimental designs to measure impact of wells/bores on local and regional scale.

## 1.2 Human-induced pathways for inter-aquifer connectivity

Most literature related to impacts from coal seam gas or shale gas production centres around the impact of hydraulic fracturing on drinking water quality and the leakage of methane gas to surficial aquifers or to the land surface (Vengosh, Jackson, Warner, Darrah, & Kondash, 2014). US EPA (2016a) considered two major subsurface mechanisms by which the injection of hydraulic fracturing fluid and the creation and propagation of fractures can lead to contamination of drinking water resources, i.e. unintentional migration of fluids and gases (i) up the production well into groundwater owing to poor casing or cementing, and (ii) through subsurface geologic formations into a drinking water resource. Well failure has been identified as a possible pathway for migration of such contaminants from the hydrocarbon reservoir to shallower aquifers. Reagan et al. (2015) identified four broad classes of plausible failure scenarios for upward migration of contaminants associated with hydraulic fracturing:

- vertically extensive fracturing of the overburden/caprock/aquitard separating the hydrocarbon reservoir from overlying groundwater owing to inadequate design and/or operation of the fracturing operation,
- reactivation of dormant fractures/faults due to hydraulic fracturing creating pathways for contaminant leakage,
- fractures from the stimulation operation intercept older abandoned unplugged wells (e.g. conventional oil and gas wells), and
- continuous and highly permeable pathways via poorly completed wells due to inadequate design, installation or weak cement.

In a review of well integrity across the conventional and unconventional gas industry in the US, Jackson (2014) illustrates the severity of well integrity failure, especially in Pennsylvania where since 2005 the Department of Environmental Protection has confirmed more than 100 cases of well-related groundwater contamination, out of more than 5,000 new wells. According to Jackson (2014), well integrity is the key to minimizing many of the risks associated with hydraulic fracturing and unconventional resource extraction. Finally, Jackson (2014) identifies the need for much more information on the structural integrity of older producing wells and abandoned wells.

In addition to leaky coal seam gas wells, inter-aquifer connectivity may also be enhanced by degraded water bores, oil and gas wells repurposed into water bores, and inappropriately decommissioned coal exploration holes. The status of water bores in the Surat and its relevance to enhanced inter-aquifer connectivity was previously discussed by Wu et al. (2018). Especially the bores constructed before 1965 were considered to be in a poor condition due to lack of proper casing or due to the steel casing being corroded. In case such bores penetrate deep aquifers that are connected to a hydrocarbon resource, leakage pathways may develop that enhance inter-aquifer connectivity and affect the groundwater balance and/or groundwater quality. Note that such leakage pathways exist even without gas extraction. The number of potentially corroded deep water bores in the Gunnedah Basin is very likely much smaller than the estimated number for the Surat. Based on data from CDM Smith (2014), the majority of water bores in the Gunnedah Basin (Namoi) are either in the Namoi Alluvium or in the Pilliga Sandstone aquifer. The number of water bores deeper than 150 m is relatively small. There is no mentioning of water bores currently accessing groundwater from the primary or secondary coal seam target formations. For this reason the likelihood for enhanced inter-aquifer leakage in the Gunnedah Basin is considered small.

## 1.3 Coal seam gas well failure rates in Australia

To date, there have been few estimates made of failure rates for coal seam gas wells in Australia. The GasFields Commission Queensland (2015) reports statistics from well integrity compliance auditing undertaken from 2010 to March 2015. During this period 6,734 coal seam gas exploration, appraisal and production wells had been drilled in Queensland. This involved both subsurface gas well compliance and surface well head compliance testing. For the subsurface equipment, no leaks were reported while there have been 21 statutory notifications (a rate of 0.3%) concerning suspect downhole cement quality during construction. After remediation, the cement failure rate was determined to be 0%. For subsurface equipment, the conclusion is that the risk of a subsurface breach of well integrity is assessed to be very low to near zero. In regards to the surface well head gas leaks, 199 leaks have been reported and have been subsequently fixed.

Estimating coal seam gas well failure rates from failure rates reported for conventional onshore/offshore oil and gas wells or from shale gas wells has to be done with care (Wu et al. 2018). Because offshore oil and gas wells are drilled in a different and more difficult environment than onshore coal seam wells, their failure rates are expected to be much higher than for coal seam gas wells. Furthermore, coal seam wells are shallower than conventional oil and gas and shale gas wells, and therefore subject to lower temperatures and pressures. Also, operating pressures for coal seam gas wells are lower and they have less casing layers (GasFields Commission Queensland 2015). Nevertheless, the findings from conventional and shale gas wells are useful in gaining understanding of possible failure mechanisms of coal seam gas wells, and for estimating upper bound failure rates.

There are some preliminary, and purely desktop-based, estimates of failure rates for water bores (Wu et al. 2018). However, estimating coal seam gas well failure rates from water bore life expectancies also has its limitations. Failure rates derived for water bores should not be simply extrapolated to coal seam gas wells for a number of reasons, including that cementing the casing in ground can be different for water bores and coal seam gas wells (National Water Commission 2012 and DNRM 2013a), and prior to the late sixties cementing was not a requirement for water bores. Nevertheless, cement plays a critical role in protecting steel casing from corroding, and hence has a significant impact on well life expectancy.

## 1.4 Gas well abandonment

Whenever a CSG well is taken out of production, or a CSG appraisal well is not developed into a production well, CSG well abandonment measures are taken to ensure the environmentally sound and safe isolation of the well, protection of groundwater resources, isolation of the productive formations from other formations, and the proper removal of surface equipment. This involves sealing the hole completely from the bottom to surface using a series of cement plugs, which provide a seal preventing any cross flow of water and gases between underground layers, as well as isolating all downhole zones from the surface (APPEA, 2012). The well head is then removed and the steel casing (filled with cement) is cut off at least 1.5 m below ground level, sealed with a metal identification plate and buried.

Literature on the performance of decommissioned and abandoned wells is scarce. One example from Alberta, Canada, is reported next. The pre-dominant method for well abandonment in Alberta is bridge plugs capped with cement placed using the dump-bailer method. Dump bailers are used for dumping cement on pre-existing bridge plugs. They consist of a wireline tool used to place small volumes of cement slurry in a wellbore. Typically, the slurry is placed on a plug or similar device that

provides a stable platform for the low-volume cement plug. It was found that this method may not be adequate in providing a sufficient cement seal in the long term (Watson and Bachu 2009). A small subset of wellbores was re-entered to investigate the efficiency of the bridge plug abandonment method. These bridge plugs had been in service for 5 to 30 years. Generally, the cement cap placed on top of the bridge plug was not evident, even though a tour-report review indicated that the cement had been dump bailed on the bridge plug. It is estimated from experience and from this small sample that, over a long period of time (hundreds of years), approximately 10% of these types of zonal abandonments will fail and allow formation gases to enter the wellbore (Watson and Bachu 2009). Other abandonment methods, such as placing a cement plug across completed intervals using a balanced-plug method or setting a cement retainer and squeezing cement through perforations are expected to have lower failure rates in the long term.

The cement used in well construction and abandonment is designed to have a long life span (NSW Chief Scientist and Engineer report 2014). Despite considerable research on petroleum well integrity (e.g. Davies et al. 2014; Popoola et al. 2013), very little information exists about the long-term (100 - 1,000 years) durability of abandoned petroleum wells (NSW Chief Scientist and Engineer report 2014). Also the current review did not find any studies on the long-term (100-1,000 years) durability of the cement under CSG well conditions in Australia. Other studies have been conducted investigating cement degradation under simulated $CO_2$ geological storage conditions (Azuma et al. 2013; Satoh et. al. 2013; Connell et al. 2015). Laboratory experimental studies have focused on the characterisation of cement and cement/rock, cement/casing interface behaviour when exposed to $CO_2$.

The long-term degradation behaviour of cement in abandoned wells under $CO_2$ geological storage conditions was evaluated by numerically simulating the geochemical reactions between the cement seals and $CO_2$ (Yamaguchi et al. 2013). The model was validated based on the laboratory experimental results by Satoh et al. (2013) prior to applying for abandoned wells. The geochemical simulation of the reactions yielded the extent (length) of the alteration of the cement seals after long time periods. For example, the alteration length of cement seals after 1,000 year exposure was approximately one metre, leading to the conclusion that cement would be able to isolate $CO_2$ in the reservoir over the long-term. The study on long-term corrosion of cement by Yamaguchi et al. (2013) assumed that the abandoned wells were in a good condition and free of defects, such as micro-annulus in the cement sheath. This assumption may be valid for abandoned wells in the specific field studied, but may not be generalised to the abandoned wells in other fields.

Popoola et al. (2013) noted that the literature on corrosion and cement degradation considers $CO_2$ stored at high pressure to be more aggressive than methane. Therefore, a conclusion can be drawn that if coal seam gas wells are properly designed, installed and maintained, the risk of long-term leakage from coal seam gas wells from both the casing and cement can be considered to be minimal, although there is scope for additional research to specifically assess the impact of abandoned coal seam gas wells over an extended timeframe (NSW Chief Scientist and Engineer report 2014).

The long-term integrity of decommissioned wells, e.g. by using a series of cement plugs, will also depend on the degree of well integrity just before such plugs are put in place. The better the structural integrity of the well, the longer its lifetime after decommissioning. Therefore, any assessment of well integrity by measuring inter-annulus pressure build up and structural integrity prior to plugging will inform what steps can be reasonably taken during decommissioning to extend a cemented well's lifetime. Subsequent monitoring after well abandonment for a subset of wells to detect gas leaks and well integrity failures around well head infrastructure may be further considered.

## 1.5 Coal exploration holes

The potential risk of coal exploration holes in the Surat was discussed by OGIA (2016) in the framework of the Surat Cumulative Management Area (CMA); because the coal exploration holes are relatively shallow (up to 200 m), they do not penetrate the isolating layers (aquitards) above the target coal seam formations in the productive coal seam gas areas. For these reasons, the risk for enhanced inter-aquifer connectivity in the Surat CMA is considered low.

A similar reasoning can be adopted for coal exploration bores in the Gunnedah Basin (Namoi), near Narrabri. The expected maximum depth of existing coal mines in the Namoi region varies from 100 m to 380 m (Northey et al. 2014). It is therefore reasonable to assume that the majority of the exploration bores have been of a similar depth, although deeper boreholes are likely to exist. However, given the great depth of the target coal formations at the well field (top of Hoskissons coal [layer 3] is 340 m deeper than top of layer 1 and top of Maules Creek [layer 5] is 470 m deeper than top of layer 1), the thickness of the overlying aquitards (480 m), and the absence of geographic intersections between the coal seam gas study area and major coal developments (Northey et al. 2014), it is very unlikely that coal exploration holes would indeed be contributing to inter-aquifer leakage in locations in the Gunnedah Basin where coal seam gas is expected to be extracted.

Based on these considerations, the calculations of the impact of enhanced inter-aquifer leakage that will be discussed in Section 4.6 will consider only for a small failure rate, i.e. 1, 2, and 5% of the well locations used. Furthermore, the analysis is considered more of an exploratory nature to illustrate potential impacts should inter-aquifer connectivity be enhanced through such pathways.

## 1.6 Monitoring well and bore integrity: review of methods

Well and bore integrity monitoring approaches adopted by different industries have been reviewed in Sections 1.6.1 to 1.6.3. A more comprehensive overview of monitoring approaches applicable to coal seam gas wells is provided in Section 6.

### 1.6.1 Water bores

Integrity of groundwater production bores has been investigated using borehole geophysical techniques (logging) and groundwater quality analysis. In the US, borehole geophysical logs were combined with groundwater quality analysis to detect if the water bores (both productive and abandoned) could have enhanced vertical connectivity between a shallow alluvial aquifer and several underlying confined aquifers (USGS 1997). The aim of the geophysical logging was to find evidence of breaks or gaps in the well casings and cement around the casings. Although the geophysical data provided evidence of a couple locations where local voids behind casing could be present, none of the evidence indicated that there are connected voids that could allow flow over substantial distances behind casing. Based on water quality parameters (VOCs, SVOCs, pesticides, PCBs, TPHs, trace elements, major ions, cyanide, and physical properties) sampled from the production bores, no evidence was found of increased connectivity.

In Australia, DERM (2011) identified that all areas of groundwater monitoring would benefit from an increased accuracy and validity of data. This includes an assessment of the integrity of the water bores to ensure that the data gathered is reflective of the aquifer status. The recommended operational instrumentation would be a down-hole video inspection camera.

### 1.6.2 Injection wells

Identification and evaluation of methods used by industry and regulatory agencies to determine aspects of mechanical well integrity for injection wells was undertaken by the US EPA (2008). Demonstration of mechanical integrity is the most common means of demonstrating that there is no movement of fluids into or between different groundwater systems. Based on their review the following methods were reported by industry and regulatory agencies to identify the presence of leaks: pressure testing and wire-line geophysical logs including cement bond, sonic, temperature, density and neutron logs.

### 1.6.3 Wellbore in a $CO_2$-rich environment

To test the integrity of a 30-year old, mainly $CO_2$ producing, wellbore installed in a high $CO_2$-bearing formation, Crow et al. (2009) combined down-hole ultrasonic imaging and vertical interference tests. Ultrasonic imaging provided measurements of acoustic impedance as an indication of cement quality, while the vertical interference test was to apply pressure across a cemented shale section and measured the response. The latter provides an indication of the extent of hydraulic communication along the exterior of the well casing between the two perforations and is a measure of the effective permeability of the barrier system.

# 2 Conceptualisation of leaky wells

## 2.1 Previous seepage pathway conceptualisations

In a recent review of national and international literature on bore and well induced inter-aquifer connectivity, Wu et al. (2018) summarised well failure mechanisms and developed several conceptualisations of plausible hydrocarbon reservoir-aquifer failure pathways. Four major pathways - and their conceptualisations - for movement of water between strata were identified: (i) pathways linked to uncased exploration bores, (ii) pathways linked to decommissioned coal seam gas production wells, (iii) pathways linked to oil and gas wells repurposed for water extraction and water bores with degraded casing, and (iv) natural pathways linked to fractures and faults between wellbores and surficial aquifers. For the purpose of this study, two out of the above four conceptualisations (i.e., (i) and (ii)) will be taken forward to (i) determine regional-scale impacts from enhanced inter-aquifer connectivity on groundwater fluxes and heads, and (ii) determine local-scale impacts from enhanced inter-aquifer connectivity on solute transport and risks for groundwater quality deterioration. Pathway (i) was selected as it likely represents a worst-case under the condition that the borehole is completely open for fluid migration; this pathway would also encompass effects due to pathway (iii). Pathway (ii) was selected as it is the only real pathway linked to CSG extraction. Pathway (iv) is out of scope as it is a natural pathway that cannot be managed.

The leakage pathway conceptualisations selected for purpose of this study are decommissioned coal seam gas production wells and uncased exploration bores. In open, abandoned exploration bores the migration pathway is through the open, backfilled or partially collapsed borehole, with likely little or no resistance to flow (Figure 2-1). Depending on the ambient hydraulic gradients across low-permeable formations (aquitards), flow can be upward or downward. Conditions where upward flow exists in one location and downward flow in another location can also occur.

Well integrity failure was only simulated after the 25-year gas production period (i.e., when wells have been decommissioned), based on the assumption that failed coal seam gas wells would be repaired or decommissioned during the pumping/production phase. In decommissioned and abandoned coal seam gas wells, loss of integrity may lead to the following pathways for water migration and solute transport (Figure 2-2):

- through a micro-annulus between the cement casing and the soil/rock matrix (1) or the steel well casing (2)
- through a deteriorated cement sheath between the well casing and soil/rock matrix (3)
- through deteriorated cement plugs used in decommissioning (4, 5), and
- through the well itself, via corrosion holes, shear or tensile damage (6).

In Figure 2-2 flow is from upper aquifer to lower aquifer based on the downward head gradient ($H_1>H_2$). This scenario may represent either a natural downward gradient or a downward gradient typical for the period of depressurisation during or long after gas extraction has ended (note that recovery to the initial hydraulic head condition in the coal seam formation may take hundreds of years (Wu et al., 2018)). This conceptualization must also assume that the coal seam gas zone has had sufficient time to re-equilibrate such that the cleat system has become re-saturated with formation water and that any remaining methane is immobile and adsorbed into the matrix of the

coal. Otherwise there is a relative permeability problem for the water to be able to move into or out of the coal zone.

When an upward gradient exists ($H_2>H_1$), flow will be from the lower to the upper aquifer. The latter condition was observed both pre-coal seam gas and post-coal seam gas extraction in several locations of a regional groundwater model that provided realistic head boundary conditions for the current study (Wu et al., 2018).

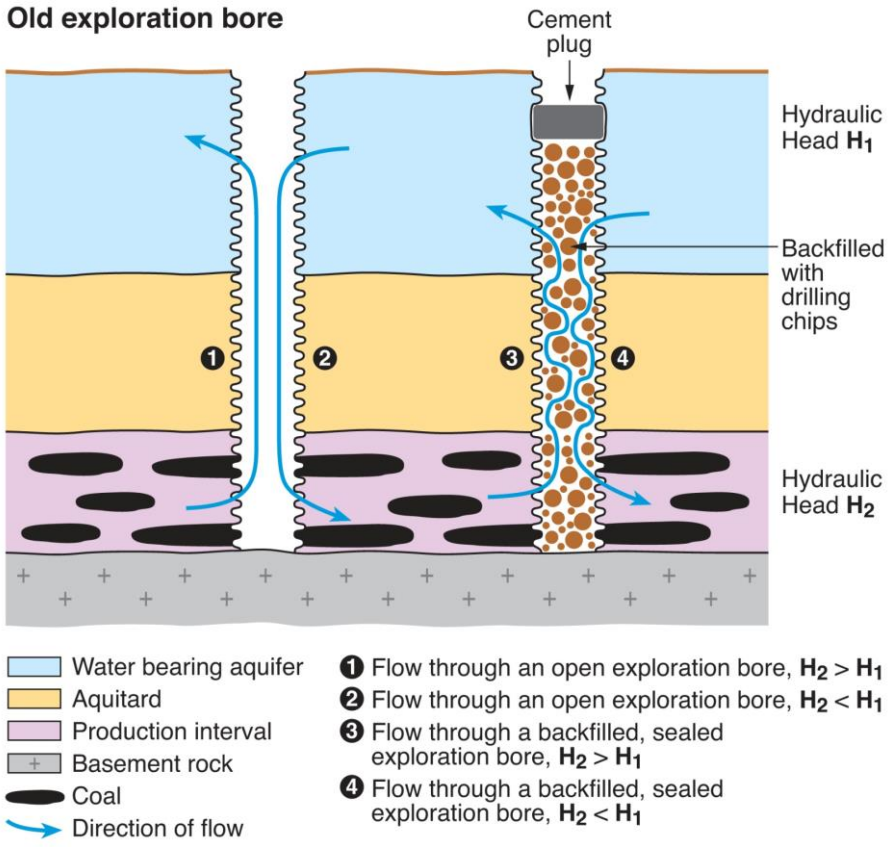


**Figure 2-1 Pathways for water movement in uncased exploration bores: (1) upward flow through an open exploration bore ($H_2>H_1$), (2) downward flow through an open exploration bore ($H_1>H_2$), (3) upward flow through an initially backfilled exploration bore whose sealing capacity has been impaired ($H_2>H_1$), and (4) flow through a backfilled, sealed exploration bore ($H_1>H_2$). All indications of flow are potential directions. Not to scale [Wu et al. 2018].**

For a single leaky well or bore, single-phase flow through the well may be represented using the Darcy flow equation with an effective well hydraulic conductivity. The flow through the well will be governed by the well or bore effective hydraulic conductivity ($K_{eff}$), the radius of the bore hole and the head difference between the top and bottom of the well (i.e., between the two aquifers). Where the effective bore conductivity is high, flow through the bore may be limited by the transmissivity of the upper aquifer and the production zone (see discussion in Section 2.2). This was demonstrated by Silliman and Higgins (1990) and Doble et al. (2018) for a simplified hydrogeological system with two aquifers separated by an aquitard. When the well conductivity is high relative to aquifer transmissivity, the aquifers can limit radial flow to or from the well location.

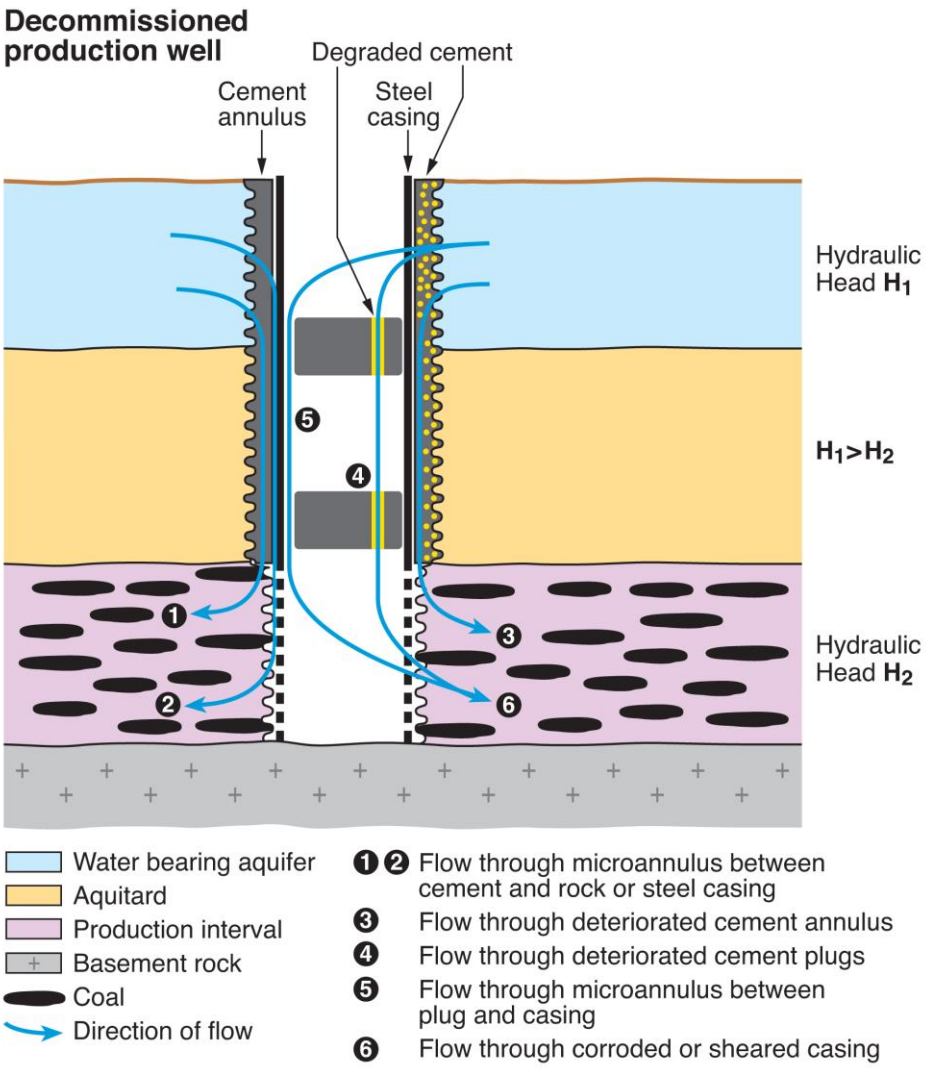


**Figure 2-2 Pathways for water movement in decommissioned cemented wellbores: flow through micro-annulus between cement and rock matrix (1) or steel casing (2), flow through deteriorated cemented annulus (3), flow through deteriorated cement plugs (4), flow through micro-annulus between plug and casing (5), and flow through corroded or sheared casing (6). Upward flow is equally possible when H2 > H1. All indications of flow are potential directions. Not to scale [Wu et al. 2018].**

## 2.2 Exploring the potential for regional-scale impacts

The potential for regional-scale impacts on groundwater quantity and quality from theoretical well leakage will be explored by using a three-dimensional groundwater flow model for assessing quantity impacts and a three-dimensional analytical solution for assessing quality impacts. The two leakage pathways considered are the decommissioned coal seam gas production wells and uncased exploration bores.

The scenarios that will be explored assume that during coal seam gas production all potential leaky gas wells will be detected and remediated. As such, there are no leaks considered during a 25-year gas (and water) production period. Leakage pathways are considered to exist only after decommissioning and abandonment of the gas production site, for reasons that casing material will gradually degrade over time; unless continued monitoring occurs of the abandoned wells, such leaks may go undetected. As mentioned above, this condition assumes that the near-well region has gone back to water saturation in the cleat system and is no longer gas-saturated. Immediately at the end of gas production, the water saturation in the gas reservoir is likely to be low and thus there are relative permeability issues. In other words, the relative permeability will remain low until the reservoir is fully water-saturated; until then, downward flow will advance slowly. These processes have not been considered here; the assumption is that this resaturation has occurred.

In the simulations the assumption will be that flow rates primarily occur through the leaky annulus, but with a realistic upper limit to the effective hydraulic conductivity of such a leaky well. Failure rates from 0 to 100% will be considered. Note, however, that the assumption of absence of leakage pathways during the gas production period does not mean that local loss of well integrity does not exist; as long as such local issues do not provide for a continuous pathway, fluid flow will not happen. Nevertheless, understanding the well integrity prior to decommissioning is important because well integrity will deteriorate over time and decommissioning measures should account for the status of well integrity to be most effective.

The scenario for the uncased exploration bores differs in two ways from the previous scenario: the effective hydraulic conductivity is much higher as backfilling with natural material is most likely less effective than for properly decommissioned coal seam gas wells, and the number of leaky bores physically located within the gas production area is considered much smaller (a failure rate up to 5% of all bores is considered based on the discussion in Section 1.5). The latter assumption reflects the observation that coal exploration bores are generally relatively shallow and/or are geographically separated from the coal seam gas production area (see discussion in Section 1.5 and Section 4.6).

# 3 Numerical groundwater flow model development

## 3.1 Case study area

The study area coincides with the area reported in the Groundwater Impact Assessment of CDM Smith (2014). The CDM Smith model was used as a guide to develop a simplified groundwater flow model of the regional impacts of well or bore integrity failure in regions where coal seam gas extraction occurs. The simplified groundwater flow model was developed in MODFLOW-USG to be consistent with the single-well groundwater flow modelling by Doble et al. (2018).

The simplified model domain consists of 5 layers, the top layer represents the main water bearing aquifer in the area (Pilliga Sandstone) which overlays a sequence of alternating aquitards (layers 2 and 4) and target coal seams (Hoskissons Coal Formation as the secondary target formation [layer 3] and Maules Creek Formation as the primary coal target formation [layer 5]). Table 3-1 outlines the layer amalgamation from the 24 layer CDM Smith model (CDM Smith, 2014) to the simplified 5 layer model. The thickness and elevation of each layer were taken as the average amalgamated layer thickness from the CDM Smith (2014) model (see Table 3-1).

The simplified model represents an enhanced version of the Doble et al. (2018) model, and maintains some of the spatial elements of the CDM Smith (2014) model. It should be noted that by representing the aquitard sequences as single layers the model will underestimate lag times in the aquitard response to pumping and overestimate drawdown in the aquifers (Frind, 1979). Indeed, a single-layer aquitard allows for the entire storage volume of the aquifer to be available, which greatly overestimates the rate of drawdown propagation through the aquifer. As such this deliberate overestimation of drawdown is appropriate as it results in a conservative estimate of impacts. Where large impacts are predicted, more refined assessments can be made in a subsequent phase.

Each layer was simulated as a confined but convertible aquifer; within MODFLOW a convertible aquifer refers to a confined aquifer that becomes unconfined if the groundwater head drops below the top of the model cell. This allows for a realistic representation of aquifer depressurisation during pumping. To limit the impact of boundary conditions, the model domain is 195 km by 151 km (29,445 $km^2$), which represents a distance of 40-60 km between the edge of the study area well field and the model boundary. The NGPA model was used as a template for the model grid structure, where the cell size ranges from 1×1 $km^2$ (at and around the well field), 5×1 $km^2$ and 1×5 $km^2$ to the east, west and north of the model, to 5×5 $km^2$ (at the northern, eastern and western edges of the model) (Figure 3-1). In a previous study on well integrity at the scale of an individual well, Doble et al. (2018) demonstrated that when using MODFLOW-USG and the CLN package the effect of cell size does not have on effect on predictions of drawdown. Cells size tested ranged from 0.5 to 1000 m.

**Table 3-1 Outline of geological units in the study area with numerical model layers based on CDM Smith (2014), and simplified model layers used in this study. NC = not considered in the model.**

| Formation | Hydrostratigraphic Unit | Model Layer | Simplified Model Layer |
|---|---|---|---|
| **Narrabri/Gunnedah Alluvium** | Aquifer | 1 | NC |
| **Liverpool Range Volcanics** | Aquitard | 2 | NC |
| **Wallumbilla Formation** | Aquitard | 2 | NC |
| **Bungil Formation** | Aquitard | 3 | NC |
| **Mooga Sandstone** | Aquitard | 4 | NC |
| **Orallo Formaion** | Aquitard | 5 | NC |
| **Pilliga Sandstone** | Aquifer | 6 | 1 |
| **Purlawaugh Formation/Garrawilla Volcanics** | Aquitard | 7 | 2 |
| **Deriah Formation/Napperby Formation** | Aquitard | 8 | 2 |
| **Digby Formation/Trinkey Formation** | Aquitard | 9 | 2 |
| **Wallala Formation/Breeza Coal Member** | Aquitard | 10 | 2 |
| **Clare Sandstone/Howes Hill Coal Member** | Aquifer | 11 | 2 |
| **Benelabri Formation** | Aquitard | 12 | 2 |
| **Hoskissons Coal (Late Permian)** | CSG reservoir | 13 | 3 |
| **Brigalow Formation** | Aquitard | 14 | 4 |
| **Arkarula Formatin** | Aquitard | 15 | 4 |
| **Melvilles Coal Member** | Aquitard | 16 | 4 |
| **Pamboola Formation** | Aquitard | 17 | 4 |
| **Watermark Formation** | Aquitard | 18 | 4 |
| **Porcupine Formation** | Aquitard | 19 | 4 |
| **Maules Creek Formation (upper)** | Aquitard | 20/21 | 4 |
| **Early Permian coal seam (Maules Creek Fm))** | CSG reservoir | 22 | 5 |
| **Maules Creek Formation (lower)** | Aquitard | 23/24 | - |

Hydraulic properties for each layer are outlined in Table 3-2, and were based on those used in the CDM Smith (2014) model. More recent aquitard hydraulic conductivity values are available from Turnadge et al. (2017). The new value for layer 2 (upper aquitard series) is more than two times lower than the value used by CDM Smith (2014); this again represent a conservative condition. For layer 4 (lower aquitard series) the new value is 2.5 times higher than the CDM Smith (2014) value; while this is not conservative, the slightly higher $K_V$ for layer 4 is likely compensated by the lower $K_V$ for the second layer. Layer boundary conditions were chosen based on the structural geology within the Bohena Trough, in which the study area is located. The coal seams (and aquitards) were deposited within the basement trough limiting their spatial extent. Therefore they represent layers of finite area and volume, as such no flow boundaries were chosen to represent this spatial

discontinuity in the simplified model (layers 2 to 5). All model boundary conditions are only applied to the edge cells.

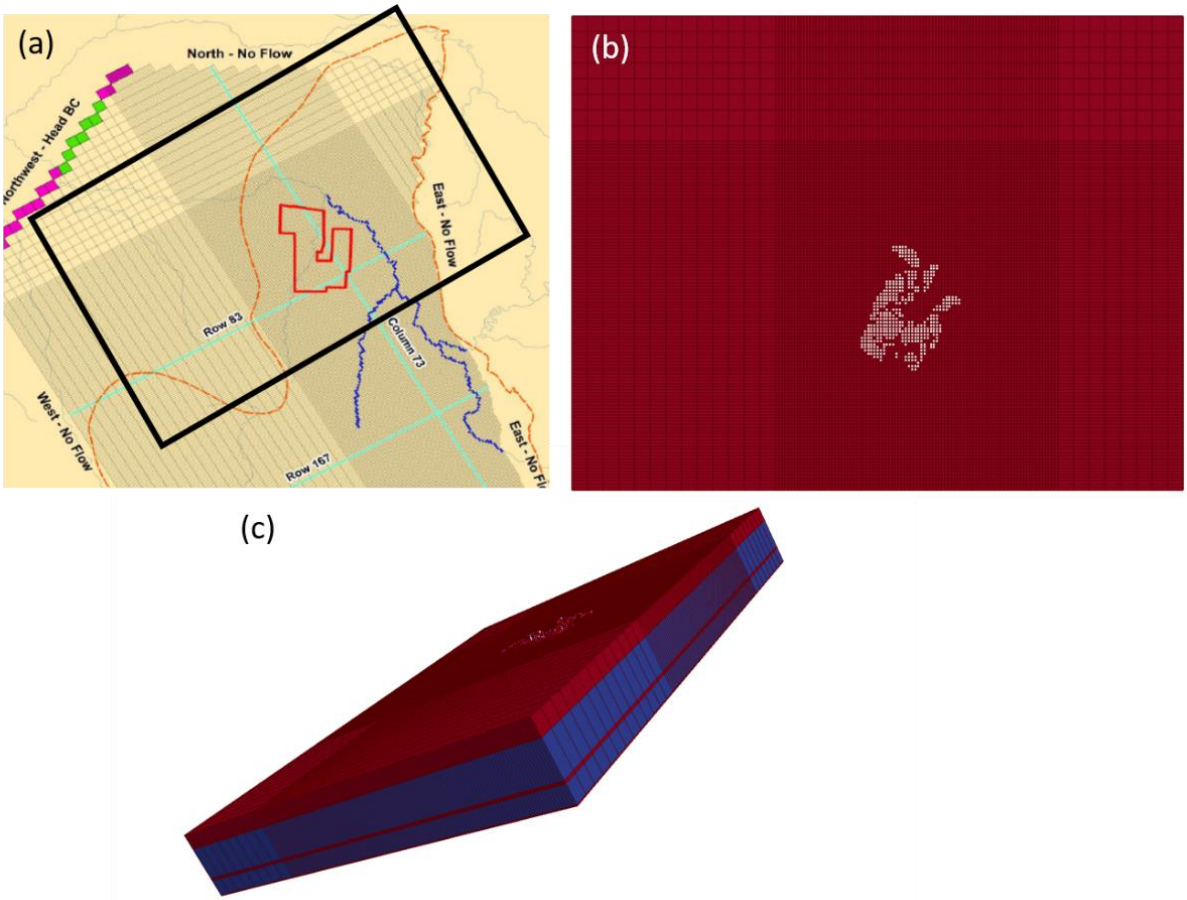


**Figure 3-1 Diagrams of the simplified model grid. (a) Black rectangle shows the area represented by the simplified model (195 km × 151 km$^2$) relative to the full CDM Smith (2014) model; (b) Simplified model grid structure and coal seam gas well locations (white dots); (c) Relative thicknesses (nearly 480 m) of the model layers of the simplified model.**

The Pilliga Sandstone (layer 1) is the most contiguous geological layer in the model, as such constant head boundaries were used in the model (Figure 3-2). The constant head boundary (layer 1) in the simplified model was based on the steady-state groundwater heads previously calculated with the CDM Smith (2014) model (Figure 3-3). This generated a realistic regional flow field within the simplified model. Initial conditions used for layers 2-5 were equal to the average steady-state heads from the CDM Smith (2014) model.

**Table 3-2 Simplified groundwater model layer discretisation and parameterisation. CHB and NFB are constant head boundary and no flow boundary, respectively. Data from CDM Smith (2014). Values in square brackets are new measurements (median from harmonically upscaled values) reported by Turnadge et al. (2017).**

| Parameter | Layer 1 | Layer 2 | Layer 3 | Layer 4 | Layer 5 |
|---|---|---|---|---|---|
| **Thickness (m)** | 111.41 | 229.41 | 17.8 | 113.21 | 7.11 |
| **Top elevation (m AHD)** | 200.28 | 88.87 | -140.54 | -158.36 | -271.56 |
| **Base elevation (m AHD)** | 88.87 | -140.54 | -158.36 | -271.56 | -278.68 |
| **Lateral Boundary** | CHB | NFB | NFB | NFB | NFB |
| **Horizontal hydraulic conductivity $K_h$ (m/d)** | $10^{-1}$ | $10^{-3}$ | $10^{-1}$ | $10^{-3}$ | $10^{-1}$ |
| **Vertical hydraulic conductivity $K_v$ (m/d)** | $10^{-3}$ | $10^{-5}$ [$4\times10^{-6}$] | $10^{-3}$ | $10^{-5}$ [$2.5\times10^{-5}$] | $10^{-3}$ |
| **Specific yield $S_y$ (-)** | 0.01 | 0.01 | 0.01 | 0.01 | 0.01 |
| **Specific storage $S_s$ (1/m)** | $10^{-5}$ | $10^{-5}$ | $10^{-5}$ | $10^{-5}$ | $10^{-5}$ |
| **Initial head (m AHD)** | variable | 265.74 | 264.27 | 263.9 | 263.65 |

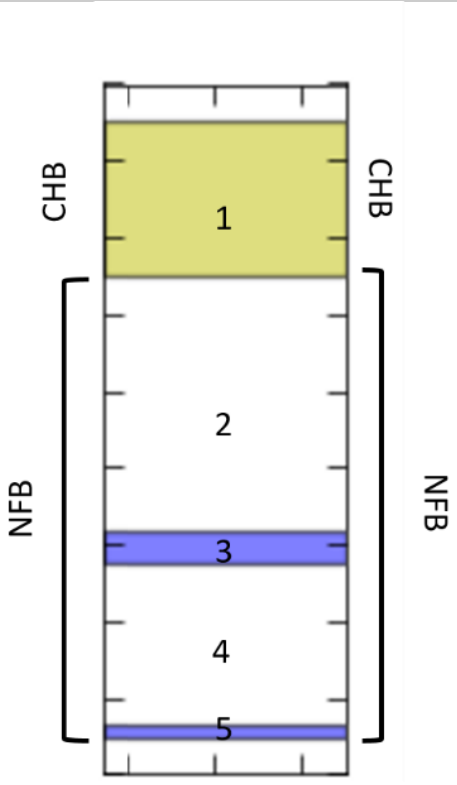


**Figure 3-2 Cross-section with model boundary conditions applied to the five model layers (layer 1 = Pilliga Sandstone aquifer; layers 2, 4 = aquitard; layers 3, 5 = coal seam gas reservoir): NFB = no flow boundary, CHB = constant head boundary.**

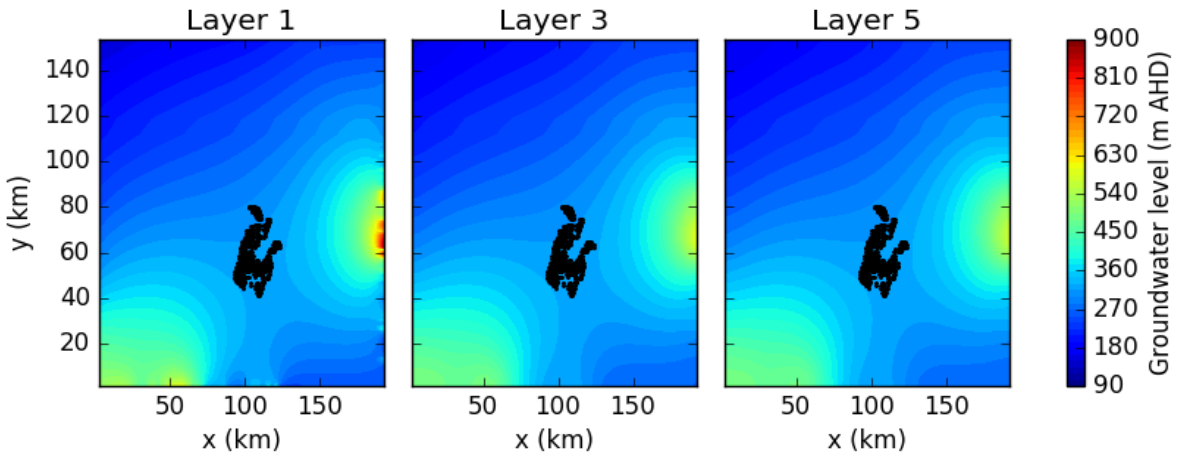


**Figure 3-3 Simplified model steady-state groundwater heads prior to gas extraction in water bearing aquifer layers 1, 3 and 5. Black dots indicate the location of the gas extraction area.**

The gas extraction area covers 425 km$^2$; within this area, 425 coal seam gas well pairs (total of 850 well screens) were considered as part of the field development plan (Figure 3-1 and Figure 3-3). A 1 km spacing was assumed for each well pair, with each pair targeting the primary (Early Permian, layer 5) and secondary (Hoskissons, Late Permian, layer 3) coal seams. These wells are grouped into 18 water extraction areas, each with a different total extraction volume and rate over the proposed 25 year production period of the gas field. The simplified model used the base case scenario extraction rate and volumes from CDM Smith (2014) model (Figure 3-4). It can be inferred from Figure 3-4 that the deeper Early Permian coal seam will undergo a more considerable depressurisation relative to the shallower Late Permian coal seam. Modflow-USG does not account for geomechanical compaction as a result of reservoir pressure reduction during extraction. This will change the net effective stress leading to a certain amount of compaction, which, in turn, may reduce the pressure depletion propagation (i.e., the groundwater head decline would become smaller). Indeed, as gas is produced from a CSG reservoir, two distinct and opposing phenomena occur that can affect the absolute permeability of the cleat system (Morad et al. 2008):

- The decrease in reservoir pressure reduces the pressure in the cleats. Cleat net effective stress (which is the difference between overburden stress and pore pressure) can cause changes in cleat permeability. Depending upon the orientation of cleats relative to the in-situ stress orientation, cleat compression or dilation may result in either the reduction or enhancement of cleat permeability, respectively.
- Desorption of gas from the coal matrix results in shrinkage of the matrix. Shrinkage causes the space within the cleats to widen and the permeability of the cleats increases.

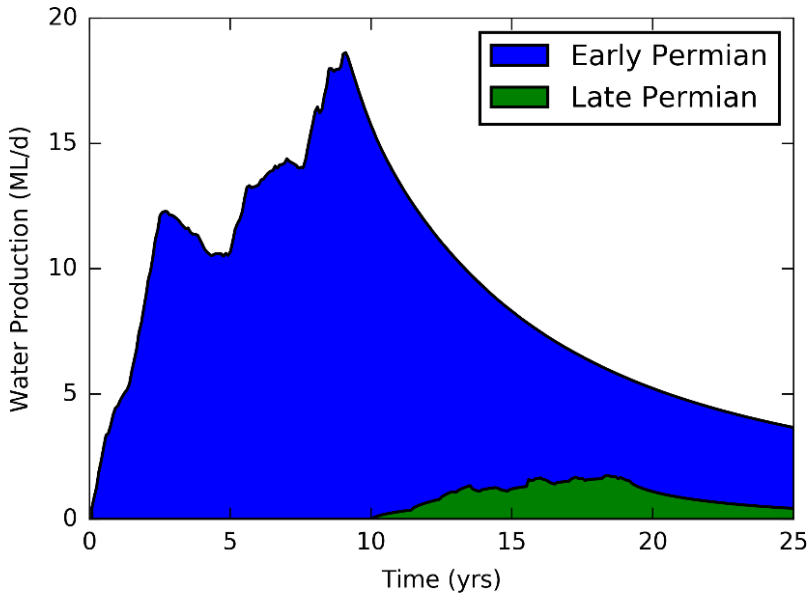


**Figure 3-4 Water Production estimates for the Narrabri Gas Project area, for the Early Permian (Maules Creek) primary coal seam gas target formation (blue) and Late Permian (Hoskissons) secondary coal seam gas target formation (green) (CDM Smith, 2014).**

The simplified model was first simulated in steady-state to allow the system to reach a pre-production equilibrium. Figure 3-3 shows the calculated steady-state head distribution in layers 1 (aquifer), 3 (coal seam gas reservoir), and 5 (coal seam gas reservoir). The regional flow induced by the spatially variable constant head boundary in layer 1 results in a head difference ranging between -89 m (upward gradient) and 276 m (downward gradient) between layer 1 and layer 3 and between layer 1 and 5, respectively. These large differences are located along the edge of the model driven by the boundary condition in layer 1 and all other layers. The average heads in layer 1, 3, and 5 are 317.9 m, 318.26 m, 318.305 m, respectively. The average head difference between layer 1 and 3 is therefore -0.33 m and the average head difference between layer 3 and 5 is -0.4 m (upward gradient across the entire vertical profile). This represents unperturbed flow conditions.

The gas production period was simulated using the estimated water production volumes over a transient 25 year period (Figure 3-4). Subsequent water level recovery was modelled for a period of 2,500 years in all layers.

**Table 3-3 Simplified groundwater model well/bore flow parameters.**

| Parameter | | Leaky well | *Open well* |
|---|---|---|---|
| **Length of well (m)** | partial | 358.64 | *358.64* |
| | full | 478.96 | *478.96* |
| **Well radius (m)** | | 0.25 | *0.25* |
| **Effective well conductivity (m/d)** | | 0.813 | *$6.25x10^{8}$* |
| **Well skin factor (-)** | | - | *10* |

## 3.2 Model implementation of leakage pathways

Well integrity failure was conceptualised using the Connect Linear Network (CLN) package from MODFLOW-USG (Panday et al. 2015). The CLN package enables simulation of flow through conduits whose size is smaller than a model grid cell without requiring further grid refinement. A string of connected CLN nodes (such as those representing a well) will allow passive flow between model layers in absence of active pumping, controlled by the head gradient along the conduit, and the resistance to flow through the conduit, between the conduit and aquifer matrix, and through the aquifer matrix (Panday et al. 2015; Doble et al. 2018). Flow through a CLN well is limited by a specified effective well hydraulic conductivity, $K_{eff}$, for example an open well or bore hole will have a high conductivity relative to the aquifer, whereas a leaky well with flow along the pathways through the well annulus will have a relatively low hydraulic conductivity (see Table 3-3). The effective well conductivity of $8.13 \times 10^{-1}$ m/d, or 1100 mD was chosen to be conservatively one order of magnitude greater than that used by Nordbotten et al. (2009).

Results for open well scenarios are provided in the context of open/unsealed water bores and exploration bores rather than coal seam gas wells. Therefore, the parameters for open bores are also provided in Table 3-3 based on those of Doble et al. (2018).

Well integrity failure was only simulated after the 25-year gas production period, based on the assumption that failed coal seam gas wells would be repaired or decommissioned during the pumping/production phase.

Each coal seam gas well pair was simulated using a single string of CLN nodes, with the nodes in layers 3 and 5 acting as pumping nodes during the production period (see Figure 3-5). After the gas and water production period, these pumping nodes became inactive but still allowed passive water flow through the well screen with the hydraulic gradient across the nodes as the only driving force. To spatially distribute the leaky wells across the gas production area, an approach was taken that would maximise the impact. This conservative approach provides assurance that impacts are not underestimated. Note that there is no physical process that would cause spatially correlated well failure. Rather this approach may reflect potential errors in installation practices or material failure which are likely to be spatially correlated as the well field is established. This approach represents a worst case scenario and thus results in biased predictions results.

A spatially correlated random failure approach was used for this purpose to spatially distribute a given percentage of all the leaky production wells (i.e., 850 well screens) (Figure 3-7). Simulation of bore failure was undertaken using an indicator kriging algorithm. Kriging assumes that there is a spatial dependence in the failure rate of two wells or bores. The failure is assumed to be dependent on the neighboring boreholes (Figure 3-6). This generates clustering of failed wells which by their cumulative effect, will yield higher impacts then when wells are spread out more uniformly. The level of clustering can be determined by setting a maximum correlation distance beyond which correlation becomes zero. Failed bores within the maximum distance are given a value of 1 and intact bores a value of 0. The individual bores are then given a weighting based on their distance to the well with an unknown status (i.e. the well being simulated), and the weighting of the failure values of surrounding bores returns a probability of failure. A random number can then be generated to determine if a bore fails. The failure rate can be initiated by “seed wells”, where a number of bores are simulated with just the failure rate. The level of clustering can be increased by increasing the maximum correlation length: in which case more wells will have a similar behaviour, also those further apart. A scenario of zero correlation can be achieved by setting the maximum correlation distance to a value smaller than the bore spacing. The effect of clustering will gradually

decrease as the well failure rate increases: the closer the well failure rate is to its maximum (100%), the more similar the distribution of leaky wells becomes to other ways of spatially distributing leaky wells, such as a random approach.

Because the generated patterns have no physical basis, the probability of the generated patterns was calculated under the hypothesis that there is no spatial correlation. As an example, without correlation the probability of five wells within a 1000m radius to fail simultaneously if the failure rate is 5% is $0.05^5 = 3\times10^{-7}$. For a 1% failure rate the probability is $10^{-10}$, while for a 50% failure rate the probability if $3\times10^{-2}$. In other words, for the more likely small failure rates, the probability of clustering is extremely small. Therefore, the risk (likelihood×consequence) calculated for any impact associated with such small failure rates will be small.

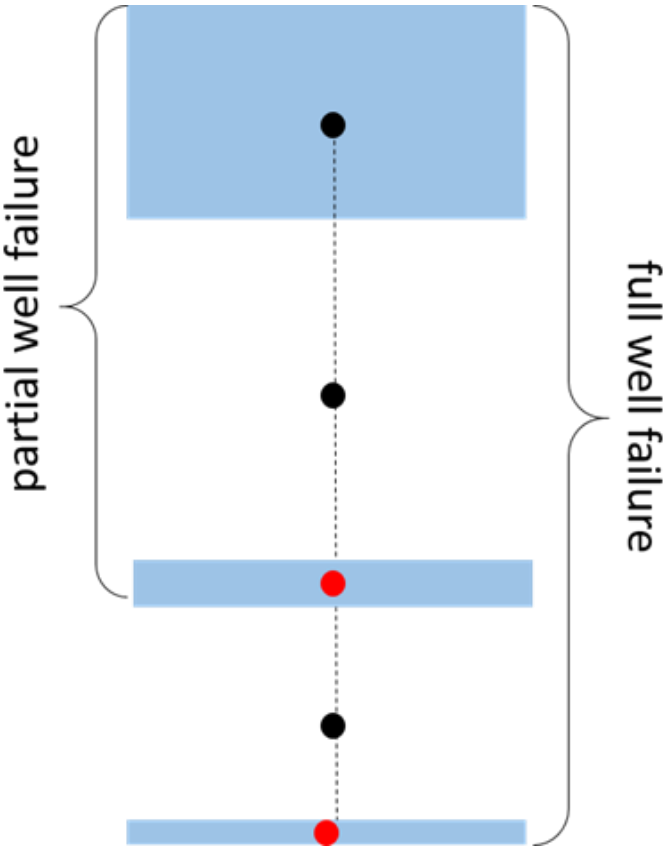


**Figure 3-5 Schematic set up of a CLN well in the simplified model. Black dots represent the CLN nodes, and red dots represent CLN nodes used as pumps during the 25-year pumping period, after which they become well screens allowing for passive water flow. The CLN nodes included in a *partial well failure* (only upper coal seam gas reservoir) and a *full well failure* (both coal seam gas reservoirs) are also indicated. During and after production period water flow is from top to bottom.**

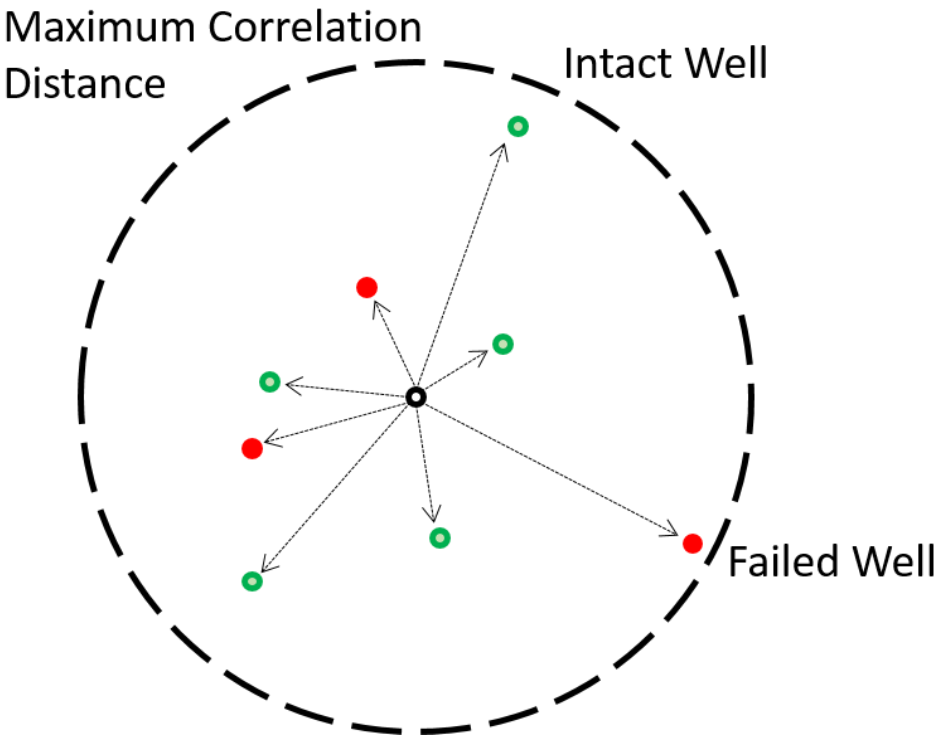


**Figure 3-6 Schematic image of the spatially correlated random well failure approach. The white circle represents the seed well, green and red dots represent intact and failed wells respectively.**

This approach further results in two types of well integrity failure; partial and full well integrity failure based on the location at which the well is completed. Partial well integrity failure occurs when the production well completed in the Late Permian coal seam (layer 3) fails. Full well integrity failure occurs when, either, the well completed in the Early Permian coal seam (layer 5) fails or when both the well in the Late and Early Permian coal seams (layers 3 and 5) fail. All well failure simulations consist of a combination of full and partial failure types because the selection approach is applied to wells in layer 3 and 5.

All wells were assumed to have the same construction and installation, therefore the properties of all failed wells was kept constant. Note that the full well failure condition is still different from the open borehole condition ($6.25\times10^{8}$ m/d) assessed by Doble et al. (2018), i.e. the full well failure in this study still assumes that flow is only through some degraded cement, usually within the annulus (for details of pathways, see Wu et al. 2018).

Parameters associated with the well failure were based on the leaky well scenario from Doble et al. (2018) and are shown in Table 3-3. The spatially correlated random failure approach uses a fixed correlation length to determine the likelihood of failure within a given radius, beyond this radius well failure potential is assumed to be negligible. The effect of using two different correlation lengths 2 and 10 km on the clustering of wells is illustrated in Figure 3-7. A correlation length of 10 km was used in the remainder of this study.

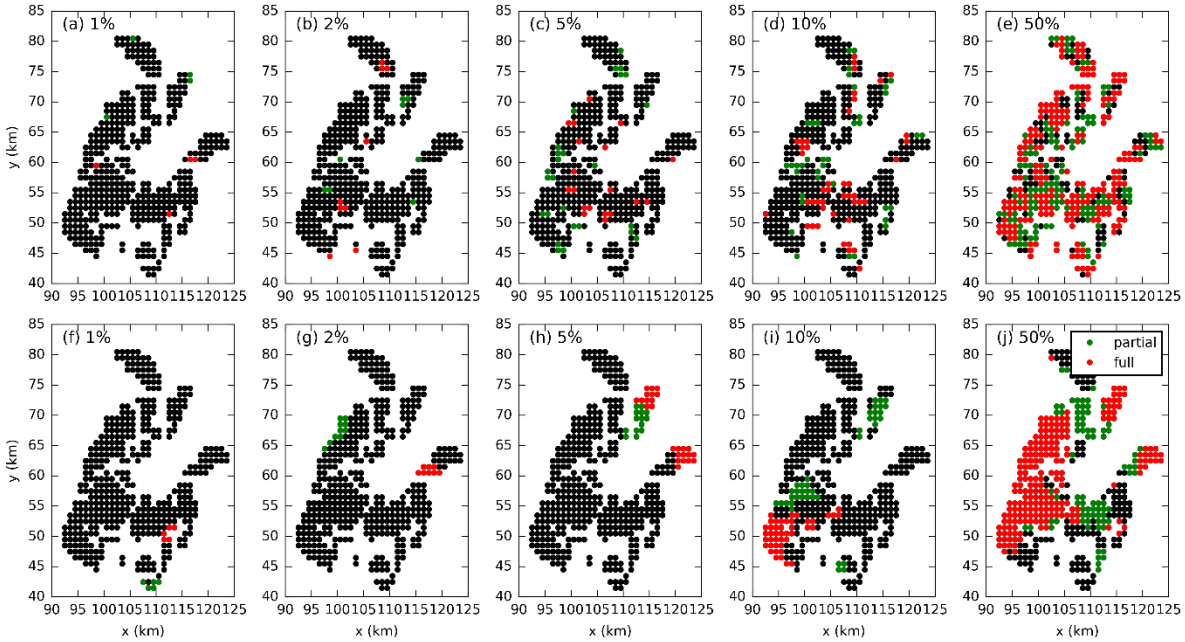


**Figure 3-7 Well failure patterns based on the spatially correlated random well failure approach for a spatial correlation length of 2 km ((a) – (e)) and 10 km ((f) – (j)). The percentage of wells that have failed is indicated at the top of each graph (from 1 – 50%). Black points indicate intact wells, green indicates a well which has partially failed and red indicates full failure (See Figure 3-5 for further description of well failure type).**

A baseline simulation of the impact of the 25-year gas (and water) production period on the groundwater balance and heads with 0% well failures was used to compare simulations where well failure enhanced inter-aquifer leakage had occurred. The baseline scenario represents aquifer recovery through seepage from the aquitards and contribution from the constant head boundary in layer 1. No recharge contributions from rainfall or rivers were considered in this study; this is a conservative assumptions that will ensure impacts are not underestimated. The impact of enhanced inter-aquifer leakage was investigated for progressive well failure scenarios where the proportion of well failures ranged from 0 - 100% (1, 2, 3, 4, 5, 6, 7, 8, 9, 10, 20, 30, 40, 50, 60, 70, 80, 90 and 100%).

## 3.3 Groundwater impact metrics

Of particular interest in this modelling exercise is the impact of the post production phase on layer 1, the Pilliga Sandstone. The Pilliga Sandstone represents the main water bearing aquifer in the area and determining how the gas (and water) extraction will affect the aquifer is important. Therefore, to determine the impact of well failure on regional scale groundwater flow and levels, the model was set up to generate the following simulation metrics:

1. timeseries of the change in Pilliga Sandstone aquifer groundwater level induced by the production period and the subsequent groundwater level recovery,
2. the contribution of failed wells to inter-aquifer groundwater exchange relative to the flux through the bulk of the aquitard (i.e. the matrix),
3. maximum drawdown and time at which maximum drawdown occurs,

4. changes to the time required to re-equilibrate the aquifer (layer 1) to a (potentially new) steady-state condition, and
5. changes to the effective flux across the aquitard:

$$Q_{eff} = = \left(\frac{Q_{aq}+Q_{well}}{A}\right)\frac{\partial z}{\partial h} \quad (1)$$

where $Q_{eff}$ is the effective flux density (m/d), $Q_{aq}$ and $Q_{well}$ are the flow into the aquitard (layer 2) and flow through the wells, respectively ($m^3/d$), $A$ is the flow area ($m^2$) e.g. (the well field [local] or the entire model domain), ∂z is the vertical discretization between layers 1 and 2 (m), and ∂h is the difference in groundwater head between layer 1 and 2 (m).

Metric (1) illustrates the impact of the production period and recovery on the groundwater levels at the point of maximum drawdown, and at distances of 10 km to the north, south, east and west of the well field for layers 1, 3, and 5 (for location of points see Figure 3-8).


**Figure 3-8 Diagram with the locations (yellow dots) at which the groundwater levels (metric 1) are shown in Figure 4-1 (within the well field), Figure 4-2 (north and south of the well field), and Figure 4-3 (east and west of the well field). Wells are shown as white dots.**

Metric (2) is concerned with the flux of water through the failed wells between the top aquifer (layer 1) and the underlying production intervals (layers 3 and 5), in comparison with the flux through the bulk of the top aquitard (layer 2). This will identify the impact of leaky wells on the model water balance.

Metric (3) addresses the impact of well failure on the head response in the top aquifer (layer 1) during the recovery phase, relative to the pre-production steady-state heads. This will give an indication of maximum impacts of well failure.

Metric (4) investigates the time required for the system (in particular layer 1) to reach a new quasi-equilibrium. This is determined as the time at which the combined flow through the aquitard (layer 2) and failed wells equals 1% of the maximum flux.

Metric (5) determines the impact of well-induced inter-aquifer leakage on the effective flux density ($Q_{eff}$) across the top aquitard (layer 2), defined as the total flux divided by the flow area.

# 4 Regional-scale groundwater impact modelling

## 4.1 Metric 1: Groundwater level response

The groundwater level response in layers 1, 3, and 5 have been derived for a series of failure rates ranging from 0 to 100 %. Time series of head variations will be discussed for the five locations shown in Figure 3-8. The maximum drawdowns induced by the production period, in model layers 3 and 5, are approximately 60 and 500 m, respectively, which occurs during the production period (Figure 4-1). The simulated drawdown in layer 5 is higher than required for optimizing desorption of gas whilst maintaining sufficient well head pressure for surface operations. This overestimation can be attributed to the use of a single layer aquitard (Frind, 1979). The maximum drawdown in layer 1 is 7.5 m and occurs, approximately 75 years after the production ceases. The lagged response in layer 1 is a result of the delay in vertical pressure propagation of the depressurisation in layer 3 and 5 from the production period. The groundwater level response is unaffected by the number of well failures, replenishment of the underlying layers is controlled by leakage through the aquitards.

The more complex model used by CDM Smith (2016) (the upper aquitard sequence had 6 numerical layers while the lower aquitard sequence had 7 numerical layers) simulated maximum drawdown in the Pilliga Sandstone, Later Permian and early Permian of < 0.5 m, 10 m, and 100 m, respectively. CDM Smith (2014) explained the effect of discretisation on drawdown as follows. The sudden decrease of hydraulic heads in the CSG reservoir due to water extraction leads to non-linear hydraulic gradients in aquitards adjacent to the CSG reservoir, particularly near the interfaces of both units. Therefore, the representation of non-linear aquitard gradients in groundwater flow models and the associated releases of water from aquitards requires appropriate vertical discretisation. The use of a single model layer per aquitard unit would imply a linear hydraulic gradient across the aquitard and a near-instantaneous release of water from storage throughout the entire thickness of the aquitard in response to water extraction. However, because the main interest is to obtain an estimate of the change in drawdown or flux relative to a base case, the overestimation will likely be cancelled out when the change is calculated.

The recovery period is markedly different in the three layers; layer 5 exhibits the fastest (relative to layer 1 and 3) recovery of groundwater heads to pre-production levels of approximately 400 years. The reason for the faster recovery in layer 5 can be attributed to the much larger depressurisation of layer 5 generating a larger gradient with the overlying aquitard; this will generate a larger flux compared to layer 1 and 3 where the vertical gradients will be much smaller. Groundwater levels in layer 3 reach pre-production levels approximately 1,500 years post production, and layer 1 is still less than the pre-production levels 2,500 years (modelled time period) post production. This model does not include recharge, therefore the time to groundwater level recovery may differ where this process is important (e.g. in the Pilliga Sandstone aquifer). This assumption is conservative, as it overestimates the impact.

The lateral propagation of drawdown at multiple points is shown in Figure 4-2 and Figure 4-3 (see Figure 3-8 for point locations at 10 km). The maximum drawdown for all locations ranges between 2-4 m, which is reached approx. 100 years after pumping has ceased. See section 4.3 for further

discussion. For all locations, groundwater levels (in all layers) take almost 2,500 years to fully recover to pre-production levels.

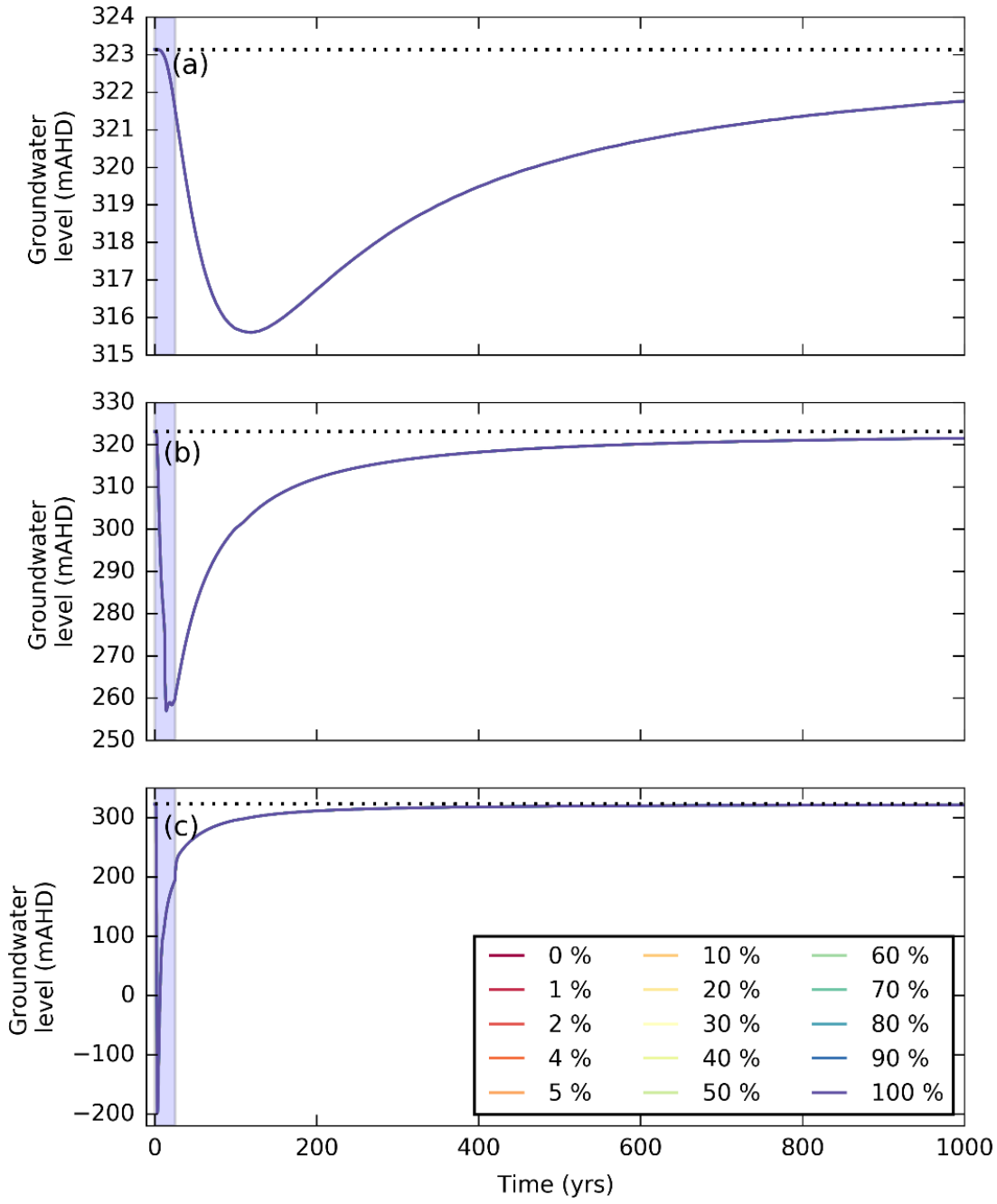


**Figure 4-1 Time series (production to recovery) of groundwater levels at the point of maximum drawdown in the well field for different well failure rates in (a) Pilliga Sandstone Aquifer (layer 1), (b) Late Permian coal seam (layer 3), and (c) Early Permian coal seam (layer 5). All simulations generate identical groundwater levels and therefore plot on top of each other. The blue bar indicates the coal seam gas (and water) production period (25 years). The dotted line represents the pre-production groundwater level (m AHD).**

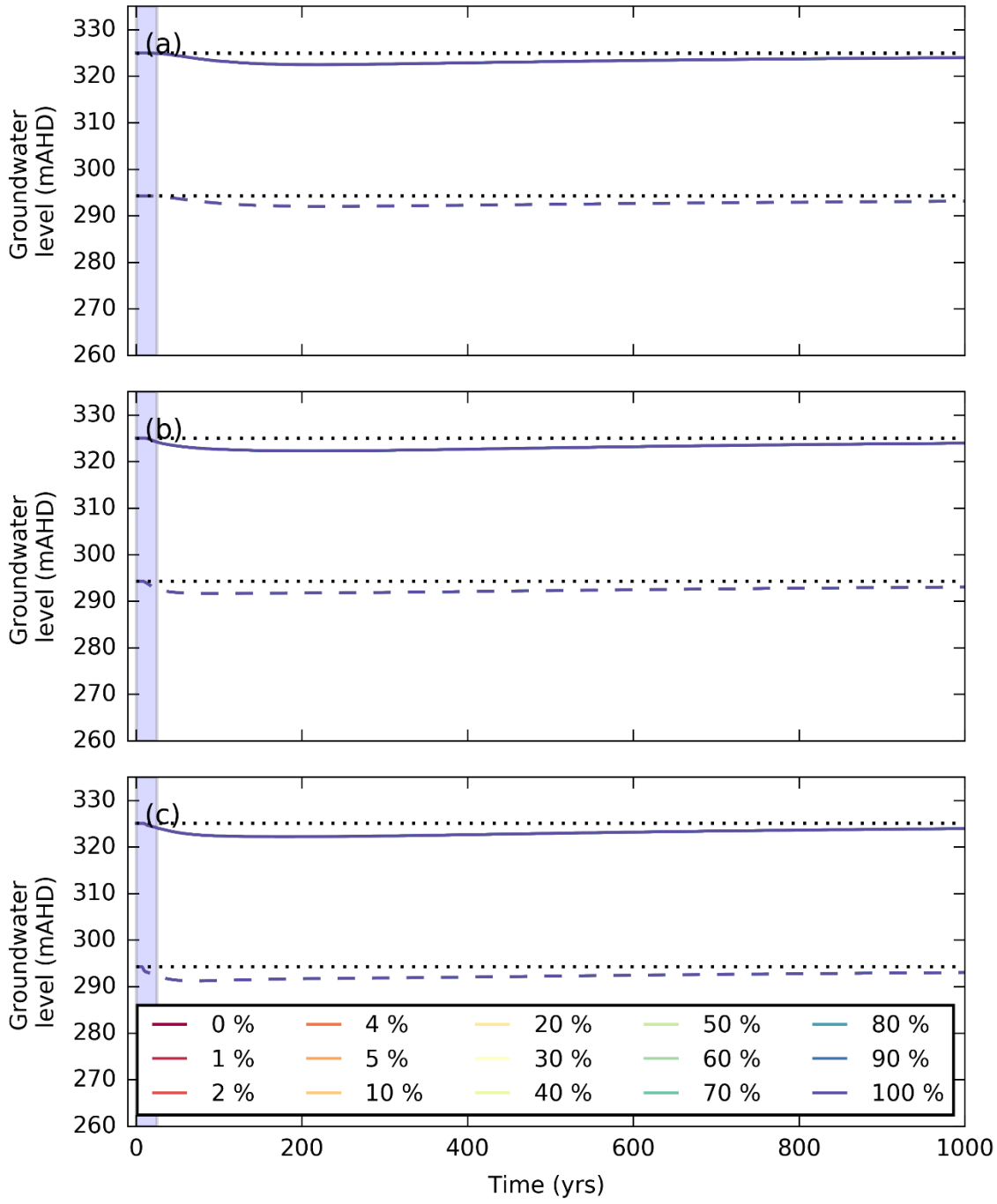


**Figure 4-2 Time series (production to recovery) of groundwater levels at a distance of 10 km to the north (solid line) and south (dashed line) of the well field for the different well failure rates in (a) Pilliga Sandstone Aquifer (layer 1), (b) Late Permian coal seam (layer 3), and (c) Early Permian coal seam (layer 5). All simulations generate identical groundwater levels and therefore plot on top of each other. The blue bar indicates the coal seam gas (and water) production period (25 years). The dotted line represents the pre-production groundwater level (m AHD).**

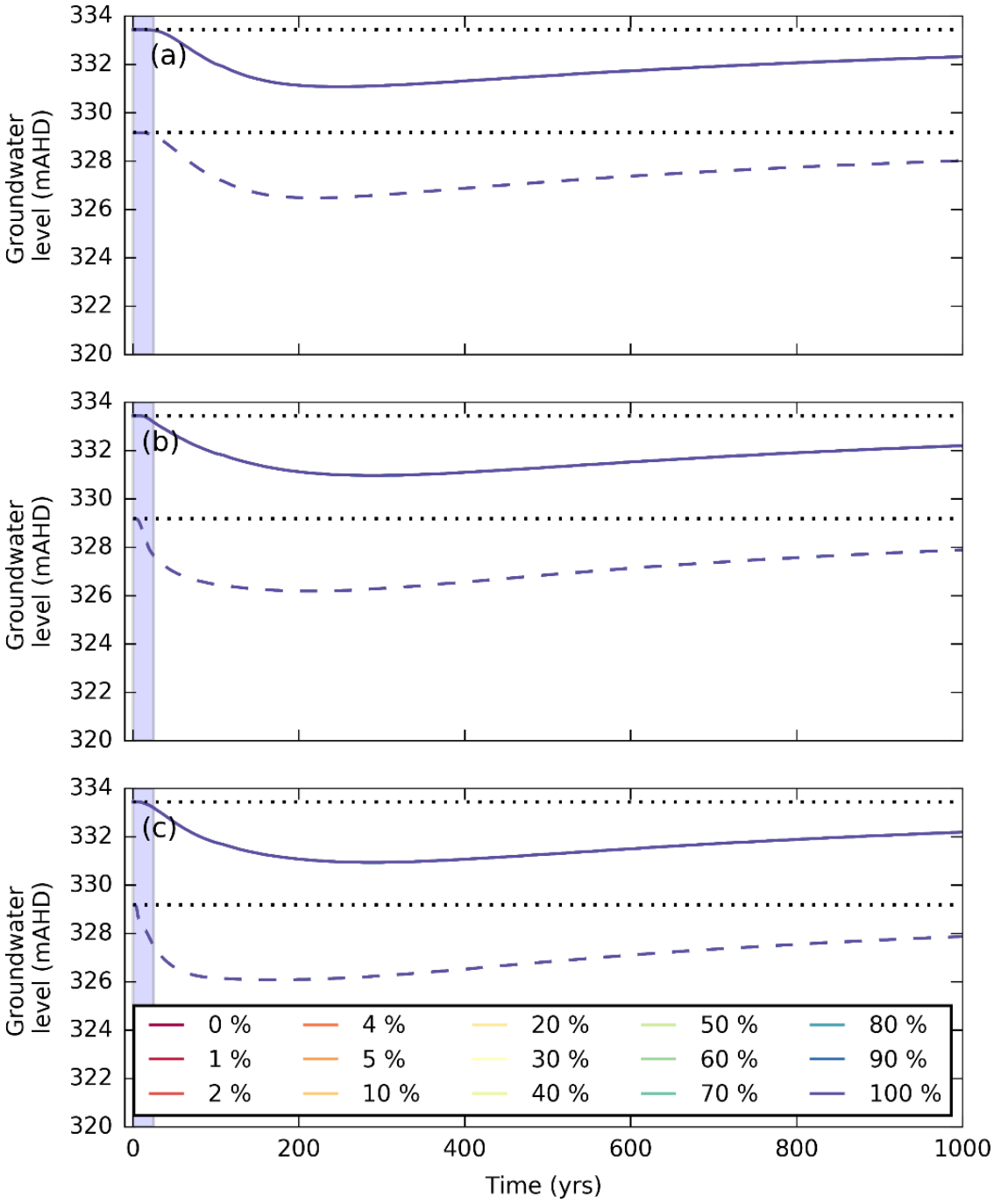


**Figure 4-3 Time series (production to recovery) of groundwater levels at a distance of 10 km to the east (solid line) and west (dashed line) of the well field for the different well failure rates in (a) Pilliga Sandstone Aquifer (layer 1), (b) Late Permian coal seam (layer 3), and (c) Early Permian coal seal (layer 5). All simulations generate identical groundwater levels and therefore plot on top of each other. The blue bar indicates the coal seam gas (and water) production period (25 years). The dotted line represents the pre-production groundwater level (m AHD).**

## 4.2 Metric 2: Contribution of well failure to overall inter-aquifer groundwater exchange

The contribution of flow through leaky wells to inter-aquifer leakage, through time, will be presented in two ways, first as a flux density (total flux rescaled to the flow area in km$^2$) and subsequently as total flux across the relevant flow area. Flux densities and total fluxes will be shown for the leakage pathway through wells and through the aquitard as diffusive flux (across the total flow domain and across the flow area of the gas project area). The flux densities for the leakage through wells are shown in Figure 4-4(a), while the corresponding regional (based on the full model area of 29,445 km$^2$) and local (based on the 425 km$^2$ gas production area) downward leakage through the aquitard (layer 2) are show in Figure 4-4(b) and Figure 4-4(c).

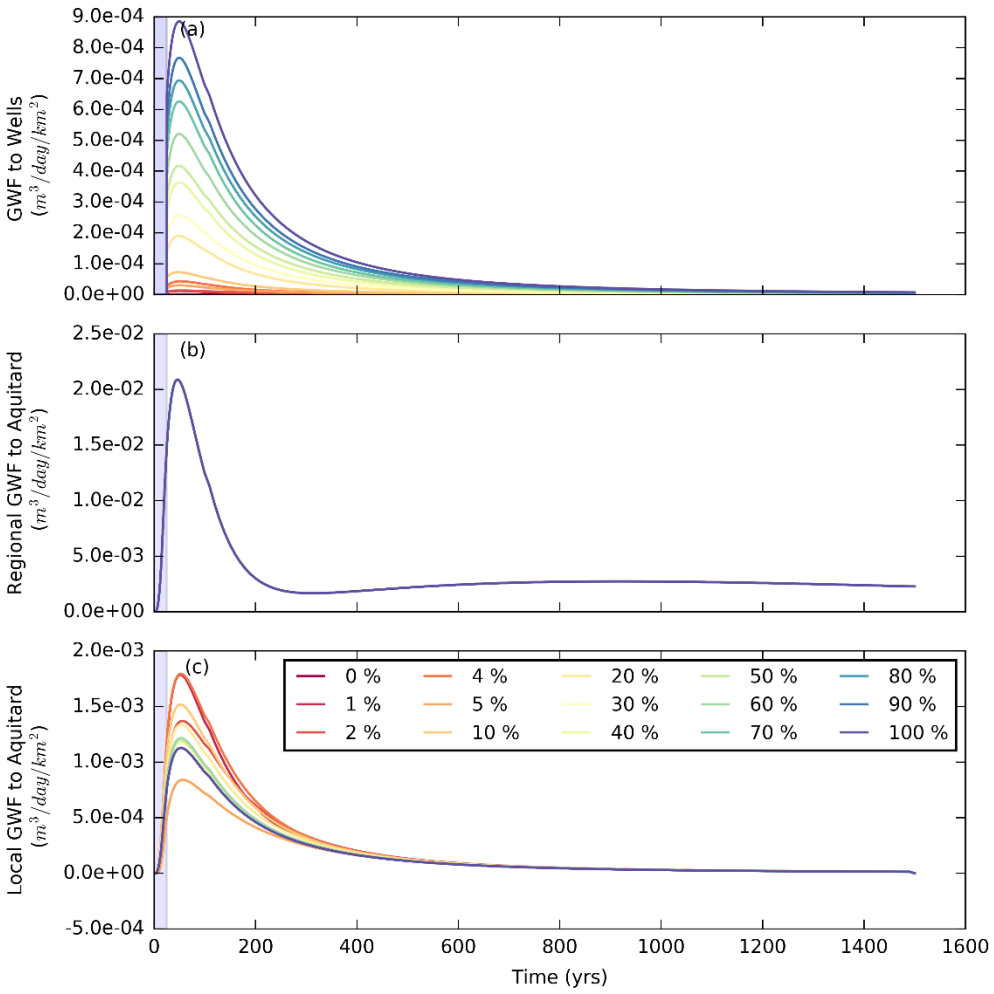


**Figure 4-4 Impact of different well failure rates on (a) the total groundwater flow density (GWF) in layer 1 to the wells (m$^3$/day/km$^2$), (b) total regional leakage density (full model domain) across the upper aquitard (m$^3$/day/km$^2$), and (c) total leakage density beneath the gas well field (425 km$^2$), from layer 2 into the underlying coal target formation (layer 3) (m$^3$/day/km$^2$). All simulations generate identical regional leakage response and therefore plot on top of each other. The blue bar indicates the coal seam gas (and water) production period (25 years).**

The fluxes through the leaky wells and aquitard (local scale and regional scale) are also shown as total flux integrated across the respective flow areas (Figure 4-5). The results are for 100% failure rate and 25 years post pumping. The overall largest flux of 600 $m^3$/day is across the regional aquitard. The second largest flux of 200 $m^3$/day is across the gas project area and is mainly driven by the downward head gradient. Comparison between regional and local flux shows that one third of the regional flux is due to the flux across the gas project area. Finally, the flux through the leaky wells amounts to 0.37 $m^3$/day, which is about 0.2% of the diffusive flux across the aquitard in the gas project area. This is a very small fraction and also means that the effective hydraulic conductivity of the aquitard has not changed. This illustrates again that even under a very unlikely scenario of 100% well failure, the total flux through the leaky wells is very small. The findings are similar to those of Doble et al. (2018) using heuristics, where the flow through the aquitard did not show any significant influence with 1 leaky well per $km^2$ (100% failure rate) a well conductivity of 0.1 m/d and a reference conductivity of $10^{-5}$ m/d (Fig 8 Doble et al. 2018).

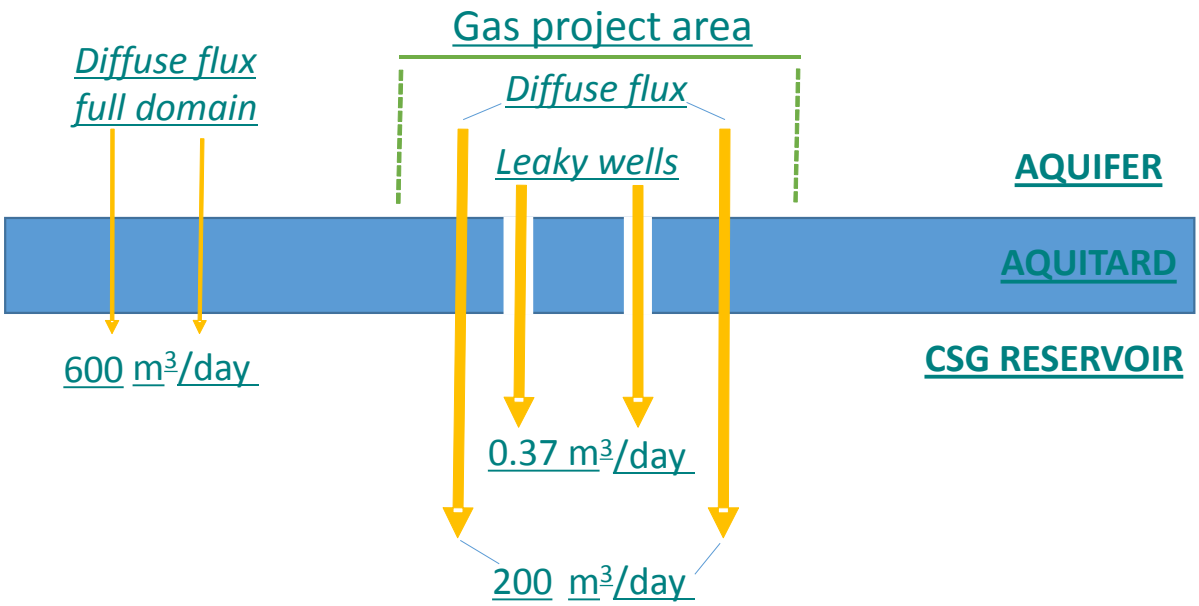


**Figure 4-5 Contributions to daily mass balance of inter-aquifer leakage from diffuse flux across aquitard (full model domain), diffuse flux across aquitard (gas project area), and flux through leaky wells (100 % well failure).**

Regional diffuse aquitard leakage appears to be insensitive to the number of well failures (Figure 4-4(b)), such that the simulated responses are identical for all scenarios, from zero well failure through to 100 % well failure. The local diffuse aquitard leakage on the other hand is influenced by the well failure rate (Figure 4-4c); the 0% and 1% well failure rates result in the highest local diffuse aquitard leakage rate. This is as expected: for a given gradient, little or no flow bypasses the bulk of the aquitard for a 0% and 1% well failure rate, hence the highest diffusive flux. For well failure rates greater than 1%, fluxes are lower and there is no clear correlation between % well failure and the local diffuse aquitard leakage. This is likely due to the way the leaky wells are allocated across the area, i.e. by using the spatially correlated random approach, linked to spatially variable water production profiles across the gas project area. In other words, a small increase in well failure rate may result in disproportionally large increase in fluxes when an area with a high water production profile is accessed.

The magnitude of flow through leaky wells, as expected, is strongly related to the number of well failures, i.e., the greater the failure rate the higher is the flow through the wells (Figure 4-4a). In addition to this, the well failure type, partial or full, also strongly influences the flow magnitude. A partial well failure only enhances inter-aquifer leakage between layers 1 and 3, whereas a full well failure connects all layers. Because Layer 5 is subject to significantly more water extraction than layer 3 during the coal seam gas production phase (see Figure 3-4), the increase in the hydraulic gradient between the layers 1, 3, and 5 will and therefore increase the potential for inter-aquifer leakage compared to the case where leakage pathways exist only between layer 1 and 3.

In all simulations, the maximum flow through leaky wells and local aquitard leakage is observed approximately 25 years after pumping has ceased. This lagged response is a function of the limited flow rate through leaky wells and the ambient gradient in the aquifers.

The calculated flux history across the relevant flow areas has also been presented as total flux (opposed to flux densities) (Figure 4-6). These results can be converted into the results shown in Figure 4-4 by dividing them by the respective flow areas (425 km$^2$ for flux through wells and diffusive flux through gas project area, and 29,445 km$^2$ for the regional flux).

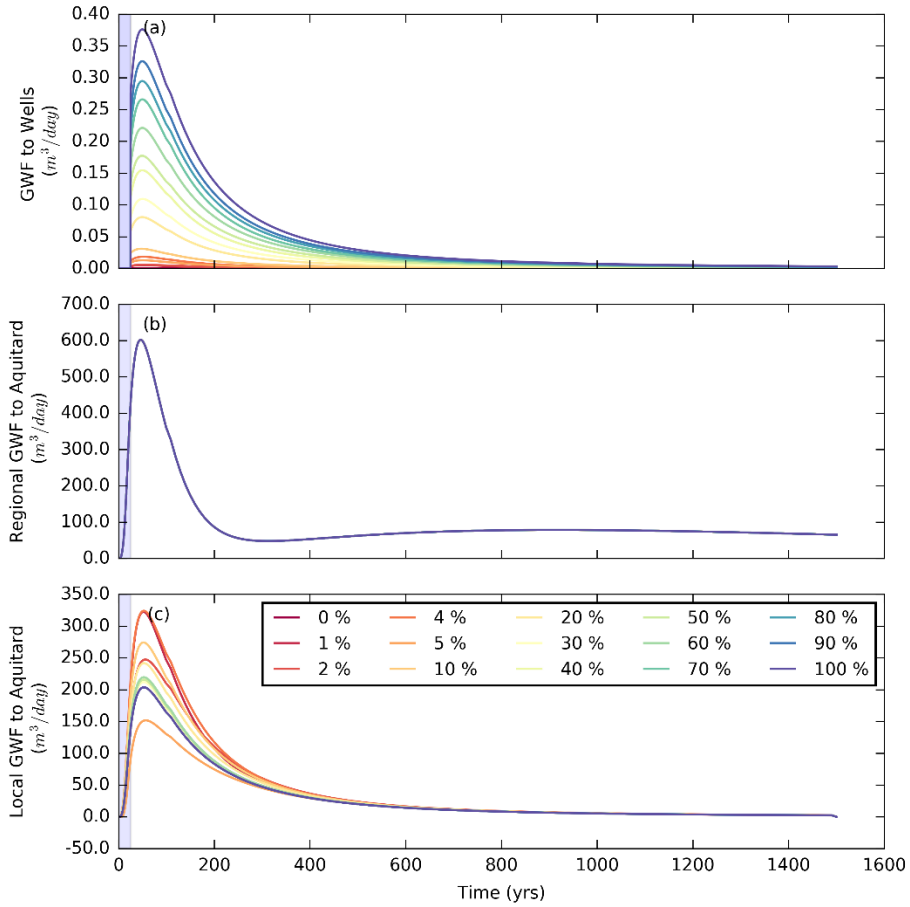


**Figure 4-6 Impact of different well failure rates on (a) the total groundwater flow (GWF) in layer 1 to the wells (m$^3$/day), (b) total regional leakage (full model domain) across the upper aquitard (m$^3$/day), and (c) total leakage beneath the gas well field (425 km$^2$), from layer 2 into the underlying coal target formation (layer 3) (m$^3$/day). All simulations generate identical regional leakage response and therefore plot on top of each other. The blue bar indicates the coal seam gas (and water) production period (25 years).**

As a reference, the three total fluxes are also shown for zero % failure rate (Figure 4-7). This represents a yardstick against which the scenarios with failure rates larger than zero can be compared. Without well leakage, the total flux through the aquitard at the gas project area is half (300 $m^3$/day) that of the total regional flux (600 $m^3$/day). For 100% leaky wells the flux through the aquitard decreases to 200 $m^3$/day as a fraction of the flux now goes through the wells.

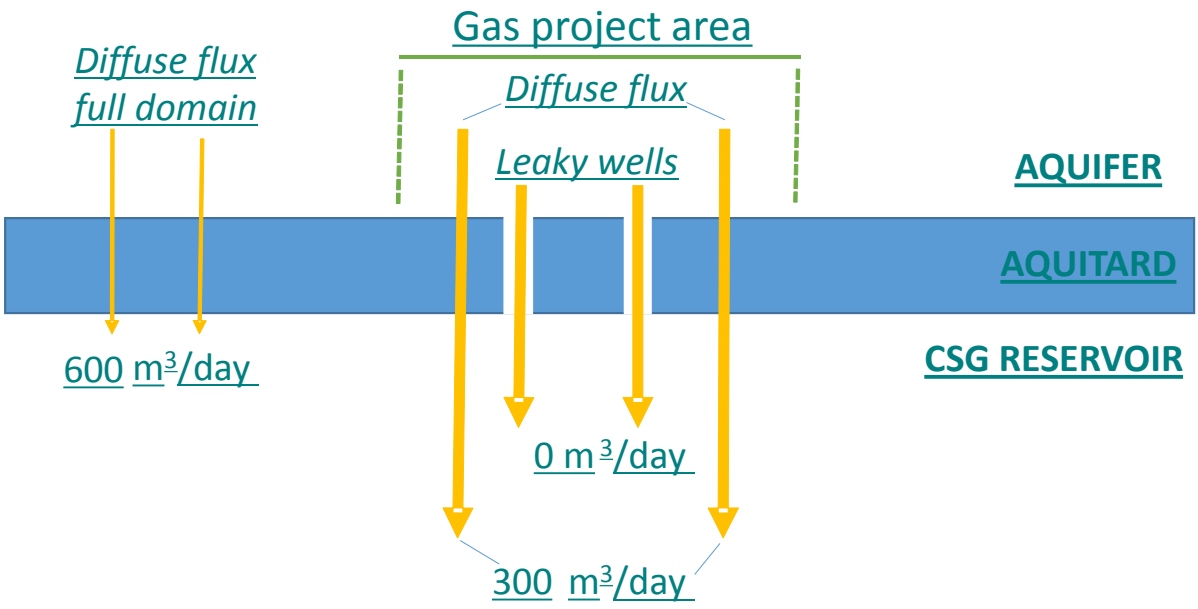


**Figure 4-7 Contributions to daily mass balance of inter-aquifer leakage from diffuse flux across aquitard (full model domain), diffuse flux across aquitard in the gas project area, and flux through leaky wells (0 % well failure).**

## 4.3 Metric 3: Maximum drawdown and time of maximum drawdown time

Simulated groundwater heads in the main aquifer (layer 1) were not significantly influenced during the 25 year pumping period in the absence of well-induced leakage. Any observed head variations can be attributed to regional leakage to the main aquitard (layer 2). All significant changes to the groundwater head occurred during the recovery phase, i.e., after pumping had ceased.

The maximum drawdown in the main aquifer (layer 1) and the time of maximum drawdown are shown in Figure 4-8 for a 0% well failure and in Figure 4-9 for a 100% well failure, respectively. The impact of enhanced inter-aquifer leakage through leaky wells appears to have no discernible impact on the drawdown, or its timing, in layer 1 of the model (see Figure 4-10 for the difference between Figure 4-8 and Figure 4-9). The limited impact of well failure on the groundwater heads is corroborated by the relatively low flow rates through the wells seen in Figure 4-4a.

During the production period, the groundwater heads in layers 3 and 5 declined from 342.5 m AHD for both layers, to a minimum depth of 256.1 and -197.7 m AHD (drawdown of 86.4 and 540.2 m respectively) (see further in Figure 4-12). Recovery in layers 3 and 5 can only occur through regional leakage across the bulk aquitard or through failed wells (if present). In the absence of any well failure, a drawdown of 0.9 m still persists in layers 3 and 5, 1500 years after pumping has ceased.

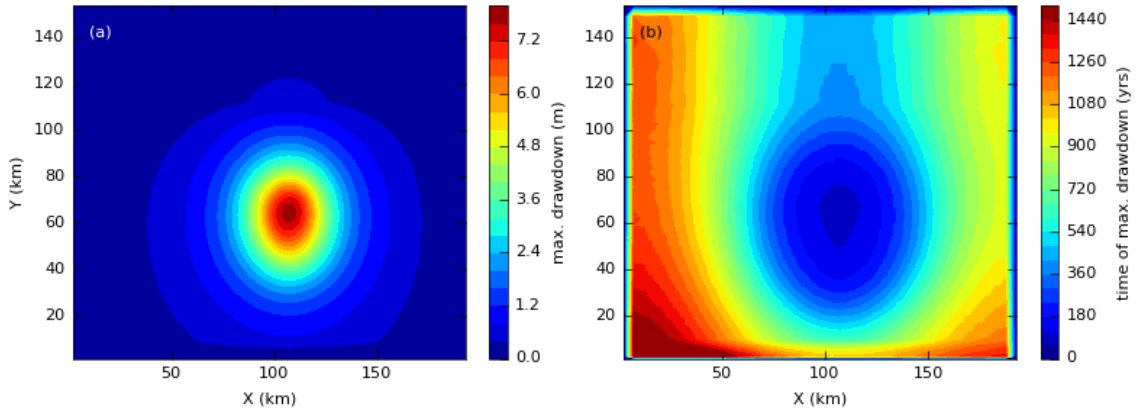


**Figure 4-8 (a) Maximum groundwater level drawdown in layer 1 for 0% well failure and (b) the associated timing of maximum drawdown relative to the initial steady-state groundwater level for 0% well failure.**

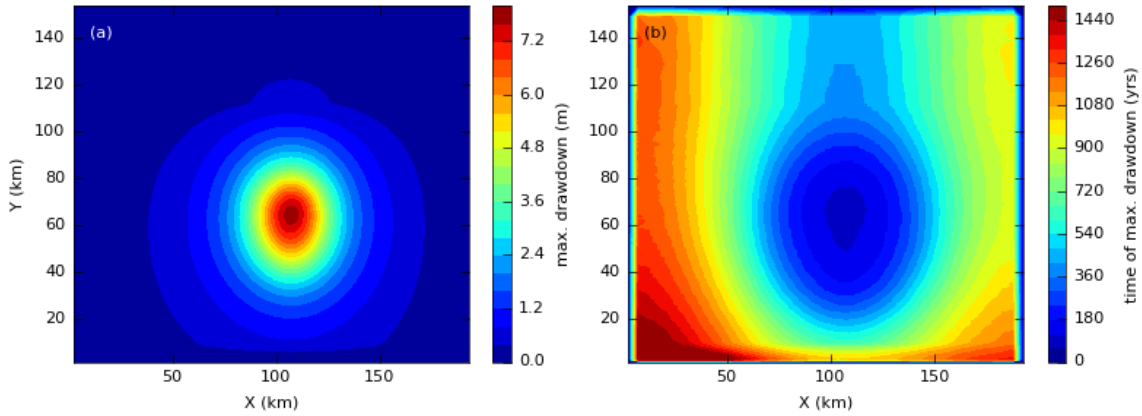


**Figure 4-9 (a) Maximum groundwater level drawdown in layer 1 for 100% well failure and (b) the associated timing of maximum drawdown relative to the initial steady-state groundwater level for 100% well failure.**

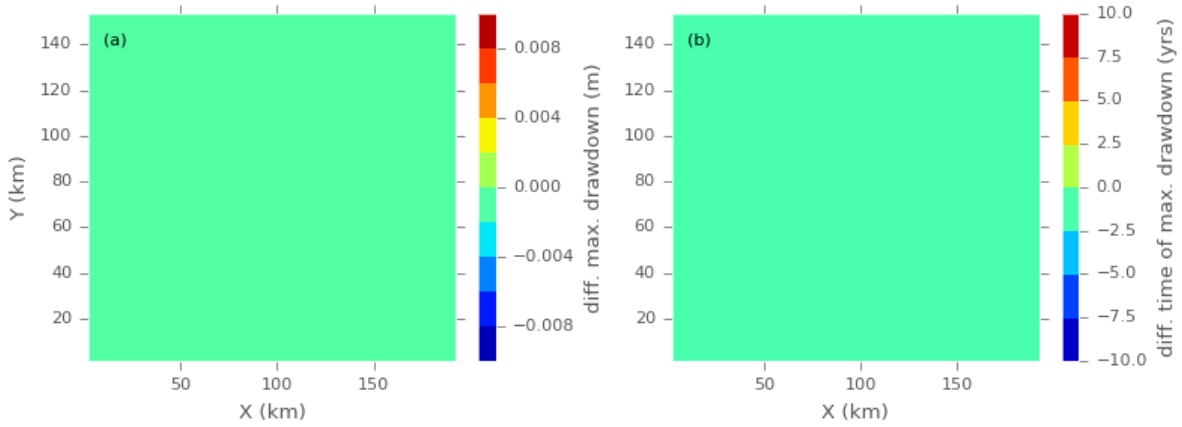


**Figure 4-10 (a) Difference in maximum groundwater level drawdown in layer 1 between 0% and 100% well failure and (b) the associated difference in timing of maximum drawdown relative to the steady-state groundwater level between 0% and 100% well failure.**

## 4.4 Metric 4: Aquifer equilibration time

Assuming hydraulic pressures equilibrate within the system, a two order of magnitude reduction in flow through the wells (i.e. 99% reduction in inter-aquifer leakage) represents a system closely approaching a new quasi-equilibrium. Figure 4-11 shows the relationship between well failure rate and the time to reach a new quasi-equilibrium. In general, the higher the percentage of well failures, the quicker the system reaches a new equilibrium (Q1). This is because the additional flow pathways provided by the wells help replenish the underlying production layers at a faster rate (based on no simulated recharge). Despite the system reaching faster equilibrium with a higher failure rate, the effect on the groundwater levels in the layer 1 is still negligible (Figure 4-10). This general trend can be observed in Figure 4-11, however there is considerable variability in the time to a new quasi-equilibrium for simulations with a low failure percentage (i.e., less than 40%). This variability can be attributed to a number of factors; 1) how the spatially correlated random failure approach selects its wells, 2) the location of the failed wells within the production zone (water extraction areas), and 3) the number of simulations. As previously shown in Figure 3-7, spatial correlation of well failure will result in clustering of selected wells, the extent of which is determined by the correlation length. A longer correlation length (i.e., 10 km such as that used in this study), which results in wells being more strongly clustered, whereas a smaller correlation length will produce a more random well selection with less clustering (see Figure 3-7a-e). The more erratic behaviour of metric Time to Q1 is most apparent for a small well failure percentage which is due to limited clustering. As the well failure percentage increases, the metric Time to Q1 becomes less erratic because wells become more clustered (producing a more homogenous result). Furthermore, where the density of failed wells is higher (i.e., in such a cluster), a new quasi-equilibrium may be obtained sooner by an increase in aquitard hydraulic connection to the underlying layers, increasing the vertical flow rate, relative to a random selection (i.e., no clustering).

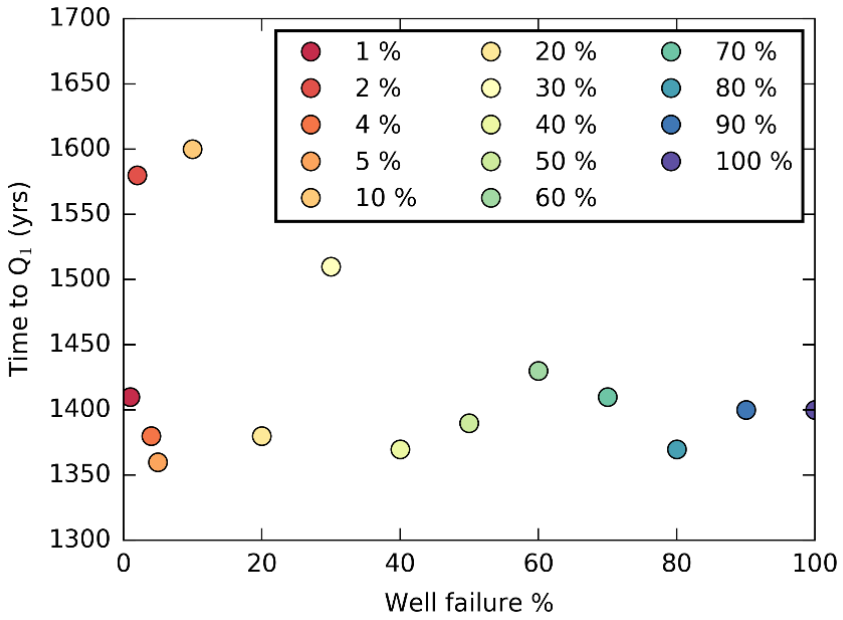


**Figure 4-11 Time required for the inter-aquifer leakage (total groundwater flow through failed wells) to reduce to 1% of its maximum flow rate ($Q_1$). $Q_1$ is calculated for different well failure rates.**

The location of the wells in the well field may also be important because the well field area is subdivided into water extraction areas, where each has its own pumping regime with water production values ranging from 5 - 18 ML/day (for details see CDM Smith, 2014). This spatial variability in pumping will influence how the failed wells contribute to inter-aquifer leakage. Should a cluster of failed wells be located in an area of high water production, the underlying layers will have undergone considerable depressurisation, relative to other areas in the well field, thereby creating a larger vertical gradient (see Figure 4-12). This will increase the potential flow rate through failed wells in these areas. It should be noted that the likelihood of a cluster of failed wells in a high production zone is lower than the likelihood of a cluster of failed wells elsewhere in the well field.

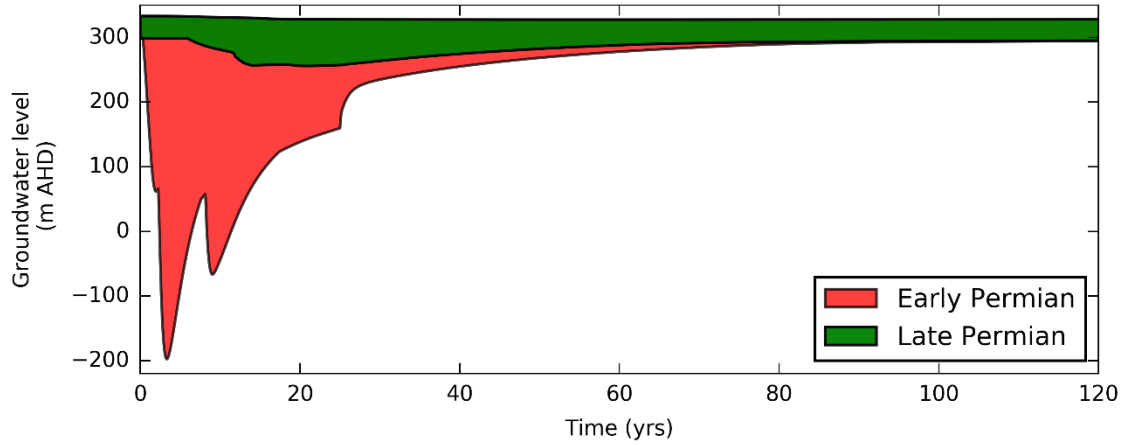


**Figure 4-12 Range in simulated groundwater level (m AHD) prior to production through to post production period, in the Early Permian Coal Seam (layer 5) and the Late Permian Coal Seam (layer 3) beneath the well field for 0% well failure.**

Further simulations of different random well failure patterns may be required to accurately determine the influence of well failure on time to a new quasi-equilibrium.

Nevertheless, it is clear from Figure 4-11 that a minimum period of 1,350 years is required for the groundwater system to approach a new quasi-equilibrium based on the simplified model used here.

## 4.5 Metric 5: Changes to the aquitard effective flux

The regional (entire model) and local (beneath the well field) effective flux ($Q_{eff}$) of the top aquitard (layer 2) are shown in Figure 4-13. The regional $Q_{eff}$ appears to be unaffected by the number of well failures, because all simulations produce the same temporal response. By comparison, the local $Q_{eff}$ of the aquitard shows some local influence of the well failure rate, most likely associated with variability in aquitard leakage associated with the different well failure rates.

The regional $Q_{eff}$ of the aquitard quickly rises to approximately $2.0 \times 10^{-3}$ m/d at the start of the recovery phase, after which it slowly drops to a minimum of $5 \times 10^{-6}$ m/d over the following 300 years, after which it rises and begins to stabilise around $10^{-5}$ m/d, similar to the vertical hydraulic conductivity for layer 2 (Table 3-2). The minor fluctuations in the regional $Q_{eff}$ for the estimated area are the result of variability in the hydraulic gradient within the model.

The response in the local $Q_{eff}$ of the aquitard is closely tied to the time of maximum drawdown in layer 5 (3 years into the production period, Figure 4-12), such that the maximum local $Q_{eff}$ ($2.6x10^4$ m/d) coincides with the maximum drawdown. Figure 4-4 (a and c) shows that there was no significant increase in either aquitard flow or leakage to the wells (assumed to fail only in the recovery stage), therefore this response is a function of the higher vertical hydraulic gradient beneath the well field induced by pumping.

$K_{eff}$ varies through time because the calculation assumes steady-state conditions, i.e. no change in storage. During the production phase, flow from layer 2 to the underlying layers will occur resulting in a decline in the layer storage. Flow into the aquitard will replenish the storage in the recovery phase therefore the flow out of the aquitard may be underestimated (flow through the aquitard is not in equilibrium) accounting for the underestimation in $K_{eff}$.

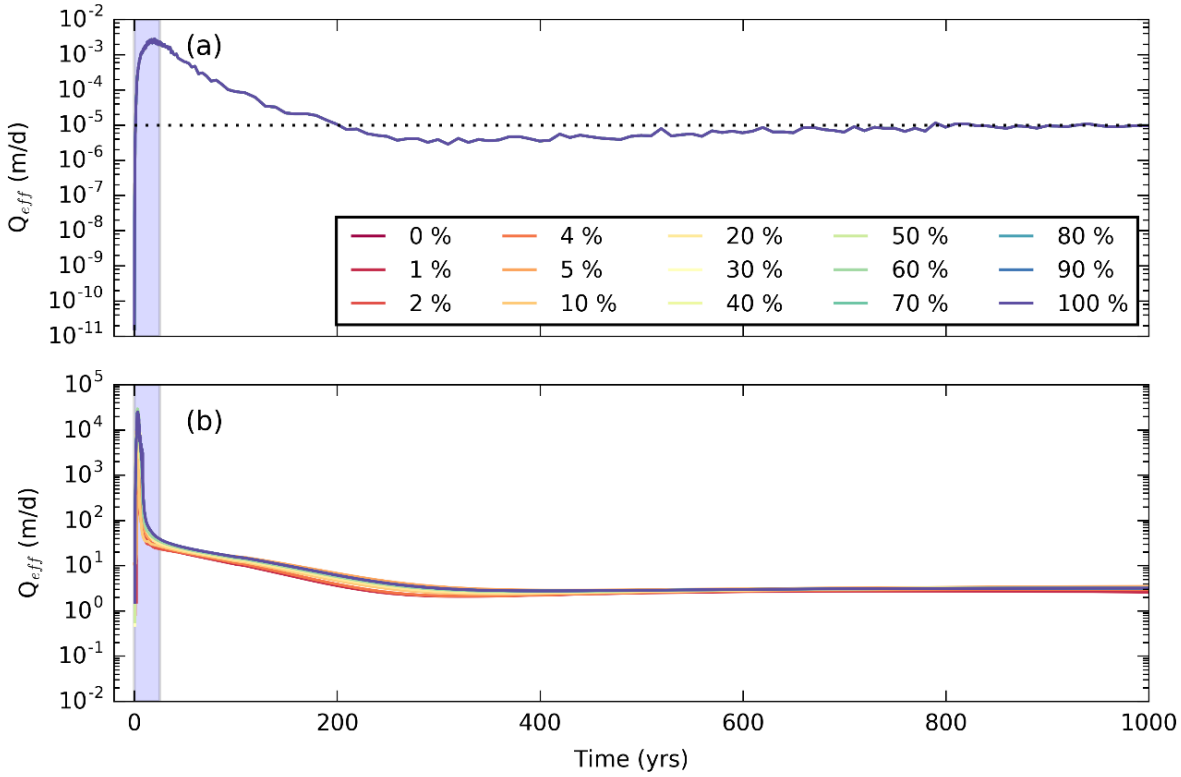


**Figure 4-13 Effective flux of the top aquitard (layer 2) through time for different well failure rates for the full model (a) and local well field (b). All well failure simulations generate identical effective flux trends (irrespective of the number of full or partial well failures) and therefore plot on top of each other. The blue bar indicates the production period (25 years), the dotted line (a) indicates the hydraulic conductivity of the aquitard (layer 2).**

## 4.6 Impacts from degraded water bores or coal exploration holes

As discussed in Section 2, water bores with degraded casing and coal exploration holes may contribute to increased inter-aquifer leakage by providing flow paths. Conceptually these bores could contribute to inter-aquifer leakage in the vicinity of a coal seam gas production area both during the gas production phase and after decommissioning of the site. In this study only the latter condition will be studied, as the depressurisation of the coal formation is still very larger even after gas and water production has ended, and because such depressurisation will continue exist for hundreds of years compared to the relatively short gas production period (couple of decades). The potential impact after the decommissioning will thus be representative for the period prior to decommissioning (period with active gas and water extraction).

The simplified Gunnedah Basin model was again used to explore potential impacts of open boreholes on the groundwater flow. These simulations provide a preliminary insight into the impacts of such open boreholes on the groundwater flow. The steady-state and production period simulation was the same as for the leaky well simulations. However, due to the high density of wells in the current model well field (1 per km), only low well failure rates (1%, 2%, and 5%, Figure 4-14) where simulated in an attempt to replicate the likely spatial distribution of open exploration wells.

The enhanced connection between layers, by an increasing number of failed open wells, is apparent in the groundwater levels in Figure 4-15a, where the maximum drawdown in layer 1 increases with a larger well failure percentage (also see Figure 4-18, Figure 4-19 and Figure 4-20). The rate of recovery in groundwater level in layer 3 and layer 5 (Late Permian and early Permian coal seams, Figure 4-15b and c) also demonstrates the same response, where the groundwater levels (and therefore recovery rate) for 5% failure simulation are 4 m above those of the 1% failure simulation. The difference in groundwater levels between the well failure scenarios diminishes 500 years post-production.

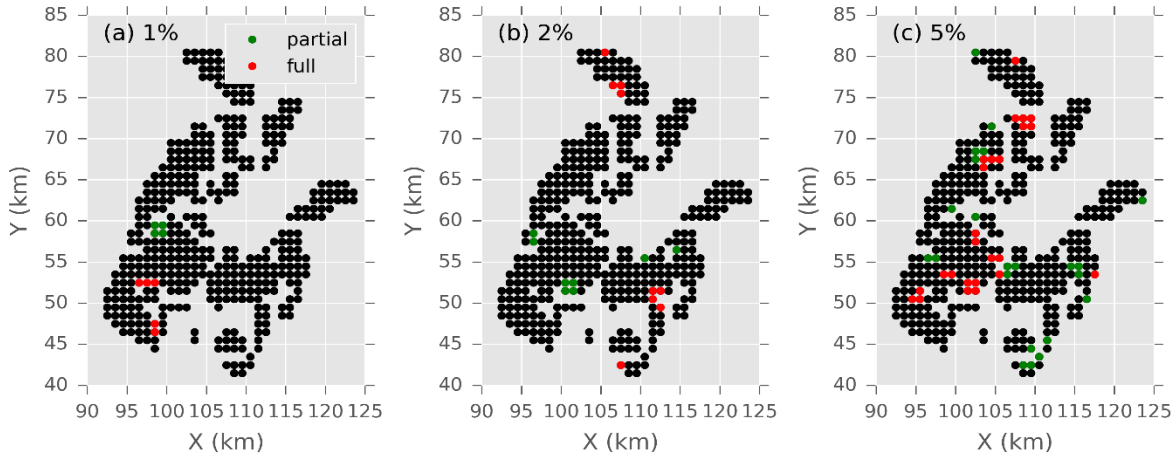


**Figure 4-14 Bore failure patterns based on the spatially correlated random bore failure approach for a spatial correlation length of 2 km ((a) – (c)). The percentage of bores that have failed is indicated at the top of each graph (from 1 – 5%). Black points indicate intact bores, green indicates a bore which has partially failed and red indicates full failure (See Figure 3-5 for further description of bore failure type).**

The spatial response in groundwater levels at greater distances from the gas production area (10 km to the north, south, east and west of the bore field) are shown in Figure 4-16 and Figure 4-17. The groundwater levels for the open bore scenarios are similar to those of the leaky well scenarios (Figure 4-2 and Figure 4-3), suggesting that the additional flow through the opens bores has a local impact on the groundwater levels rather than a regional impact. At higher failure rates and/or wider spatial distribution of failed bores, a more regional response may occur.

The spatial impact of the production period and open bore leakage is shown as the maximum drawdown in layer 1 for 1 % (Figure 4-18), 2% (Figure 4-19) and 5% (Figure 4-20) bore failure. The impact of increasing the number of open bores is small but apparent when comparing the results from 0% failure to 5 % bore failure (Figure 4-21). Likewise, there appears to be only minor differences in the timing to the maximum drawdown between the 0%, 1%, 2%, and 5% bore failure rates. The area affected by the 5% failure rate is approximately 7,500 $km^2$, based on a minimum additional drawdown of 0.1 m.

Figure 4-22 clearly demonstrates that the groundwater flow to the open bores is the primary mechanism to replenish the underlying layers, being two orders of magnitude higher than the local flow through the aquitard and twelve orders of magnitude larger than the regional flow through the aquitard. This will reduce the time to a new quasi-equilibrium from approximately 1,400 years for 100% leaky well failure (Figure 4-11) to approximately 500 years for 1 - 5% open bore failure.

An analysis of the total fluxes can be made on the basis of Figure 4-23. The overall largest flux is through the leaky bores, i.e. around 1,500 $m^3$/day for a 5% failure rate. This is about three times larger than the total regional flux (approximately 350 $m^3$/day for a 5% failure rate), and nearly six times larger than the diffusive flux across the gas project area (about 150 $m^3$/day for 5% failure rate). Compared to the fluxes for a zero failure rate (see Figure 4-5), both the total regional flux and the flux through the gas project area have decreased by nearly a factor two, i.e. from 600 to 350 $m^3$/day and from 300 to about 150 $m^3$/day. Note that these results are very conservative due to the simplified model.

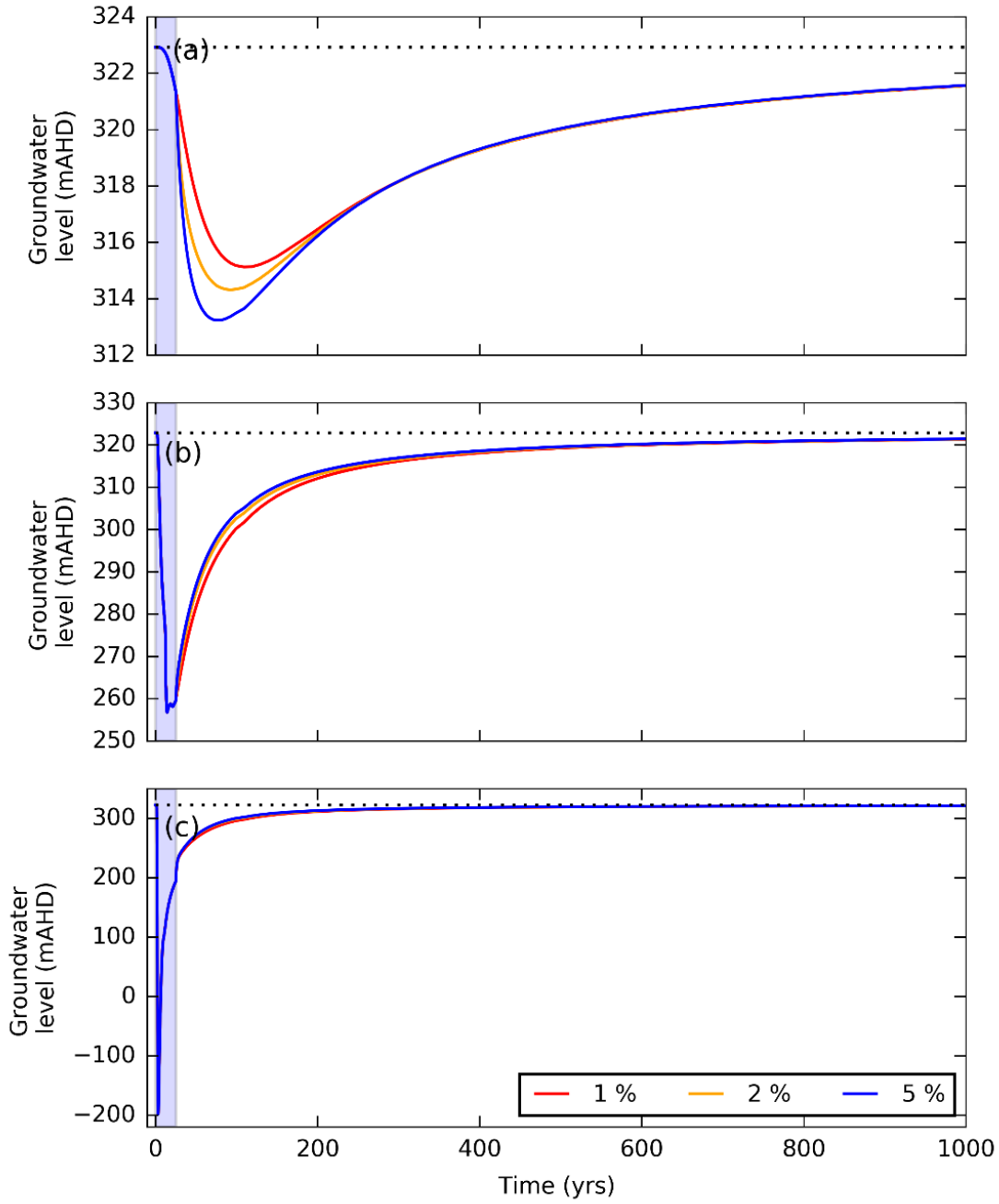


**Figure 4-15 Time series (production to recovery) of groundwater levels at the point of maximum drawdown in the bore field of different bore failure rates in (a) Pilliga Sandstone Aquifer (layer 1), (b) Late Permian coal seam (layer 3), and (c) Early Permian coal seal (layer 5). For layer 5 all simulations generate identical groundwater levels and therefore plot on top of each other. The blue bar indicates the coal seam gas (and water) production period (25 years). The dotted line represents the pre-production groundwater level (m AHD).**

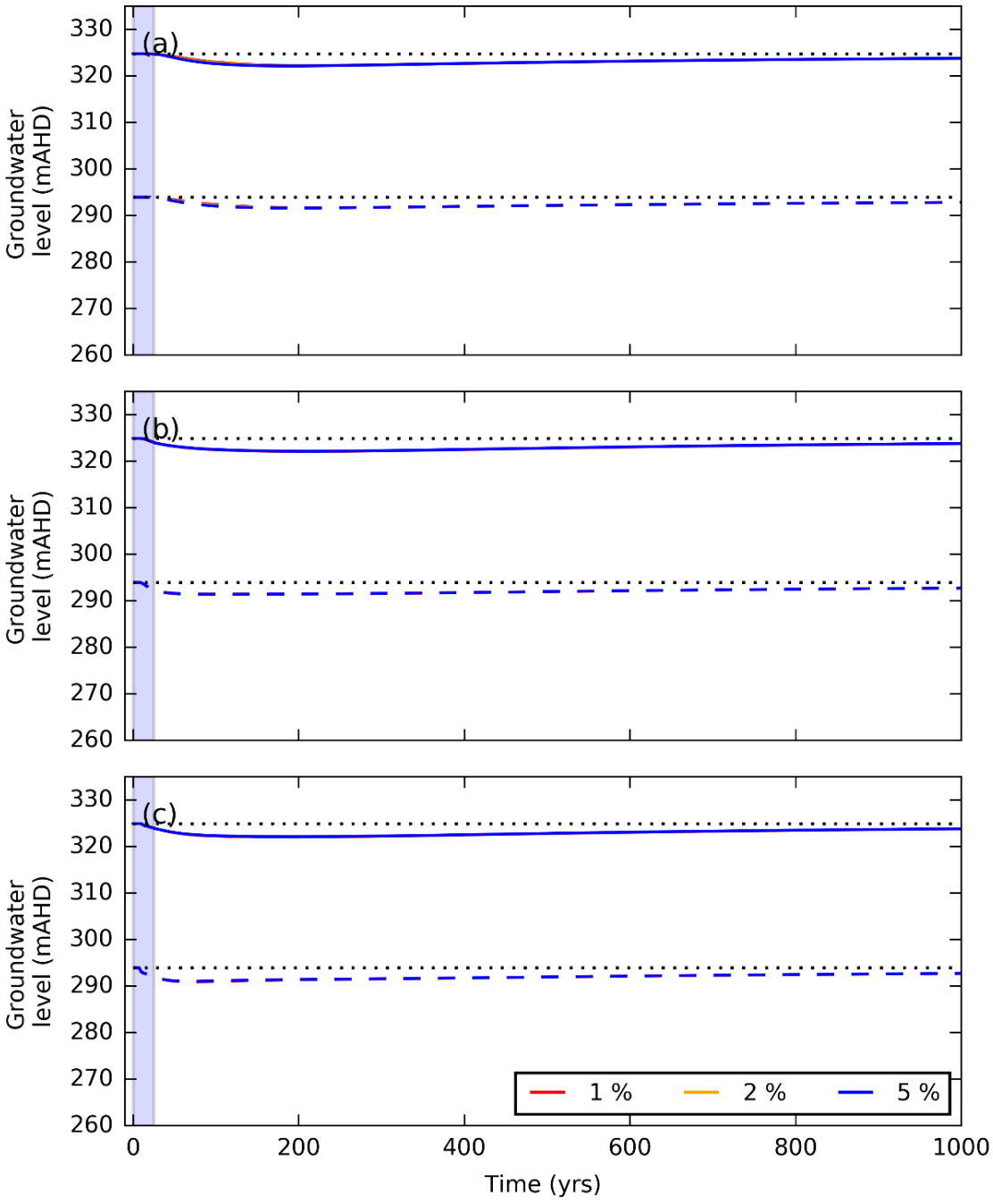


**Figure 4-16 Time series (from production to recovery of groundwater levels) of groundwater levels at a distance of 10 km to the north (solid line) and south (dashed line) of the bore field for the different bore failure rates in (a) Pilliga Sandstone aquifer (layer 1), (b) Late Permian coal seam (layer 3), and (c) Early Permian coal seal (layer 5). All simulations generate identical groundwater levels and therefore plot on top of each other. The blue bar indicates the coal seam gas (and water) production period (25 years). The dotted line represents the pre-production groundwater level (m AHD).**

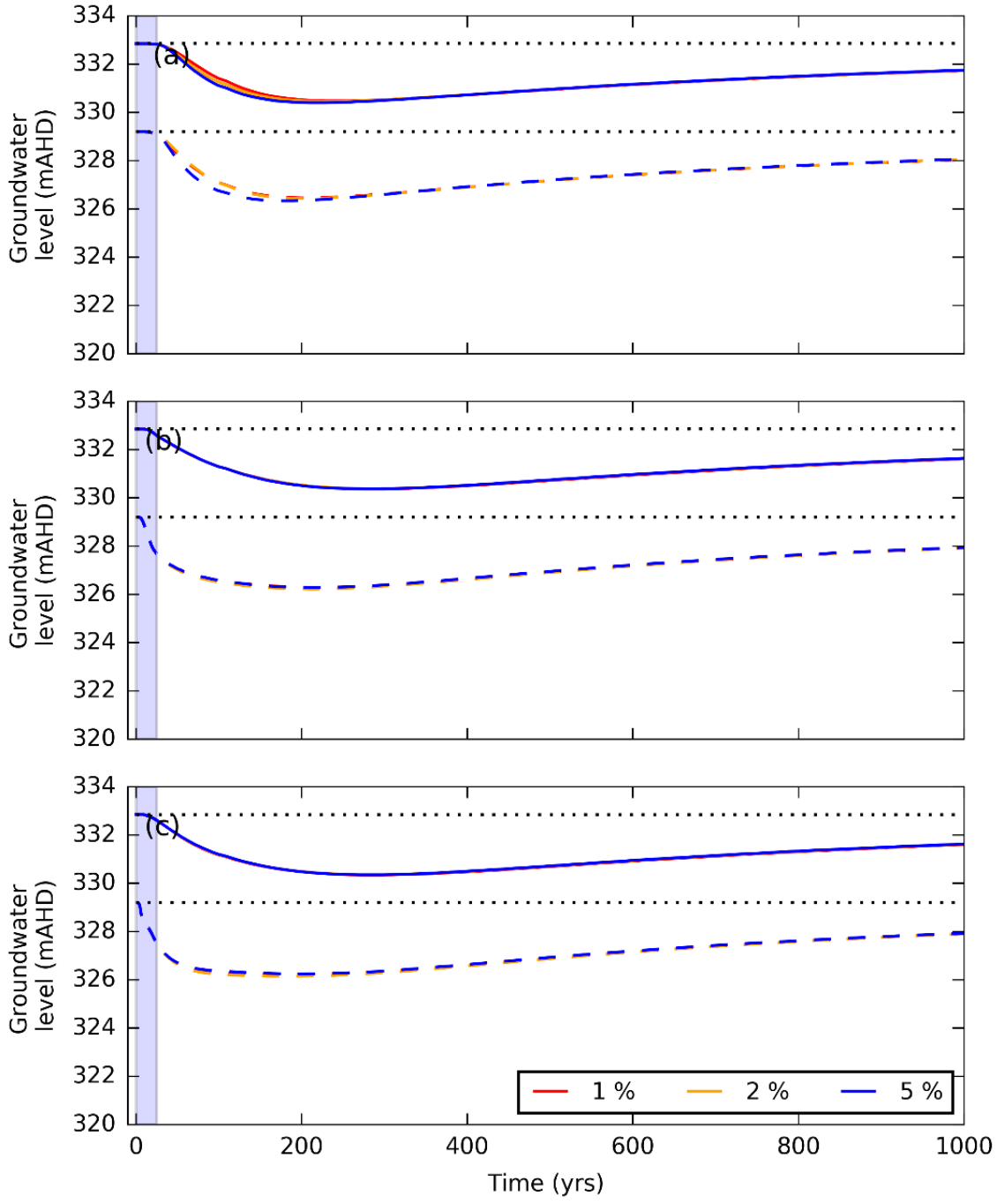


**Figure 4-17 Time series (from production to recovery of groundwater levels) of groundwater levels at a distance of 10 km to the east (solid line) and west (dashed line) of the bore field for the different bore failure rates in (a) Pilliga Sandstone aquifer (layer 1), (b) Late Permian coal seam (layer 3), and (c) Early Permian coal seal (layer 5). All simulations generate identical groundwater levels and therefore plot on top of each other. The blue bar indicates the coal seam gas (and water) production period (25 years). The dotted line represents the pre-production groundwater level (m AHD).**

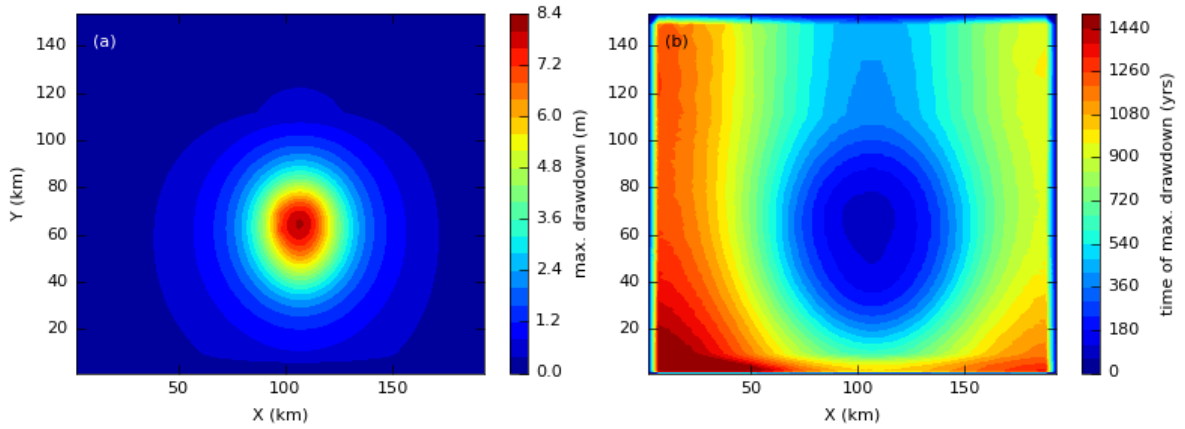


**Figure 4-18 Maximum groundwater level drawdown for 1% bore failure and (b) the associated timing of maximum drawdown relative to the initial steady-state groundwater level for 1% bore failure.**

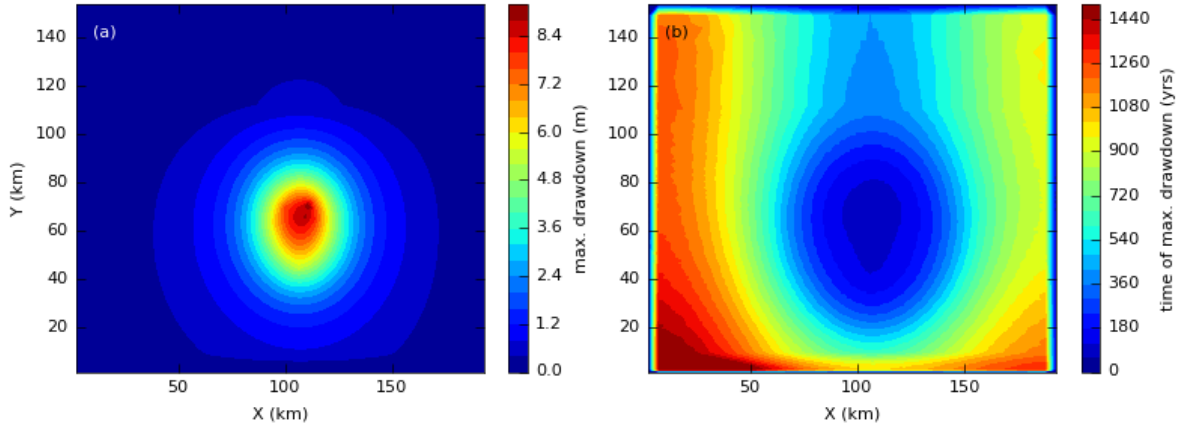


**Figure 4-19 Maximum groundwater level drawdown for 2% bore failure and (b) the associated timing of maximum drawdown relative to the initial steady-state groundwater level for 2% bore failure.**

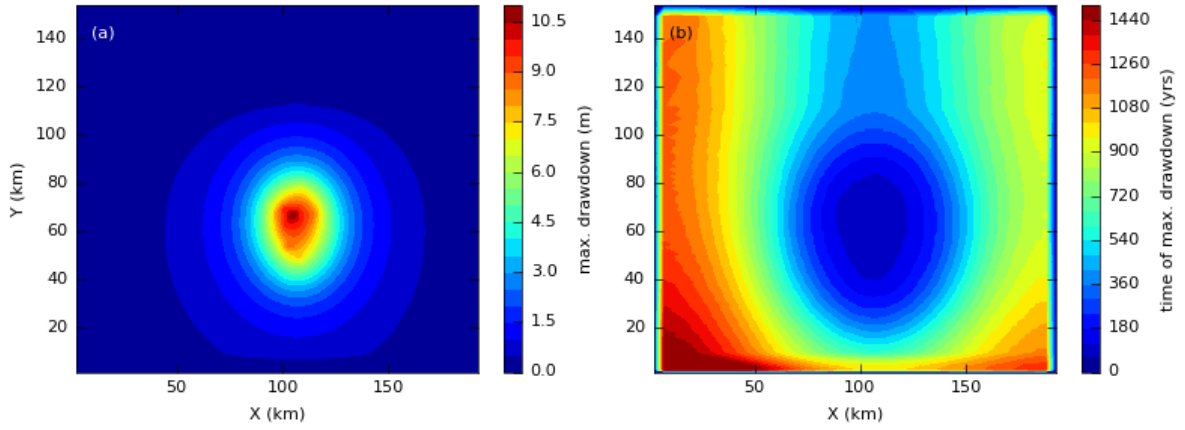


**Figure 4-20 Maximum groundwater level drawdown for 5% bore failure and (b) the associated timing of maximum drawdown relative to the initial steady-state groundwater level for 5% bore failure.**

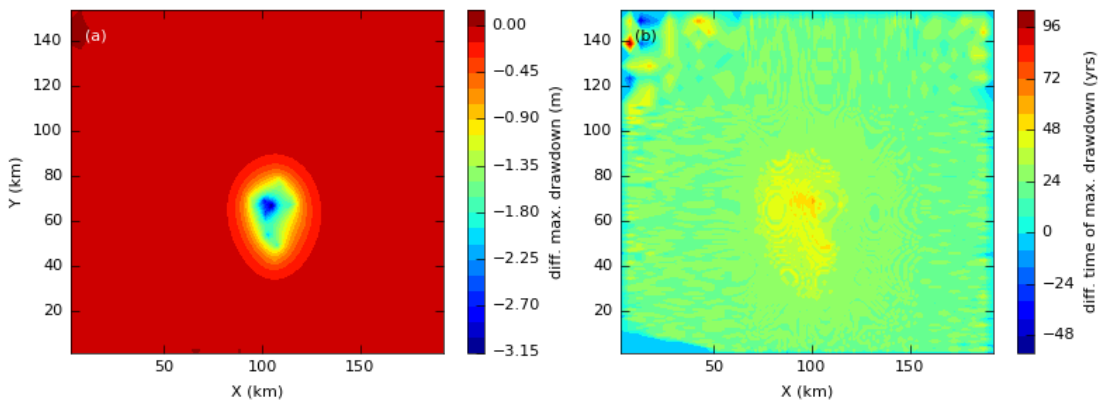


**Figure 4-21 Difference in maximum groundwater level drawdown between 0% and 5% bore failure rate and (b) the associated difference in timing of maximum drawdown relative to the initial steady-state groundwater level between 0% and 5% bore failure rate.**

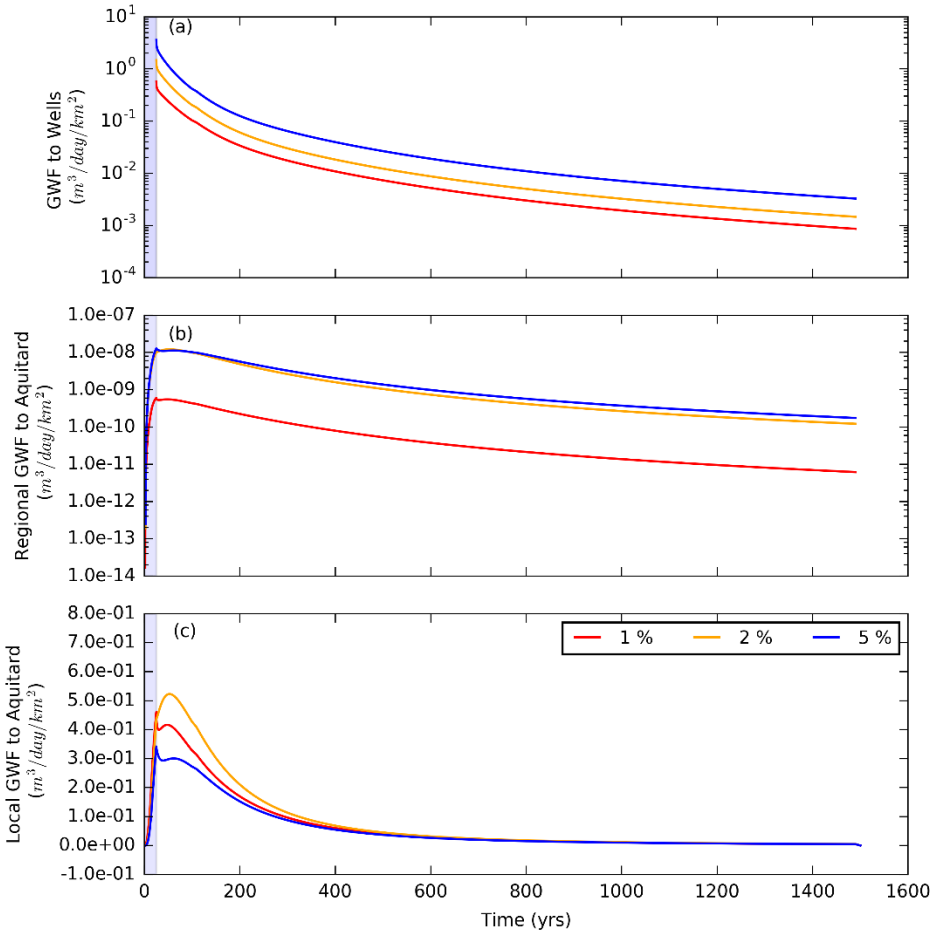


**Figure 4-22 Impact of different bore failure rates on (a) the total groundwater flow density (GWF) in layer 1 to the bores ($m^3$/day/$km^2$), and (b) total regional leakage density ($m^3$/day/$km^2$), and (c) total leakage density beneath the coal seam gas well field ($m^3$/day/$km^2$), from layer 2 into the underlying coal target formation (layer 3). All simulations generate identical regional leakage response and therefore plot on top of each other. The blue bar indicates the coal seam gas (and water) production period (25 years).**

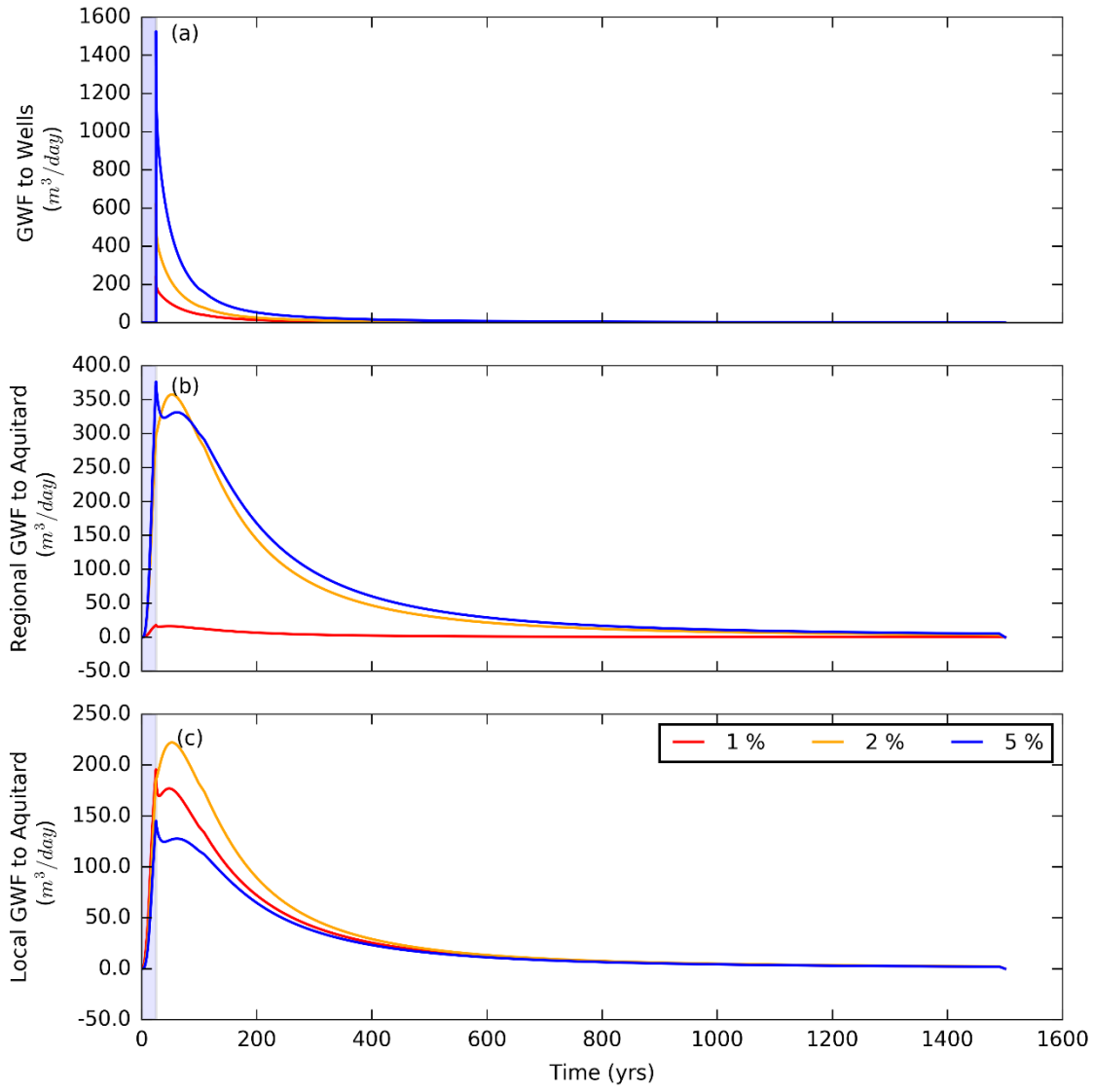


**Figure 4-23 Impact of different bore failure rates on (a) the total groundwater flow (GWF) in layer 1 to the bores, (b) total regional leakage, and (c) total leakage beneath the coal seam gas well field, from layer 2 into the underlying coal target formation (layer 3). All simulations generate identical regional leakage response and therefore plot on top of each other. The blue bar indicates the coal seam gas (and water) production period (25 years).**

## 4.7 Discussion

Inter-aquifer leakage does not appear to be materially enhanced by the presence of "leaky wells" in a coal seam gas well field. This is confirmed by negligible additional head decreases in the top aquifer and by a robust aquitard effective flux that is relatively insensitive to various failure rates. This agrees with the findings of Doble et al. (2018) for the leaky well case (i.e. partially leaky well), which showed that the inter-aquifer leakage was primarily controlled by the effective well conductivity (i.e., the flow rate within a connected well). In all scenarios tested here the effective well conductivity was relatively low (approx. 0.813 m/d). The impact of a higher effective well

conductivity will likely have a more significant effect on the regional groundwater flow system, with the magnitude of the effect depending on the well failure rate. Based on the effective well conductivity in this study, the minimum time required to reach a new equilibrium is approximately 1,350 years. Note this equilibrium is defined on the basis of the inter-aquifer flux reaching a nearly constant value. The likelihood of requiring a longer period to reach a new quasi-equilibrium increases as the proportion of well failures decreases. Should the effective well conductivity be lower than that used in this study, the time to a new quasi-equilibrium will likely increase (and vice versa for higher effective well conductivities).

The effective aquitard flux of the top aquitard is only enhanced for a period of 200 years post-production, following this the effective flux stabilises at approximately the unperturbed aquitard vertical hydraulic conductivity. However, the presence of leaky wells remains, thus the aquitard parameters remain perturbed. In this scenario the flow equilibrates after approximately 800 years, and the aquitard flux reaches steady-state. However, as long as there is a gradient inter-aquifer leakage will occur, as will transport of chemicals and potential contaminants between aquifers. As soon as the gradient increases again due to pumping (for whatever purpose), $Q_{eff}$ will go up again.

It should be noted that the pumping rates used in this model were determined using a reservoir model, and are based on the necessary aquifer depressurisation to enable gas desorption and extraction. When applied to a single phase groundwater flow model, such as MODFLOW-USG, the flow and pressure relationships are not representative of a dual phase system. Because fluxes in a single phase groundwater model are driven by pressure, this will effectively be a misrepresentation of a dual phase system, and can lead to potential errors.

The influence of open bores (e.g. coal exploration bores) on inter-aquifer leakage is considerable by comparison to the leaky well scenarios. Open bores clearly form preferential flow paths, which when located in proximity to an active well field will have a significant impact on the groundwater response. In particular, open wells enhance the drawdown in the top aquifer by enabling water to replenish those layers depressurised by pumping. In hydrogeological systems where a vertical gradient exists between geologic layers, such open wells will have a similar impact (leakage between layers) in the absence of pumping induced drawdown.

# 5 Local-scale solute transport modelling

The aim of the solute transport modelling is to assess the consequences of well and bore hole enhanced inter-aquifer connectivity, by assessing the number of required connective pathways to create a range of noticeable impacts. Impacts will be assessed by changes in solute concentration within aquifers (e.g., salinity).

Changes in aquifer chemistry (e.g. salinity) will be assessed using analytical solutions at the local scale (individual bore hole); alternatively numerical solutions[1] may be used to account for a complex geology at the regional scale and/or to account for density effects cause by saline groundwater. This section describes the use of an analytical solution to determine the changes in aquifer salinity from a single leaky bore at a local scale.

## 5.1 Modelled scenarios

Twelve scenarios were selected for impact modelling to identify under which scenarios, if any, aquifer contamination could occur; the scenarios include worst-case conditions identified in the Narrabri region (Table 5-1).

The first principal condition important for solute transport modelling is whether the groundwater flow across an aquitard is upward (Figure 5-1), i.e. from the gas production zone to the overlying water bearing aquifer, or downward, i.e. from the water bearing aquifer to the underlying gas production zone and (Figure 5-2). Of critical concern is that saline groundwater, or groundwater containing drilling or hydraulic fracturing fluid from the production zone, could migrate through leaky wells or bores into the aquifers that are relied upon for irrigation, stock and domestic water supplies. A secondary possibility, in case of downward groundwater flow during the depressurisation phase, is that fresher water from the water bearing aquifer flows into the coal target formation and changes the chemical composition of groundwater in the production zone. This may lead to accelerated oxidisation and corrosion of any remaining coal seam gas well infrastructure.

The first scenario assumes the maximum upward flow from the Maules Creek coal seam gas production zone to the Pilliga Sandstone water bearing aquifer reported in the Narrabri MODFLOW model (Doble et al. 2018). Doble et al. (2018) reported an upward flux of 11.6 $m^3d^{-1}$ under pre-production conditions through an open exploration or repurposed well. In fact this scenario is unrelated to coal seam gas extraction and only serves as another example of a leakage pathway. The second scenario assumed the maximum reported downward flow from the Pilliga Sandstone Aquifer to the Maules Creek units. This occurred immediately after production ceased, through an open exploration bore or repurposed well, with a flux of 51.4 $m^3d^{-1}$ (Doble et al. 2018). This flux was around five times higher than the upward flux scenario. They both represent worst case scenarios of leaky well or bore enhanced inter-aquifer leakage.

The second condition that influenced solute transport is the background horizontal flow velocity in the aquifer, which influences the proportion of solute that is detected downgradient of a leaky well. To evaluate this condition three situations are considered. Firstly, the median horizontal velocities

[1] A potentially useful simulator is SEAWAT (Langevin et al. 2007), which has (conservative) salt transport capabilities and is a MODFLOW plugin.

within the Pilliga Sandstone aquifer and Maules Creek Formation (gas production zone) are used based on the CDM Smith (2014) model. Secondly, the maximum horizontal flow velocity from the same model are used. Finally, we recognise that the flow of water through a leaky well or bore may significantly increase the local flow velocities within the aquifer. As a worst-case example, the inflow velocity from the open bore into the aquifer is calculated to be the highest possible horizontal velocity within the aquifer.

**Table 5-1 Scenarios for impact modelling.**

| Scenario descriptions | Pilliga Sandstone (upward flow) Median TDS | Pilliga Sandstone (upward flow) Max/Min TDS | Maules Creek formation (downward flow) Median TDS | Maules Creek formation (downward flow) Max/Min TDS |
|---|---|---|---|---|
| Median aquifer velocity | Scenario 1a | Scenario 1b | Scenario 2a | Scenario 2b |
| Maximum aquifer velocity | Scenario 1c | Scenario 1d | Scenario 2c | Scenario 2d |
| Inflow velocity through open bore | Scenario 1e | Scenario 1f | Scenario 2e | Scenario 2f |

The final condition that influences solute transport is the difference in salinity (total dissolved solids) between the water bearing aquifer and the production zone; the greater the initial difference in concentration between aquifer and production zone water quality, the greater is the impact on water quality. Two examples have been selected, based on the measured concentrations of total dissolved solids (TDS) described by CDM Smith (2014). The first condition uses median TDS values in both aquifer and production zone to represent average water quality conditions. The second condition considers the minimum observed TDS concentration in the water bearing aquifer (freshest condition) and the maximum TDS in the production zone (most saline). This condition represents the worst case that may lead to the largest impact on water quality.

## 5.2 Description of analytical solutions

An initial approximation to modelling the impact of solute migration from aquifer to production zone and vice versa (typically a pre-CSG development condition) through a leaky well is by using analytical solutions of the advection-dispersion equation. The conceptual model assumes that the well has full contact with the water bearing aquifer or production zone as the solute exits the leaky bore. This ensures that the solute is distributed evenly across the thickness of the water bearing aquifer or the production zone (Figure 5-1 and Figure 5-2).

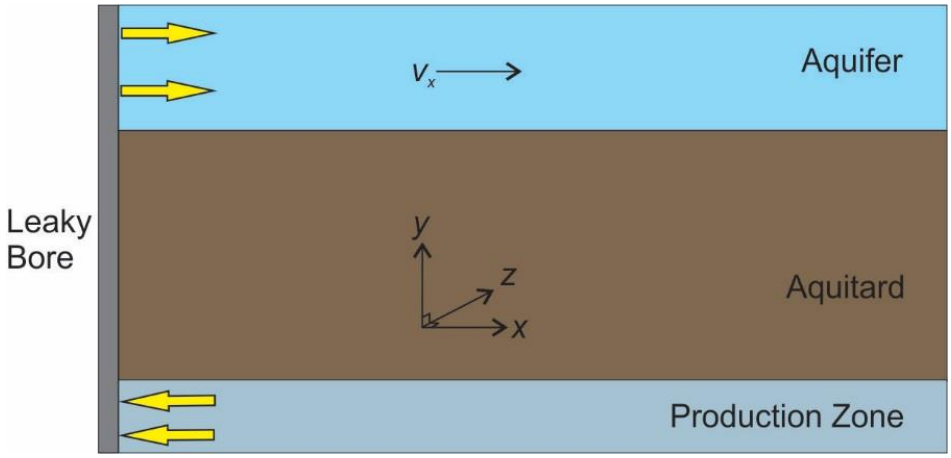


**Figure 5-1 Contaminant leaking upward from the gas production zone to the aquifer (e.g., pre-production condition).**

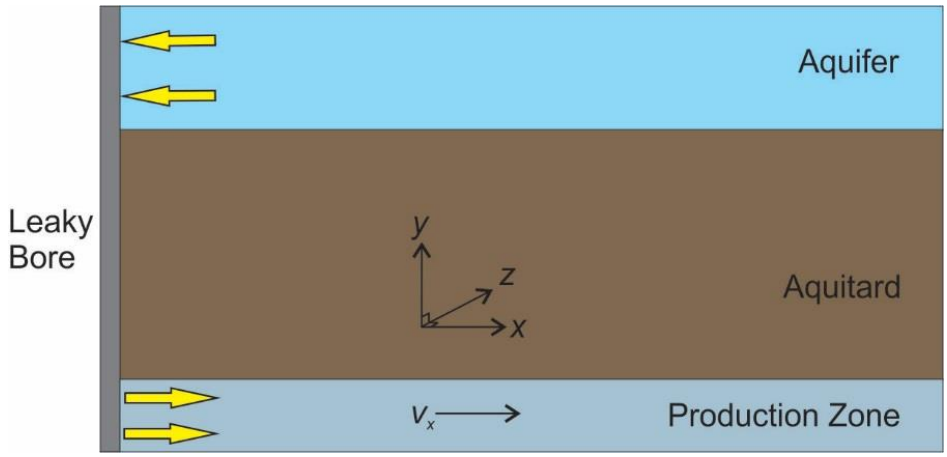


**Figure 5-2 Contaminant leaking from the aquifer to the production zone (e.g., CSG production or post-CSG production condition).**

The 3D advection-dispersion equation without solute production or decay can be written as (Šimůnek et al.(2008); van Genuchten et al. 2012):

$$R\frac{\partial C}{\partial t} = -v\frac{\partial C}{\partial x} + D_x\frac{\partial^2 C}{\partial x^2} + D_y\frac{\partial^2 C}{\partial y^2} + D_z\frac{\partial^2 C}{\partial z^2} \qquad (2)$$

$$for:\ t > 0, \qquad 0 \le x < \infty, \qquad -\infty < y < \infty, \qquad -\infty < z < \infty$$

where $C$ is the solute concentration, $R$ is the retardation factor, $t$ is time, $v$ is the pore-water velocity, and $D_x$, $D_y$ and $D_z$ are the hydrodynamic dispersion coefficients in the x, y and z directions respectively.

## 5.3 Implementation and parameterisation of analytical solutions

The advection-dispersion equation (Equation 2) was solved to find the solute concentration at any time and point in the modelled 3D domain using the STANMOD 3DADE (3D advection-dispersion equation) package (Lei and Bradford (1994); Šimůnek et al. (2008), van Genuchten et al. ((2012).

The solute source was conceptualised as a rectangular source at the well or bore, as indicated in Figure 5-3, but with the x-axis representing flow in the horizontal direction, the y-axis representing vertical flow and the z-axis representing lateral flow. The solute source had dimensions of 0.5 m along the z-axis (*b*), representing the diameter of the leaky well or bore, and either 114 m or 21 m along the y-axis (*a*), representing the full thickness of the water bearing aquifer or the production zone of this study area, respectively (Table 5-2).

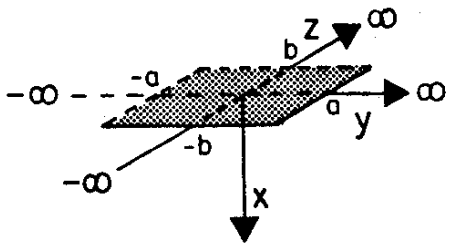


**Figure 5-3 Conceptualisation of solute source. For the leaky well problem this figure should be rotated 90° about the z-axis so that the y-axis is vertical and the x-axis is horizontal (Leij and Bradford 1994).**

The advection-dispersion equation was evaluated within a volume representing the thickness of the water bearing aquifer or production zone (114 m or 21 m) in the *y* dimension ($y_{max}$), 1,000 m in the *x* dimension away from the leaky well ($x_{max}$), and 1,000 m in the *z* dimension ($z_{max}$): 500 m either side of the leaky well. The equation was evaluated for 10 years ($t_{max}$ of 3,650 days) at intervals of 36.5 days (Table 5-2). Observation wells were established 10 m, 50 m, 100 m, 500 m and 1,000 m from the leaky well.

**Table 5-2 Parameters used in the 3D advection-dispersion equation**

| Parameter (units) | Downward flow scenario | Upward flow scenario |
|---|---|---|
| $v$ ($md^{-1}$) | Various scenarios | Various scenarios |
| $C$ ($mgL^{-1}$) | 1 | 1 |
| $C_b$ ($mgL^{-1}$) | 0 | 0 |
| Pulse length (d) | 3,650 | 3,650 |
| $R$ (-) | 1 | 1 |
| $D_x$ ($m^2d^{-1}$) | 1 | 1 |
| $D_y$ ($m^2d^{-1}$) | 1 | 1 |
| $D_z$ ($m^2d^{-1}$) | 1 | 1 |
| $a$ (m) | 21 | 114 |

| Parameter (units) | Downward flow scenario | Upward flow scenario |
|---|---|---|
| $b$ (m) | 0.5 | 0.5 |
| $t_{max}$ | 3,650 | 3,650 |
| $x_{max}$ | 1,000 | 1,000 |
| $y_{max}$ | 21 | 114 |
| $z_{max}$ | 1,000 | 1,000 |

The background concentration, $C_b$, for the analysis of relative change in TDS was 0 $mgL^{-1}$, and the concentration of the water leaking through the open well was 1 $mgL^{-1}$. This provided a unit response function for the contamination break through curves that could be scaled according to the relative difference in TDS concentration. The pulse length or duration of leaking was the full ten years or 3650 days of analysis. The retardation factor *R* was 1, which corresponds to a non-reactive chemical. The dispersion coefficients in the x, y and z directions are 1 $m^2d^{-1}$.

Example solute concentrations were obtained from the CDM Smith (2014) summary of field measured TDS in the Narrabri aquifer systems (Table 5-3). Maximum, minimum and median TDS concentrations were used for two scenarios: (i) the median difference in TDS concentration between the Pilliga Sandstone and Maules Creek formation, and maximum difference in TDS concentration, given by the maximum concentration in the Maules Creek formation and the minimum concentration in the Pilliga Sandstone.

The background groundwater velocity varied for each of the scenarios and was calculated using cell-to-cell flow information extracted from the CDM Smith (2014) groundwater model. The groundwater velocity in the Pilliga Sandstone aquifer was predicted to be more variable than that in the Maules Creek formation, with a median velocity two orders of magnitude lower than the Maules Creek formation, but a maximum velocity two orders of magnitude higher. This is thought to be because horizontal flow within the Pilliga is affected by spatially variable localised recharge and topography, whereas variability of groundwater flow into and out of the Maules Creek formation is damped by the lag time between infiltration and water reaching the formation.

Wherever groundwater flows out of leaky well or bore in the receiving aquifer, the groundwater velocity around such a leaky well will likely be higher than the background velocity of the receiving aquifer. The velocity will decrease further out from the well as the cross sectional area perpendicular to flow increases. As a worst-case scenario, the velocity of water flowing out of a leaky well, immediately adjacent the well, was calculated for the two examples outlined in Doble et al. (2018), i.e. flow through a leaky well and flow through an open, uncased borehole. The flow velocity was calculated by dividing the flow rate through the well by the cross sectional area of the well surface area adjoining the hydrogeological unit (Table 5-3).

$$v = Q/2\pi ry \quad (3)$$

where *v* is the groundwater velocity attributed to flow out of well or borehole, *Q* is the volumetric flow rate of water through the leaky or open well, *r* is the radius of the well and *y* is the thickness of the aquifer receiving the water.

When Equation 3 was used to calculate the groundwater velocity *v* from the leaky well, it was found to be less than or equal to the median background groundwater velocity. Therefore, for the leaky

well the background velocity was used to calculate solute migration. The solute transport Equation 2 was evaluated for three velocity conditions: (i) the median background velocity in the aquifer, (ii) the maximum background velocity in the aquifer and (iii) the localised inflow velocity from an open borehole.

**Table 5-3 Water quality and hydrogeological parameters from the CDM Smith (2014) model and expected well leakage flow rates and flow velocities from (Doble et al., 2018).**

| Parameter (units) | Pilliga Sandstone aquifer | Maules Creek formation |
|---|---|---|
| Median TDS ($mgL^{-1}$) | 600 | 11,000 |
| Max TDS ($mgL^{-1}$) | 5,000 | 17,000 |
| Min TDS ($mgL^{-1}$) | 500 | 5,200 |
| Median velocity ($md^{-1}$) | 2.93E-06 | 1.83E-04 |
| Max velocity ($md^{-1}$) | 2.92E-02 | 5.70E-04 |
| Inflow flow leaky well ($m^3d^{-1}$) | 4.20E-03 | 1.70E-02 |
| Inflow open borehole ($m^3d^{-1}$) | 11.6 | 51.4 |
| Leaky well surface area ($m^2$) | 179 | 33 |
| Inflow velocity leaky well ($md^{-1}$) | 2.35E-05 | 5.15E-04 |
| Inflow velocity open borehole ($md^{-1}$) | 0.06 | 1.56 |

## 5.4 Simulated concentrations linked to leaky pathways

Concentrations have been simulated for a leaky well at median and maximum groundwater velocity and for an open borehole (for velocity values see Table 5-3). For both the leaky well and the open borehole, upward and downward flow was considered (Figure 5-4). The condition of a leaky well is discussed first. A relative change in TDS concentration for upward and downward flow through a leaky well was observed only at distances of up to 10 m downgradient of a leaky well for all conditions, with concentrations slightly less than 4% of the inflow concentration. The upward flow scenario results in slightly larger concentrations than the downward flow scenario.

For the open borehole under conditions of upward flow results are similar to those for the leaky well. For downward flow through a fully open borehole, with a head difference representing the hydrogeological conditions immediately after gas production ceased (Figure 5-4), the concentrations

are much larger. In this extreme case, the relative change in TDS at 10 m is nearly 12% of the inflow concentration. The higher velocity results in a larger solute mass flux bringer more solutes into the aquifer per unit of time. At distances of 500 m and further from the well the concentration has decreased to less than 1% of the inflow concentration. Further research is needed to determine what this means in terms of concentrations for individual contaminants of concern.

When the absolute TDS concentrations are considered (Figure 5-5), the combination of a median background groundwater velocity and median difference in TDS concentrations (scenario 1a) will lead to an increase in TDS concentration in the Pilliga Sandstone of 330 $mgL^{-1}$, i.e. from 600 $mgL^{-1}$ baseline to 930 $mgL^{-1}$ at a distance of 10 metres from the leaky well (Figure 5-5). At distances of 50 m from the well the increase is only 54 $mgL^{-1}$, and at 100 m it is 16 $mgL^{-1}$. At the next distance where concentrations were modelled (i.e. 500 m) the changes in TDS are no longer detectable.

For maximum background groundwater velocity and maximum difference in TDS concentration (scenario 1d), the increase in TDS in the Pilliga Sandstone was 590 $mgL^{-1}$, from a baseline of 500 $mgL^{-1}$ to 1090 $mgL^{-1}$. The increase in TDS concentration declines rapidly with distance from the well, and the impact is limited to within 100 m of the leaky well (Figure 5-5).

The most extreme combination of conditions – a velocity equal to that of water exiting an open bore, and a maximum difference in TDS conditions still only relates to an increase in TDS concentration of 650 $mgL^{-1}$ (from 500 $mgL^{-1}$ to 1150 $mgL^{-1}$) (Figure 5-5). While this may have an impact on salt sensitive water uses where water extraction bores were within 100 m downgradient of a leaky bore, it is unlikely that it will cause an impact at a regional scale.

When downward solute transport is considered, dilution within the Maules Creek formation occurs owing to inflow of less saline groundwater from the overlying Pilliga Sandstone aquifer. The maximum dilution of the Maules Creek formation groundwater TDS concentration was 2,000 $mgL^{-1}$ (from 17,000 $mgL^{-1}$ to 15,000 $mgL^{-1}$) at a distance of 10 m from an open well. This will not impact water users accessing the upper aquifers, but there is a possibility that the change in chemistry (if it contains corrosive elements) may accelerate degradation (corrosion or clogging) of any valuable coal seam gas infrastructure at that depth. At distances of more than 500 m downgradient from a leaky well, the dilution decreases to 152 $mgL^{-1}$ less than the original 17,000 $mgL^{-1}$. As CGS wells are generally spaced more than 500 m apart, it is unlikely that the dilution effect from one failed coal seam gas well will impact one of its neighbouring wells. There is a possibility that decommissioned coal seam gas wells may be impacted by nearby exploration bores that have not been appropriately decommissioned.

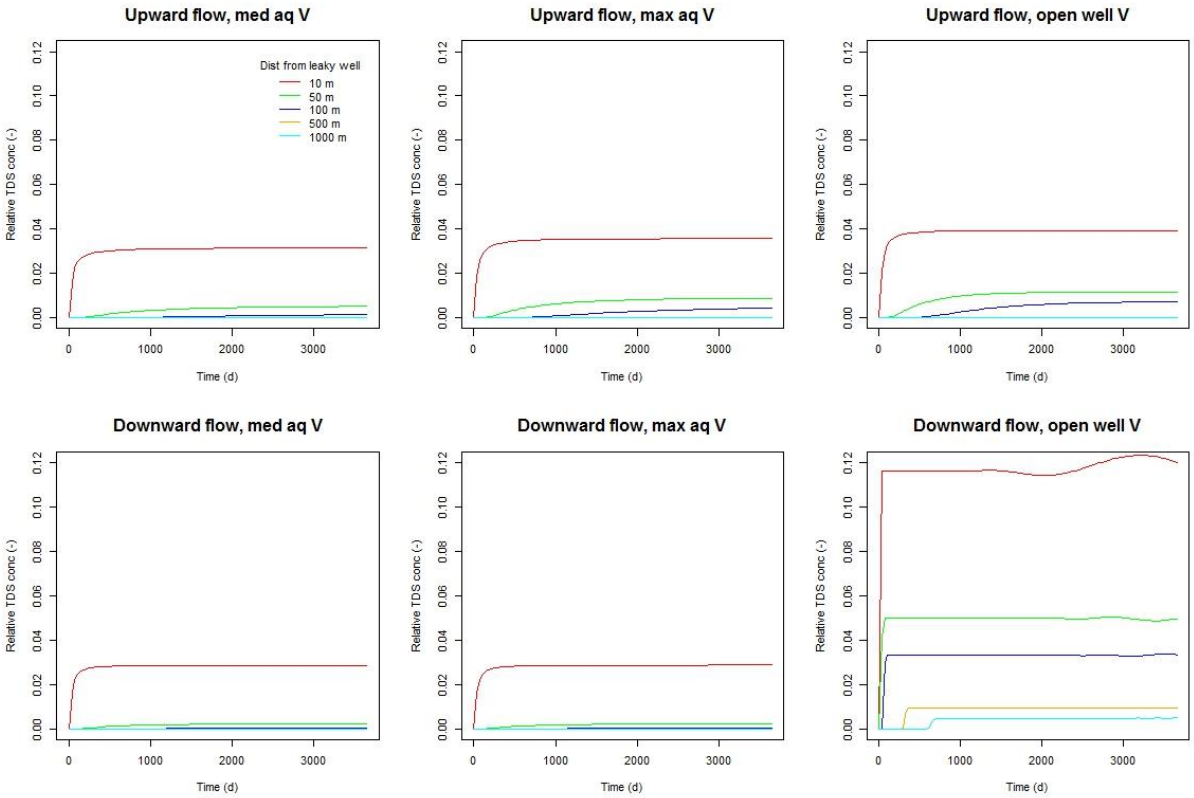


**Figure 5-4 Relative change in TDS concentration with time at 10 m, 50 m, 100 m, 500 m and 1,000 m observation points, for upward (top row) and downward (bottom row) flow scenarios through a leaky well using median (first column) and maximum (second column) aquifer velocity and the flow velocity through an open bore (third column). Hypothetical unit input concentration used. Concentration calculated as $(C_x\text{-}C_b)/C_b$, where $C_x$ is the solute concentration estimated at a point at distance $x$ metres downgradient from the well, and $C_b$ is the background solute concentration of the aquifer in a location unaffected by the leaky well. Top row represents typical baseline pre-CSG conditions where the shallow aquifer becomes more saline. Bottom row represents typical post-CSG conditions where the CSG production zone becomes diluted.**

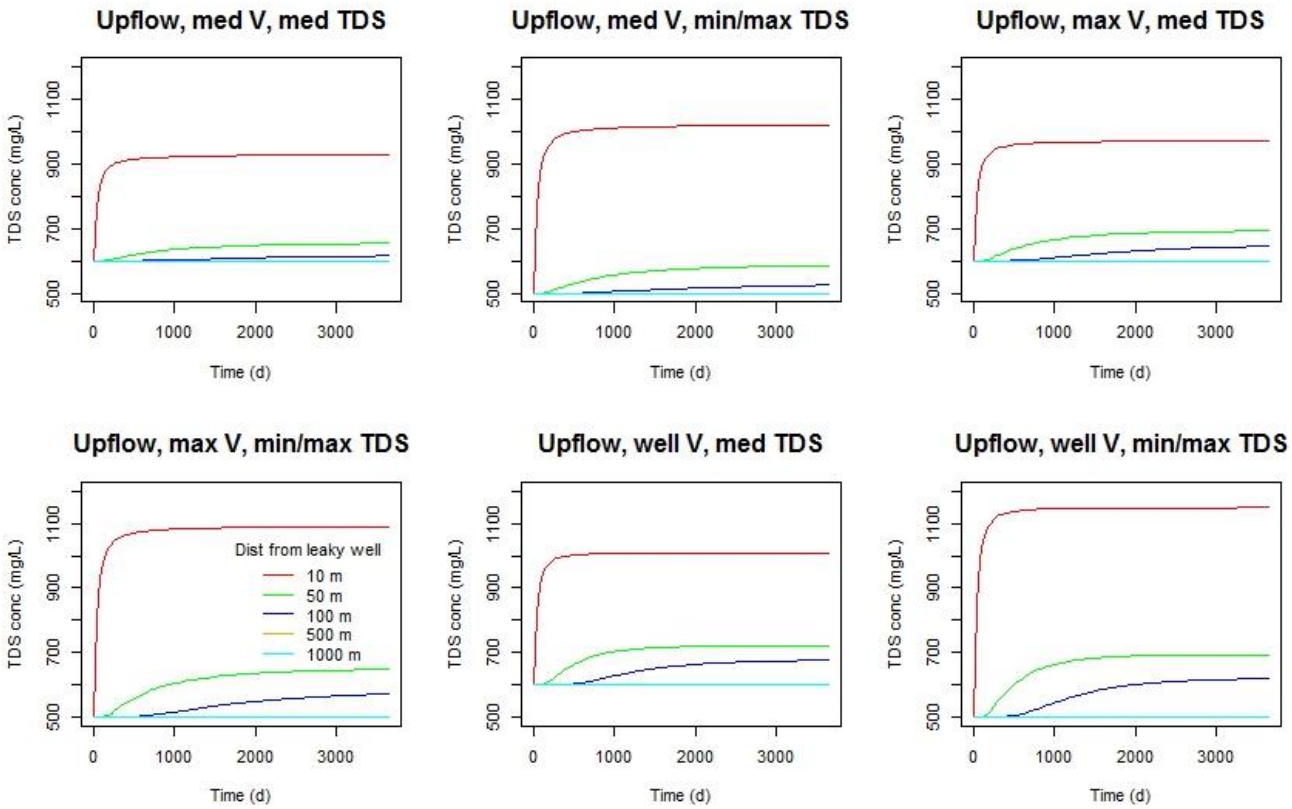


**Figure 5-5 Increases in TDS concentration in the Pilliga Sandstone aquifer with time at the five observation points due to higher TDS water from the Maules Creek formation leaking through a compromised well. Examples shown represent aquifer velocities calculated from median modelled velocity, maximum modelled velocity and maximum velocity of water leaking from an open borehole, and for aquifer TDS differences selected from the median TDS observed in each of the units, and the maximum and minimum TDS differences in each of the units. Both top and bottom rows represent typical baseline pre-CSG conditions where the shallow aquifer becomes more saline.**

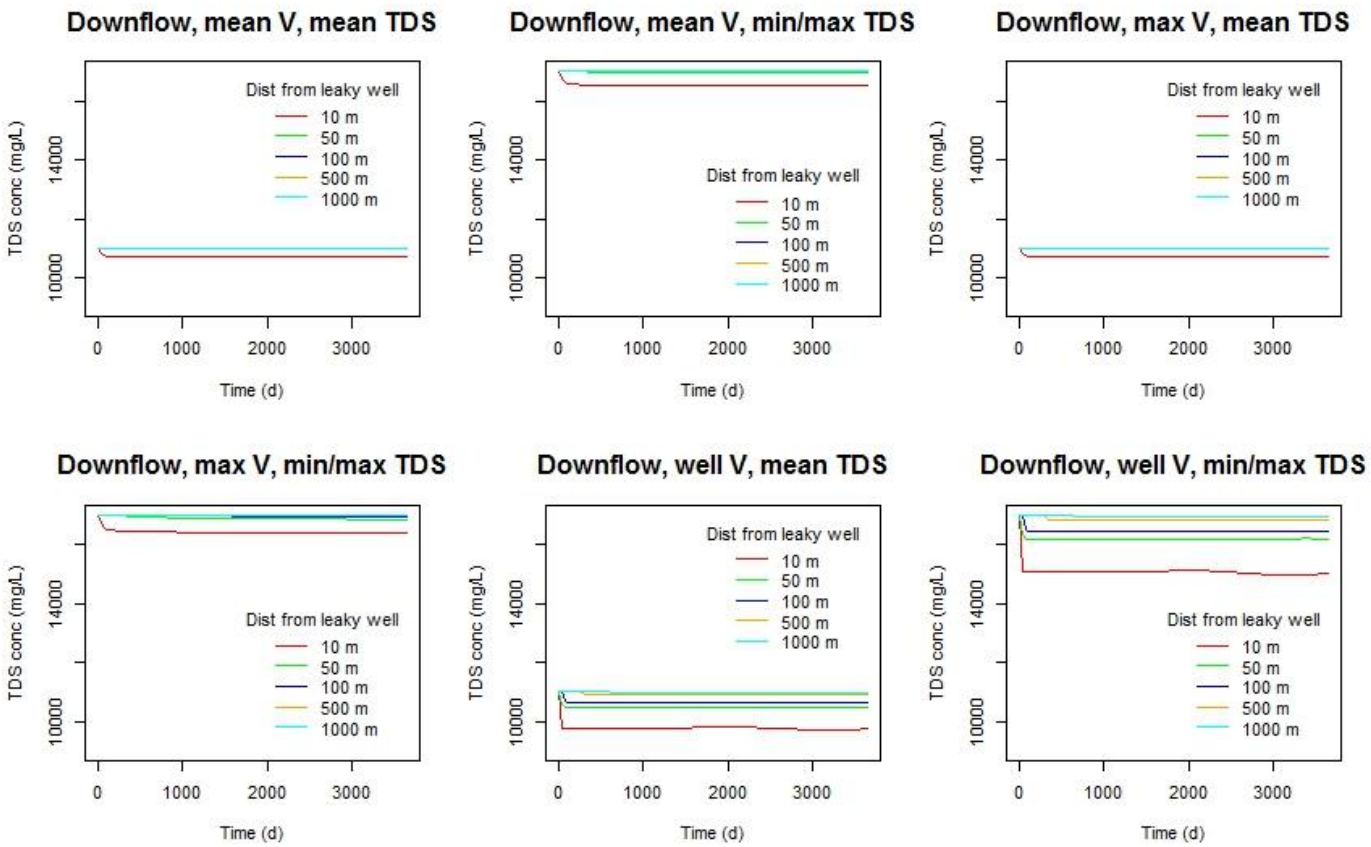


**Figure 5-6 Dilution of TDS concentration in the Maules Creek production zone (lower aquifer) with time at the five observation points due to lower TDS water from the Pilliga Sandstone leaking through a compromised well. Examples shown represent aquifer velocities calculated from median modelled velocity, maximum modelled velocity and maximum velocity of water leaking from an open well, and for aquifer TDS differences selected from the median TDS observed in each of the units, and the maximum and minimum TDS differences in each of the units. Maules Creek minimum, median, and maximum TDS is 5,200, 11,000 and 17,000 mg/L. Pilliga Sandstone minimum, median, and maximum TDS is 500, 600 and 5,000 mg/L. Both top and bottom rows represent typical post-CSG conditions where the CSG production zone becomes diluted.**

## 5.5 Discussion

The solute transport model used in this analysis assumes that the two sources of water, i.e. the background groundwater and the inflowing water from the leaky well or open borehole, are fully mixed. They do not account for density dependent flow. If the TDS concentrations of the water in the upper aquifer and lower production zone are significantly different, then water leaking upward from the production unit will preferentially settle at the base of the water bearing aquifer, leading to higher than predicted concentrations (assuming that the TDS is higher in the coal than in the upper aquifer). Such a situation would exist during the pre-CSG development phase. However, the plume will therefore spread over a smaller downstream distance from the leaky well or bore. Similarly, water leaking downward from the water bearing aquifer will preferentially be distributed to the top of the production zone, leading to higher than predicted dilution. This represents a condition typical of post-CSG development.

The highest potential for contamination of the water bearing aquifer will be associated with extraction wells that are within 100 m of, and downgradient from the leaky well. For high differences in TDS concentrations between the aquifers, potential contamination will also be highest for water bores that are screened close to the bottom of the aquifer.

# 6 Proposed approaches to well integrity monitoring

Wells, like any constructed asset, will deteriorate with age, with operational and site specific conditions influencing the rate of deterioration. This can lead to the well no longer being suitable for the intended use, and/or may result in contamination of groundwater. Well monitoring and maintenance is required to preserve the well and its component parts in good repair for the life of the well (DTI 2012; DNRM 2013). Potential well failure mechanisms for petroleum wells and coal seam gas wells in their entire life span were discussed in Wu et al. (2018), some of which could lead to enhanced inter-aquifer leakage. While additional failure pathways were discussed in Section 2, the focus here is on coal seam gas wells throughout different stages of a gas project. The subsequent sections discuss possible strategies, tools and technologies, and an outline of a proposed experimental program for monitoring inter-aquifer leakage in a coal seam gas field. The specific goal is to develop a monitoring approach that is preventive (or at least identify loss of integrity soon after it occurred) rather than corrective, and that is aimed at maintaining CSG well integrity beyond the well decommissioning phase. Although the focus is on CSG wells, several of the tools and technologies can also be used to investigate failure pathways associated with water bores or exploration bores.

## 6.1 Monitoring strategy

### 6.1.1 Assumptions relevant to loss of well integrity and its monitoring

A comprehensive definition of loss of bore or well integrity was provided in Wu et al. (2018):

*bore or well failure (or loss of integrity) is specifically defined […] as: failure to safely contain and control the flow of all fluids within or connected to a well. It can be caused by any of various forms of 'well breach' (including failure of cement sheaths/plugs/bonds, casing, and downhole and surface sealing components) and may result in hydrological breach (fluid movement between geological formations – including formations not targeted for exploitation) and environmental breach (contamination of or water balance impact to water resources).*

It is important to clarify that the loss of integrity does not require environmental change to be detected, reported, and legal liability proven in court, although it does require all the barriers (e.g. production tubing, casing, cement) to fail and the establishment of a pathway that enables leakage into the surrounding environment.

Well/bore, hydrological and environmental breaches are closely linked to each other where well/bore breach may cause hydrological breach and possibly even environmental breach. If the hydrologic breach results in significant changes in an aquifer's baseline hydrochemistry and/or changes to an aquifer's water balance, an environmental breach has occurred. Therefore, hydrological and environmental breaches would not occur if the mechanisms responsible for well breach are eliminated or properly managed. Well and hydrological breaches and their potential environmental impact across the entire life span of a well (design and/or construction, production and abandonment phase) are reported by Wu et al. (2018). Without proper management and given enough time, all the barriers put in place to ensure well integrity will degrade, including cement plugs (see Section 1.4). The more aggressive the pore-waters ($CO_2$, $H_2S$, salinity, etc.) that come in

contact with well casing material, including steel and cement, the faster the degradation (Bazzari 1989, Kreis 1991, Lyons and Plisga 2004, Elsener 2005).

As discussed in detail by Wu et al. (2018), overseas experience with conventional oil and gas wells and coal seam gas wells shows that gas production wells do lose integrity across all of the three main phases of a well. In Section 6.2 an overview is given of various monitoring techniques that can be applied to detect loss of barrier (one or more) or well (all barriers) integrity as long as access to the borehole can be secured. Monitoring of well integrity will be focussed around hydraulic fracturing (prior to), during remedial/maintenance works (e.g. pump repairs, well deepening, plugging back, pulling and resetting liners, squeeze cementing and re-perforating) and before decommissioning. Because access to the wellbore is facilitated after such operations, the down-hole monitoring devices discussed in Section 6.2 are relevant.

During active gas production, however, access to the boreholes will be very limited and therefore detection of well failure requires other techniques such as gas monitoring at the well head (surface-casing-vent flow), casing head pressure testing, and measurement of fugitive gas emissions from well casings (see further).

The most challenging phase for monitoring well integrity evolution is after decommissioning, when down-hole access is no longer possible. Direct measurement of fugitive emission of methane remains an option, e.g. through use of the gas flux chamber installed next to a decommissioned well (see Section 6.2.5).

### 6.1.2 Scope for monitoring

Some general principles for well integrity monitoring are discussed as a basis for developing a monitoring approach that is preventive rather (or at least identify loss of integrity soon after it occurred) than corrective, and that is aimed at maintaining well integrity beyond the well decommissioning phase. This requires, as a minimum, that well integrity monitoring is applied across the entire lifecycle of a well.

The following principles are considered key to an effective monitoring strategy:

- Establishment of an agreed conceptual understanding of failure mechanisms and their evolution throughout and beyond the lifecycle of a well; a reasonable escalating conceptual model would include progressive failure from an initial pressure build-up in an inner annulus, to containment breach, followed by leakage of gas and fluids,
- Establish baseline conditions regarding groundwater hydrochemistry against which potential leaks can be compared,
- Routine surveillance monitoring or bore integrity would seem a reasonable precautionary measure,
- Design a monitoring approach that facilitates early detection and remediation of leaks,
- Consider a combination of down-hole and other monitoring techniques for use prior to decommissioning (design and/or construction, active production and work-over and decommissioning phase), and after decommissioning,
- To optimise efficiencies and limited regulatory and financial resource, a tiered approach of escalating intensity and increasing specificity would seem to be a reasonable approach (see for example the tiered Decision Support System for analysis of increased gas in water bores developed by Mallants et al. 2016).

### 6.1.3 Preferred monitoring approach

The preferred monitoring approach is applicable to the following four phases: well construction and completion, well production and work-over, decommissioning, and after decommissioning. A non-exhaustive list of monitoring equipment for each phase is provided in Table 6-1; details of the tools are provided in Section 6.2. The following phases are considered:

- Well construction and completion: tools that measure mechanical integrity to provide a baseline assessment of integrity,
- Well production and work-over:
    - tools that measure inter-annulus pressure build-up and/or surface casing vent flow to provide episodic assessments of integrity;
    - tools that measure mechanical integrity after work-over operations (e.g. pump repairs, well deepening, plugging back, pulling and resetting liners, squeeze cementing and re-perforating);
    - tools that measure gas leaks around well head infrastructure. Although the impact calculations in Section 4 and 5 did not consider multi-phase flow and gas transport, monitoring gas leaks is probably one of the easiest ways to detect the presence of a leakage pathway. Gas leaks may be early warnings of a hydrological breach (fluid movement between geological formations), which may potentially lead to an environmental breach (i.e., contamination of or water balance impact to water resources);
    - tools that measure changes in groundwater hydrochemistry, contaminant concentrations or environmental isotopes. These 'tracers' may be indicators of leakage pathways through coal seam gas wells, poor-integrity water bores, open coal exploration holes, or natural pathways.
- Well decommissioning: tools that measure inter-annulus pressure build-up and mechanical integrity to inform well decommissioning design and operation,
- After well decommissioning: tools that measure gas leaks around remains of well head infrastructure; tools that measure changes in groundwater hydrochemistry, environmental tracers and/or contaminants.

**Table 6-1 Possible monitoring tools for different phases of a well lifecycle.**

| Monitoring tool | Construction-completion-production-decommissioning | Post decommissioning | Requirements |
|---|---|---|---|
| *Down-hole* | | | |
| Wire-line and ultrasonic logging | Highly suitable | Not suitable | Headworks are off |
| Testing and sampling | Highly suitable | Not suitable | Headworks are off |
| *Other* | | | |
| Surface-casing-vent flow | Highly suitable | Not suitable | Do not require heads to be taken off |

| Monitoring tool | Construction-completion-production-decommissioning | Post decommissioning | Requirements |
|---|---|---|---|
| Casing head pressure test | Highly suitable | Not suitable | Bradenhead testing valve; Do not require heads to be taken off |
| Fugitive emissions of methane | Highly suitable | Suitable | Gas flux chamber for post-decommissioning phase |
| Hydrochemistry, environmental isotopes, contaminants | Suitable | Suitable | Detectable chemical compound in produced CSG water or monitoring bores |

## 6.2 Tools and technologies for monitoring inter-aquifer leakage

Conventional and coal seam gas wells have typically a series of nested casings and cemented well annulus (Figure 6-1). The cement sheath placed between the casing and wellbore is expected to provide the zonal isolation and prevent inter-aquifer leakage throughout and beyond the life of the well. However, this depends on the proper placement of the cement, the mechanical and physical properties of the cement and the stress, and pressure and temperature conditions in the wellbore. Duguid and Tombari (2007) outlined a number of cased well logging technologies and tests for measuring well integrity in $CO_2$ injection wells. Some of these technologies may also be applicable to monitor inter-aquifer leakage through the well annulus in a coal seam gas production well.

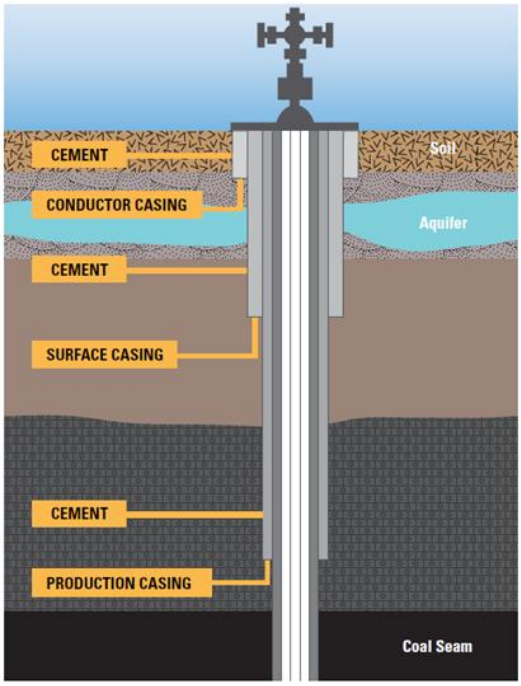


**Figure 6-1 A schematics of typical coal seam gas well (Arrow Energy, 2011).**

### 6.2.1 Wireline sonic and ultrasonic logging tools

#### CBL and VDL tool

The cement bond log (CBL) is based on the principle that a sonic signal transmitted through a casing unsupported by cement will ring strongly and the waveform will attenuate slowly; while that same signal will ring weakly and attenuate quickly when transmitted through a well casing supported by cement (Bellabarba et al. 2008). The measurement is omni-directional, responding to the average of contributions from around the circumference of the casing. The measurement is normally accompanied by a variable density log (VDL). This VDL may also yield an indication of cement bond to the formation. Increased attenuation indicates better quality bonding of the cement to the outer casing wall. In simple cases, the interpreted log response can provide good information about cement quality.

The CBL-VDL logging tool is routinely applied to well cement evaluation. The measurement responds well to solidity, works well in most fluids in the hole, is unaffected by internal casing condition and provides an indication of cement-formation bond. However, the traditional sonic CBL-VDL tool does not provide radial or azimuthal information to differentiate among channels, contaminated cement, micro-annuli and tool eccentricity.

#### Ultrasonic imaging tool (USI)

Figure 6-2 shows the cased hole ultrasonic imaging tool basics. This tool addresses the CBL-VDL tool's weaknesses to evaluate cement quality azimuthally, using a high frequency pulse-echo technique (Morris et al. 2007). A single rotating transducer is used and rotated at high speed and operates at high frequencies. The tool evaluates cement around the entire circumference of the casing, and provides the added benefit of corrosion and wear information on the casing. The tool yields 36 or 72 separate waveforms at each depth. These are processed to yield the casing thickness, internal radius and inner wall smoothness as well as an azimuthal image of the cement acoustic impedance (essentially the quality of the cement sheath).

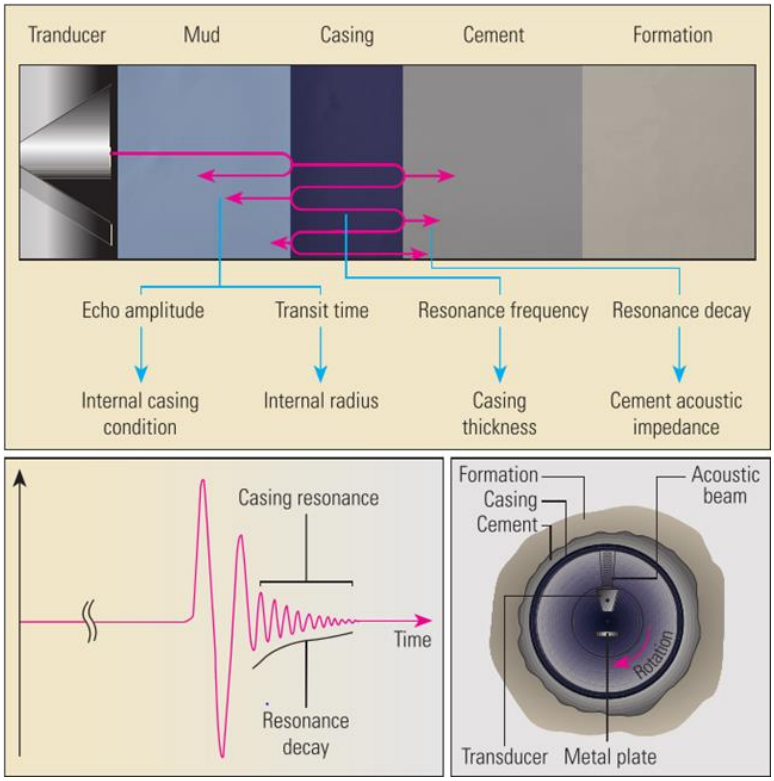


**Figure 6-2 An ultrasonic tool transducer sends a slightly divergent beam—an acoustic wave generated by a transducer when electrical power is applied to it—towards the casing to excite the casing into its thickness resonance mode. The USI UltraSonic Imager tool scans the casing at 7½ revolutions per second to render an azimuthal resolution of 5 or 10 degrees. This yields 36 or 72 separate waveforms at each depth. These are processed to yield the casing thickness, internal radius and inner wall smoothness—from the initial echo—as well as an azimuthal image of the cement acoustic impedance—from the signal resonance decay (top). The acoustic impedance of the cement (essentially the quality of the cement sheath) can be derived from the resonance decay (bottom). A good casing- cement bond results in immediate resonance decay, while free pipe rings bottom (generates echoes) for an extended period (Bellabarba et al. 2008).**

The tool provides four main measurements: a) condition of internal casing surface; b) internal casing radius; c) casing thickness; and d) quality of the cement sheath behind the casing.

While the ultrasonic imaging tool addresses the problem of azimuthal coverage for the CBL-VDL tool, it is susceptible to certain conditions encountered in the well when making the measurement: a) heavy drilling mud or borehole fluid; b) thick casings; and c) difficult to differentiating between a drilling fluid and a lightweight or mud-contaminated cement of similar acoustic impedance.

## Improved ultrasonic imaging tool

The improved ultrasonic imaging tool addresses the main shortcoming of the USI tool - the ability to accurately identify low-density cements and contaminated cements (Bellabarba et al. 2008). Low density cements are used to cement casings in formations with low fracture gradients or loss zones, such as deep water wells and coal seam gas wells (Tan et al. 2012). The acoustic impedance of lightweight and contaminated cements extends into the range of the acoustic impedances common for drilling and completion fluids which may be present in the annulus behind the casing. This tool combines the classic pulse-echo technique that is used in the USI tool with the latest flexural wave imaging technology to accurately evaluate any type of cement in the annulus.

The improved tool maintains the measurement provided by the USI tool, while adding flexural-wave imaging with one transmitter and two receivers aligned obliquely. The transducer transmits a high-frequency pulse beam of about 250 kHz to excite a flexural mode in the casing. As the wave propagates, this mode radiates acoustic energy into the annulus. This energy reflects at interfaces that present an acoustic contrast, such as the cement/formation interface, and propagates back through the casing predominantly as a flexural wave to reradiate energy into the casing fluid. The two receiving transducers are placed to allow optimal acquisition of these signals. Processing of the signals provides information about the nature and acoustic velocity of the material filling the annulus, the position of the casing in the hole and the geometrical shape of the hole, and information on the third interface (cement/formation).

### 6.2.2 Testing and sampling tools

#### Vertical interference test

The vertical interference test (VIT) is a downhole test designed to measure hydraulic communication of the outside-of-casing wellbore barrier system over a selected well section in shale (Gasda et al. 2013). The test involves perforating the well casing and cement in two separate one-foot intervals typically separated by three to thirteen meters. The two perforated intervals should be located in the same aquitard. Once the intervals are isolated with an inflatable packer, a pressure is applied to the upper perforated interval from the surface and held at a constant pressure for a number of hours or days. The pressure is monitored in the upper zone with a modular reservoir probe-single (MRPS) module gauge. Simultaneously, the transient pressure response in the lower isolated zone is measured using a second modular reservoir probe-dual packer assembly (MRPA) gauge (Figure 6-3). The transient data are used to infer the extent of hydraulic communication, i.e. flow, through the barrier system. If good isolation is maintained inside the casing, then any detectable pressure signal indicates fluid flow along the exterior of the casing. The effective wellbore permeability can be estimated through numerical analysis of the VIT data.

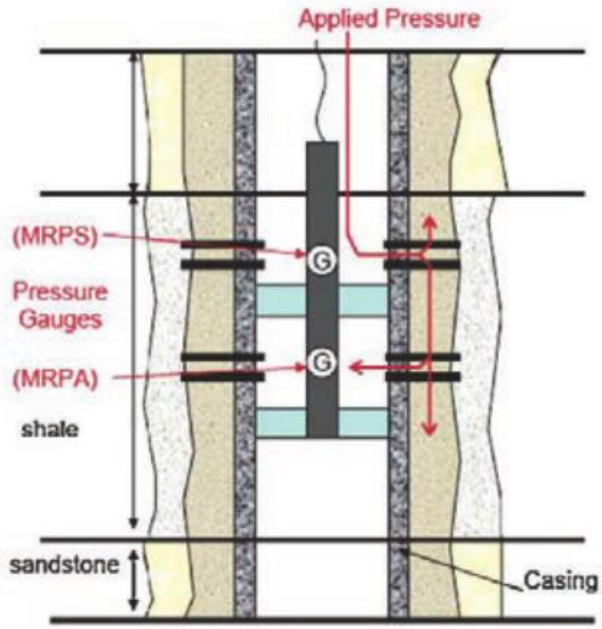


**Figure 6-3 Schematic of vertical interference test performed across a well section in the shale interval above the production zone (indicated as sandstone) (Gasda et al. 2013).**

### Mechanical sidewall coring tool

Sidewall coring tools can be used to take sidewall cores from a cased well. The tool has a coring bit capable of cutting through the casing, cement, and formation and retrieving a composite core sample containing each material. The samples are about an inch in diameter and a few inches long. The retrieval of sidewall cores allows the detailed inspection of wellbore materials for damage by micro characterization and micro-imaging techniques. The disadvantage of taking sidewall cores is that it is a destructive technique that leaves an, approximately, one inch hole in the side of the well (Duguid and Tombari, 2007).

### Cased-hole mobility and fluid analysis tool

Cement and formation permeability behind casing can be measured in situ using tools that can drill holes several inches deep through the casing, cement and formation rock (Burgess et al. 2001). The measurements involving pressure drawdown and build-up periods are then made on the newly exposed material. The mobility and permeability of the material can be calculated based on its response to pressure drawdown and build-up. It is possible to have multiple measurements through the same point in the casing where the hole in the sidewall is made deeper between the measurements and changes in mobility of the cement and/or formation can be measured. It is also possible to take fluid samples through the hole in the casing using a fluid sampling module to analyse the formation fluid in situ and to collect and retrieve it for further laboratory analysis (Duguid and Tombari 2007).

## 6.2.3 Surface-casing-vent flow

Well leakage at the surface may be recorded as surface-casing-vent flow (SCVF); this represents gas flow through wellbore annuli and gas migration along the outside of the casing. The SCVF occurs when gas enters the exterior production-casing annulus from a source formation below the surface-casing shoe and flows to surface when the casing vent is open or builds gas pressure in the annulus when the casing vent is closed. Gas migration occurs when gas migrates along the outside of the cemented surface casing. It is important to note that while gas leaks can occur in one barrier, secondary barriers will contain the pressure and prevent a leak to the outside (King and King 2013). In Alberta, Canada, the Alberta Energy Resources Conservation Board requires that all wells drilled and cased be tested for SCVF within 60 days of drilling-rig release and before final abandonment. Wells that have positive SCVF and exhibit gas flow rates greater than 300 $m^3$/day, or have a stabilised surface casing build-up pressures that is greater than the water hydrostatic pressure gradient to the depth of the surface casing shoe, or have liquid hydrocarbon flow or saline-water flow, must be repaired immediately (Watson and Bachu [2009]).

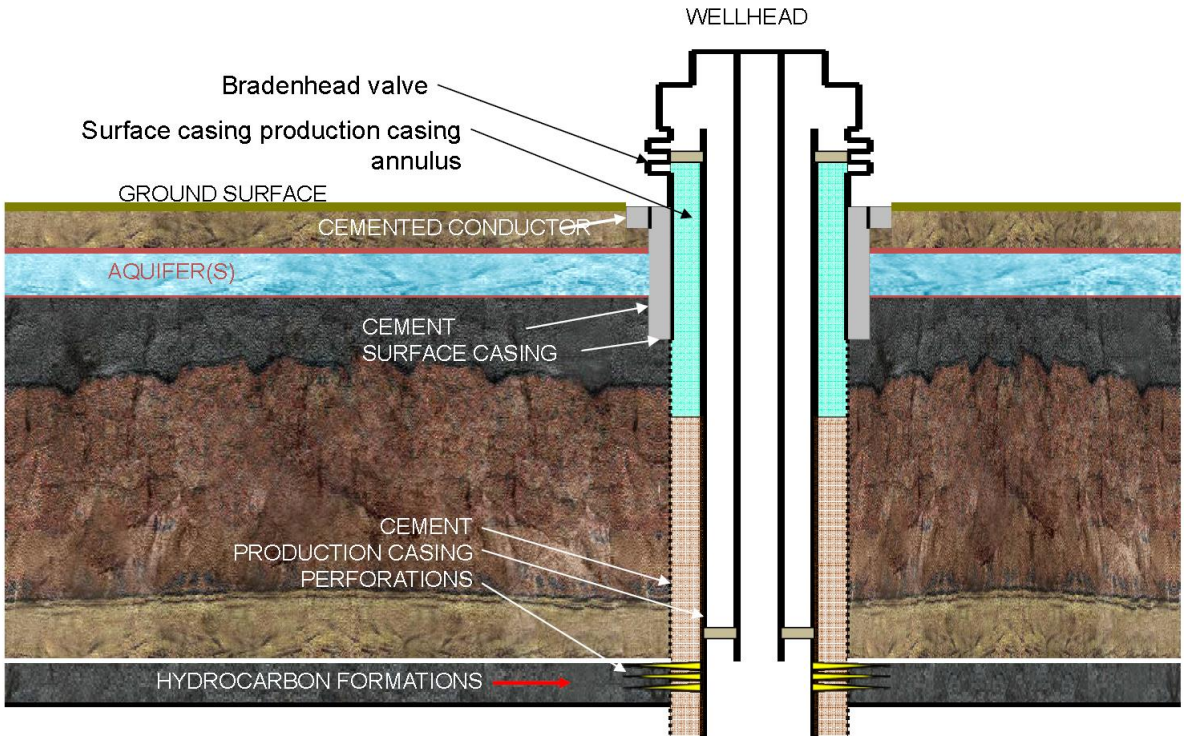


**Figure 6-4 Bradenhead testing (or casing head pressure testing) for identification of defective gas wells (COGCC 2013).**

### 6.2.4 Casing head pressure testing (or bradenhead testing)

Casing head pressure testing (or bradenhead testing) has been instrumental in identification of defective gas wells (Figure 6-4). The San Juan Field Office of the Bureau of Land Management has aggressively pursued bradenhead testing for casing head pressure measurement since 1991 (BLM 2010). Operators in the Basin are required to survey all wells and measure and record tubing, casing and intermediate casing pressures. Should casing pressures be encountered, a mandated testing protocol is used to determine if they are due to leaky casing. Beginning with the casing head valve, annular spaces are opened sequentially and the blow down time and flow rates recorded. As each annular space is blown down, the pressure in the adjacent annulus is monitored for any changes at five minute intervals for up to 30 minutes. A drop in pressure in the adjacent annular space usually indicates a leak. Wells with residual pressures after a 30 minute test interval may also indicate a casing leak. A threshold pressure of 172 kPa (25 psi) for wells in a non-critical area or 34.5 kPa (5 psi) for wells in a critical area is established as the minimum threshold pressure required for sampling and laboratory analysis of both produced and casing head gases. If the gases are similar in composition, and/or if a casing leak is detected, the operator must file and implement remedial action plans (Armstrong et al. 2009). The critical groundwater areas constitute an approximate 1 mile buffer zone surrounding domestic wells where methane has historically been documented at concentrations higher than 1.0 mg/L and casing pressures exceed 34.5 kPa (5 psi). All the other areas are designated as non-critical areas.

### 6.2.5 Fugitive emissions of methane

Measurement of fugitive emissions of methane from gas production wells may be another way of detecting issues with well integrity. Examples of methane emission monitoring in NSW Queensland are available from Day et al. (2014). Of the 43 wells examined, only three showed no emissions. The

remainder had some level of emission but generally the emission rates were very low, especially when compared to the volume of gas produced from the wells. The principal methane emission sources were found to be venting and operation of gas-powered pneumatic devices, equipment leaks and exhaust from gas-fuelled engines used to power water pumps. Although the well pad emissions were low, a separate, larger source of methane was found on a gas relief vent on a water gathering installation close to one of the wells examined during this study. During the field measurements, no evidence of leakage of methane around the outside of well casings was found at any of the wells included in this sample. Methane measurements were made using a Picarro Model 2301 Cavity Ring-down Spectrometer $CH_4/CO_2/H_2O$ analyser coupled with a Picarro Mobile Measurement Kit. To determine if $CH_4$ was escaping from the well casing, the flux chamber method was applied at each well site to measure the emission rate of any leakage from around the outside of the casing. Measurements were made on the ground surface near well heads to determine if $CH_4$ was migrating around the outside of well casings or through casing walls. These measurements were made using a surface flux chamber, a technique frequently used to measure emission rates of soil gases.

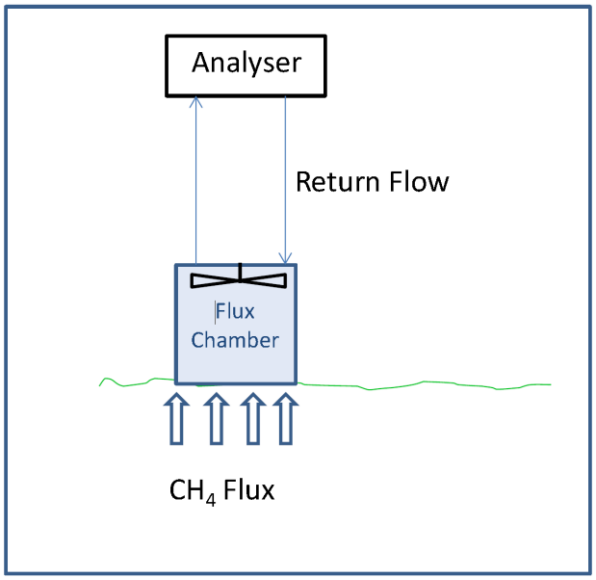


**Figure 6-5 Schematic diagram of the flux chamber system used for well casing leak determinations.**

### 6.2.6 Groundwater hydrochemistry, environmental isotopes, contaminants

The objective of this section is to provide a few illustrative examples of studies where measurement of environmental tracers in groundwater have been used successfully to detect interaquifer connectivity, possibly linked to hydrocarbon extraction, coal exploration bores, or degraded water bores. The objective is not to attempt to provide a comprehensive overview of all relevant literature on the use of tracers to detect anthropogenically enhanced interaquifer connectivity. More extensive recent reviews on such subjects are available from, e.g. US EPA (2016).

The hydrochemistry of groundwater together with concentrations of environmental isotopes and contaminants (organic and inorganic) can provide information about connectivity, natural or anthropogenically induced, between a hydrocarbon reservoir and aquifers. However, the typical composition in terms of hydrochemistry, isotopes or contaminants may be modified by reactions along their pathway and mixing processes. Therefore, groundwater sampling should occur in close proximity to potential leakage pathways to avoid complicating factors in the analysis. The use of

groundwater hydrochemistry, tracers and contaminants is relevant to the active gas production phase and to the post decommissioning phase, as the following international examples illustrate.

In a geochemical study of potential connectivity between Marcellus shale and shallow groundwater, Warner et al. (2012a) classified 426 water samples from shallow groundwater in an 80 × 160 km area of northeastern Pennsylvania currently being developed for gas using hydraulic. The classification consisted of 4 groups based on Br, Cl, Na, Ba, Sr, and Li concentration and the isotopic ratios of $^{87}Sr/^{86}Sr$, $^{2}H/H$, $^{18}O/^{16}O$, and $^{228}Ra/^{226}Ra$. Evidence that diluted residual brine had migrated from deep formations along cross formational pathways was found in the chemistry of one group with high Br/Cl and Sr/Ca but low $^{87}Sr/^{86}Sr$. By referring to the source as the ''Marcellus'', Warner et al. (2012a) implied that leakage was from the Marcellus and they suggested that the pathways of natural gas leakage might also be areas of higher risk for leakage of residual hydraulic fracturing fluid. Warner et al. (2012b) argued that (i) there is evidence for natural migration of brine and subsequent dilution in shallow drinking water aquifers, and (ii) if hydraulic fracturing intercepts natural pathways (i.e., faults/fractures) that connect the Marcellus to overlying units, the migration of fluids, including gases, remains possible.

Jackson et al. (2013) analysed 141 drinking water bores across the Appalachian Plateaus (northeastern Pennsylvania, US) examining natural gas concentrations and their isotopic signatures with proximity to natural gas wells. Analytes included methane ($CH_4$), ethane ($C_2H_6$) and propane ($C_3H_8$), their isotopic signatures ($\delta^{13}C$ and $\delta^{2}H$ for methane and $\delta^{13}C$ for ethane), hydrocarbon ratios, and the ratio of the noble gas $^{4}He$ to methane in groundwater. For two out of three hydrocarbons the average concentrations in drinking water samples from relatively shallow bores (60-90 m depth) were significantly higher (six times for methane, 23 times for ethane) at distances < 1 km from gas wells. Based on the isotopic and hydrocarbon ratios, groundwater was found to be characteristic of a thermally postmature Marcellus-like source (the Marcellus Formation is the primary hydrocarbon resource ranging in depth from 1200-2500 m) in some cases. Jackson et al. (2013) hypothesise that the higher dissolved gas concentrations observed in drinking water are the result of (i) faulty or inadequate steel gas well casings and (ii) imperfections in the cement sealing of the annulus or gaps between casings and rock that keep fluids from moving up the outside of the gas well.

Environmental tracers such as noble gases constitute an appropriate complement to hydrocarbon geochemistry. Especially radiogenic noble gases ($^{4}He$, $^{21}Ne$, and $^{40}Ar$) provide conservative tracers (i.e., unaffected by chemical reactions or microbial activity) and their well-characterized isotopic compositions in the crust, hydrosphere, and atmosphere make noble gases ideal tracers of crustal fluid processes. When paired with hydrocarbon composition and inorganic water chemistry, noble gases can help differentiate (“fingerprint”) between natural geological migration of hydrocarbon gases and anthropogenic contamination. Darrah et al. (2014) documented fugitive gases in eight clusters of domestic water wells overlying the Marcellus and Barnett Shales in the US, including declining water quality through time over the Barnett. Gas geochemistry data including noble gases (e.g., $^{4}He$, $^{20}Ne$, and $^{36}Ar$) indicated leaks through annulus cement (four cases), production casings (three cases), and underground well failure (one case) rather than gas migration induced by hydraulic fracturing deep underground. Further examples of the use of organic and inorganic chemistry in combination with dissolved gases and their isotopic to identifying leakage pathways associated with unconventional gas extraction can be found in Warner et al. (2014), Llewellyn et al. (2015), and others.

Detection of change in concentrations of organic and inorganic constituents and tracers can be an indication of a leakage pathway linked to bore or well integrity. Being able to detect change requires however a proper baseline condition against which change can be measured. This includes characterisation of potentially local differences due to geology and understanding of temporal trends. Relevant research is that by Golding et al. (2013), Hamilton et al. (2012 and 2014), and

Papendick et al. (2011) on fingerprinting the actual coal-bearing formations by using stable isotopes. When sufficient data are available, trend analysis can be undertaken. The purpose of trend analysis is to identify any short or long-term trends that might indicate that leakage pathways exist and are impacting water quality. Note, however, that changes in chemistry consistent with a short or long-term trends are not necessarily evidence of any relationship to groundwater changes linked to well leakage of fluids or of methane gas. On the other hand, there may also be conditions when presence of methane does not immediately result in changes in hydrochemistry, e.g. when buoyancy-driven gas occurs in a bore screened in a coal seam aquifer. Water quality data and trend analysis can be performed by geographic mapping, plotting data on time-concentration plots, performing Mann-Kendall trend analysis, and evaluating results of compositional analysis of methane (AMEC Geometrix 2011; Esterby 1996; Hirsch et al. 1982).

Furthermore, it is important to understand if the chemical variability of groundwater is representative for an entire aquifer or only for a particular region. To account for spatial clustering in hydrochemical data that could be related to local differences in geology (such as variable aquifer composition) or hydrology (e.g. recharge processes and aquifer connectivity), a hierarchical cluster analysis can be undertaken. Because such clustering may lead to higher values existing in one part of an aquifer compared to other parts of an aquifer, there is a need to detect such clusters and identify the cause of higher (or lower) values. Insight in site specific differences helps to understand whether high concentrations of a particular parameter represent the natural background concentrations or are due to anthropogenic processes.

Mallants et al. (2016) determined the natural variability in hydrochemistry for key aquifers in the Surat Basin using up-to-date data. A rigorous statistical analysis of about 560 water samples collected from 2010 to 2013 was undertaken to determine natural variability of hydrochemical parameters. This included a hierarchical cluster analysis to identify any spatial patterns in hydrochemical parameters. Figure 6-6 shows the distribution of groundwater chemistry clusters for all aquifers. The hierarchical cluster analysis resulted in the identification of seven major clusters with distinct ion concentrations and ratios. These may then be used as a set of baseline conditions against which to test change in hydrochemistry, potentially linked to well or bore leakage.

Another potentially useful approach to detect inter-aquifer leakage during the coal seam gas production phase is the detection of tracers in produced coal seam gas water. If well or bore leakage exists between an overlying aquifer with younger water and a deeper gas reservoir with older groundwater (due to the downward hydraulic gradient caused by the depressurisation of the hydrocarbon formation, the water flow will be from the young to old groundwater), then tracers specific to the younger groundwater may possibly be detectable in the produced water. This will mainly depend on the degree of dilution that occurs around the coal seam gas well, where a likely very small flux of younger groundwater is mixed with a larger volume of older groundwater, prior to moving up the well as produced water.

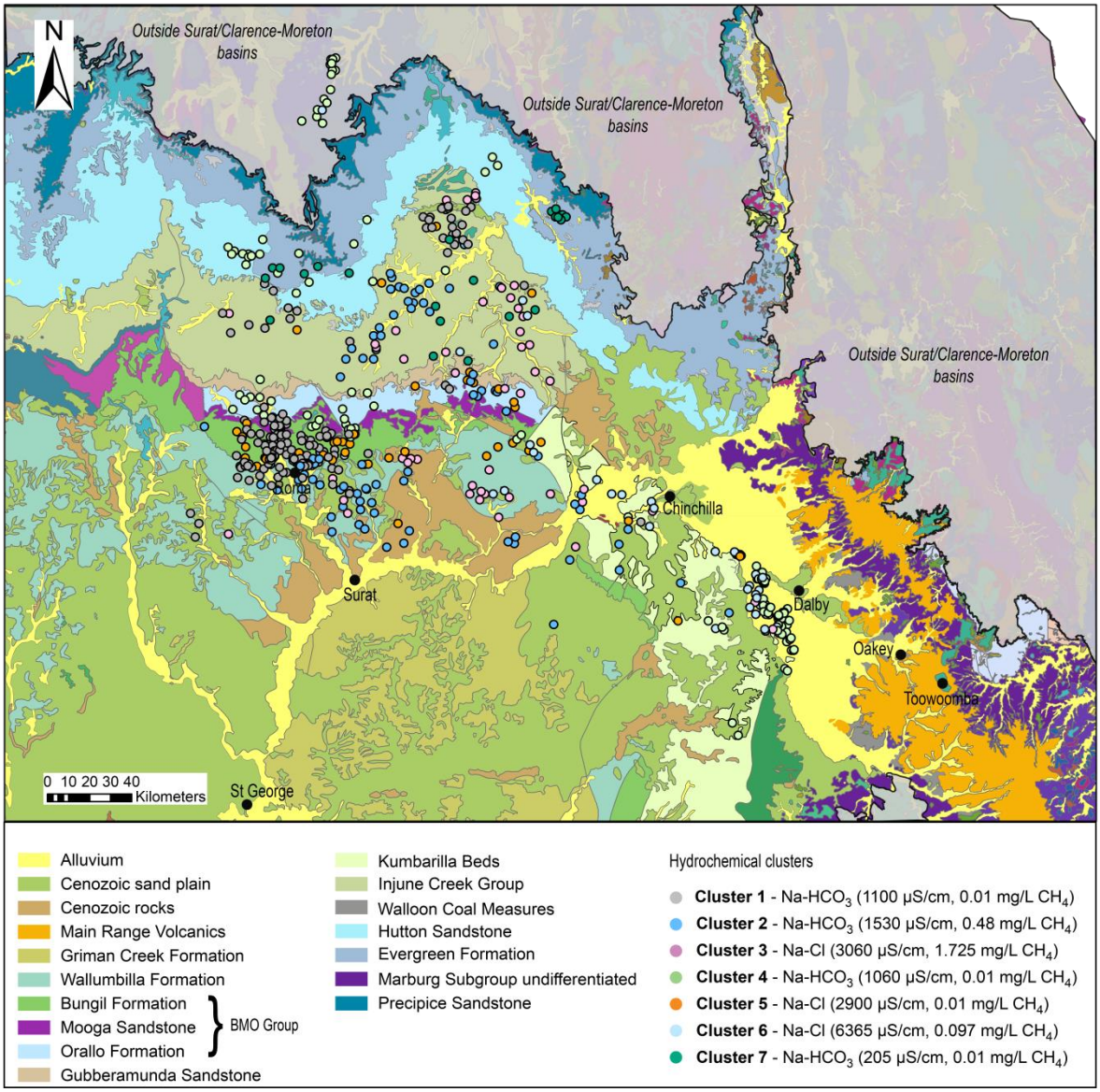


**Figure 6-6 Distribution of clusters in the Surat and western Clarence-Moreton basins and simplified surface geology for all aquifers. Major characteristics such as water type and median electrical conductivity and methane concentrations are also shown (Mallants et al. 2016).**

## 6.3 An outline of a proposed experimental program for monitoring inter-aquifer leakage in the field

Throughout the life of a coal seam gas production well, well conditions must be monitored on an on-going basis to ensure integrity of the well and well equipment (DTI, 2012). Mechanical integrity and pressure monitoring and evidence of corrosion are used to determine the mechanical integrity of casing and other well equipment during production, well treatment or well intervention and workover operations. Some of these on-going monitoring, such as surface casing annulus pressure monitoring (DNRM 2013) and fugitive gas detection around a well casing (Day et al. 2014) may be used to infer sub-surface leaks that may be induced by or result in inter-aquifer leakage. The gas

detection techniques can also be applied to the post decommissioning phase. A summary of potential well integrity testing methods is provided in Section 6.3.1.

Groundwater bores are another potential contributor to enhanced interaquifer connectivity due to loss of casing integrity once the steel casing has reached its usable life. Based on the optimistic life time of steel in water bores (i.e. 45 years), it was assumed that water bores constructed prior to 1955 will now have poor integrity, i.e., they have experienced well failure (Commonwealth of Australia 2013). This assumption is based on the fact that prior to 1955 nearly all of the water bores would have been constructed using steel casing. The water bores constructed between 1955 and 1967 were also considered to have poor integrity, i.e., well failure is implied on the basis that the steel casing from prior to 1968 would be significantly corroded by now. Integrity of groundwater production bores has been investigated using borehole geophysical techniques (logging) and groundwater quality analysis (see Section 6.3.2 for further details).

### 6.3.1 Coal seam gas well integrity testing

The proposed field-based experimental program is suitable to monitor the inter-aquifer leakage along a coal seam gas well during the entire lifecycle of a well. The list of approaches is not meant to be exhaustive; the techniques discusses are typical examples of current industry practice. A sufficiently large cohort of wells should be selected for the analysis. The experimental program is proposed to comprise four components, and focuses on detection of well failure prior to and after well decommissioning:

- Desk study. This stage reviews well completions report (including drilling, well cementing and stimulation reports), well logging data and reports, well production performance and on-going surface monitoring data. This desk study is designed to identify candidate wells and provide baseline data for further study in the next two stages;
- Cased well logging and inspection. This stage is designed to run wireline sonic and ultrasonic logging tools to directly monitor inter-aquifer leakage of the candidate wells. This stage may be separated into several steps to ensure the casing is in good condition prior to more comprehensive cement evaluation tools being run. For example, prior to running sonic and ultrasonic wireline logging tools to evaluate cement sheath and cement bond integrity, the condition of the casing inside surface and casing connections should be measured/inspected by a multifinger caliper and/or a downhole camera. If these measurements/inspection indicate that the casing has good integrity, then, sonic and ultrasonic tools should be run. These logging data will yield conditions for cement sheath and cement bonds with casing and rock formation as well as casing condition. These conditions should then be compared with the similar data obtained in earlier logging runs, including the one during well construction. This comparison could reveal if the well integrity condition deteriorate with time and operation of the well.

  Since the cased well logging and inspection is non-destructive, this operation may be performed not only prior to decommissioning, but multiple times during a well's life span to evaluate how well integrity change with time. Furthermore, this operation will require all the equipment downhole to be removed, it will need to be scheduled together with other major well operations, such as well workover for replacing the de-water pump.
- Vertical interference test and sidewall core sampling and testing. This stage is designed to measure effective well permeability within an aquitard, a direct measurement of the well integrity (see Figure 6-3 for details). These tests are destructive ones and should be

performed on wells that are going to be abandoned or to be used as one of the several wells representative of a field of existing wells. In addition, selection of the test intervals for the vertical interference test should be guided by the result of sonic and ultrasonic logging runnings. Prior to the vertical interference tests, it is proposed that the cased-hole mobility and fluid measurements are taken. These measurements yield a good understanding of the permeability in different materials (cement and formation rock) in the radial direction behind the casing as well as provide essential parameters in interpreting the vertical interference test results.

Sidewall coring should be performed following the vertical interference testing, and the location for coring should be guided by the sonic and ultrasonic tool runs and the requirement for interpreting the vertical interference tests. The sidewall core samples can be used for examining the cement bonds with the casing and the formation rocks, hole cleaning condition prior to cementing as well as for measurements on physical, mechanical and hydraulic properties and for mineralogical analyses.

- Provided baseline groundwater hydrochemistry knowledge is available, sampling of groundwater hydrochemistry, tracers and contaminants in the produced water to assess any inter-aquifer leakage. To ensure detectability of leakage against spatially and temporally variable background chemical conditions, specific tracers may need to be used whose concentrations would be present only (or in much larger concentrations) in groundwater infiltrating a hydrocarbon reservoir.
- Post decommissioning: Provided groundwater bores or monitoring wells are available within the hydrocarbon reservoir, sampling of groundwater hydrochemistry, tracers and contaminants to detect any deviation from the baseline. Forensic analyses can be used to identify causes for any changes to the baseline information. A well-known example is the identification of distinguishing features of the different possible sources of methane. Different types of analytical methods can be used to help determine if methane gas is of biogenic or thermogenic origin, or a mixture of the two. The analytical methods used to differentiate between the two types of methane are summarized in Kaplan et al. (1997). In some publications this is referred to as ‘fingerprinting’ (Coleman, 1989; Tilley and Muelenbachs, 2012).
- Undertake fugitive gas emission measurements in the vicinity of the well head using the gas flux chamber method.

### 6.3.2 Water bore casing integrity testing

In the US, borehole geophysical logs have been combined with groundwater quality analysis to detect if water bores could have enhanced vertical connectivity between a shallow alluvial aquifer and several underlying confined aquifers (USGS 1997). The aim of the geophysical logging was to find evidence of breaks or gaps in the well casings and cement around the casings. The geophysical investigations were supplemented with analysis of water quality parameters: volatile organic compounds (VOCs), semivolatile compounds (SVOCs), pesticides, polychlorinated biphenyl (PCBs), total petroleum hydrocarbons (TPHs), trace elements, major ions, cyanide, and physical properties.

In Australia, DERM (2011) identified that all areas of groundwater monitoring would benefit from an assessment of the integrity of the water bores to ensure that the data gathered is reflective of the aquifer status. The recommended operational instrumentation would be a down-hole video inspection camera.

GHD (2010) provide a comprehensive overview of techniques to assess groundwater bore deterioration. Three classes of bore condition assessment techniques are discussed:

- Geophysical techniques for casing assessment include downhole camera, caliper log, microflow log, casing collar locator, termperature and conductivity logs, specialised (oilfields) tools, and lithological tools.
- Physical testing such as pumping tests.
- Water quality monitoring involving analysis of groundwater and solid samples.

# 7 Conclusions

The potential effect of leaky coal seam gas wells and open boreholes (e.g. coal exploration bores) on enhanced inter-aquifer connectivity and subsequent impact on the groundwater balance (i.e. groundwater heads) and groundwater quality (i.e. salinity) was investigated with simulation models. The analysis of potential impacts on groundwater heads was undertaken with a focus on regional-scale impacts, while the impact on groundwater quality involved a local-scale analysis considering a single leaky well or open borehole.

A simplified 3D numerical groundwater flow model was developed for a 195×151 $km^2$ study area in the Gunnedah Basin, NSW, which included the following sequence of five model layers: aquifer-aquitard-coal seam gas reservoir-aquitard-coal seam gas reservoir. It was designed to test worst case scenario of potential impacts of leakage between aquifers. The leak rate for gas wells at 425 locations in the model was varied from 0 to 100%. Leakage was assumed to occur only after cessation of the gas production period, and involved water flow through the partially degraded well annulus which increased the effective hydraulic conductivity of the well to a value of approximately 0.813 m/d. Simulations across all failure rates demonstrated inter-aquifer connectivity does not appear to be materially enhanced by the presence of such “leaky wells” in a coal seam gas well field. This is confirmed by negligible additional head decreases in the aquifer and by a robust aquitard effective flux that is relatively insensitive to various failure rates. This agrees with the findings of Doble et al. (2018) for an individual leaky well case (i.e. partially leaky well), which showed that the inter-aquifer leakage was primarily controlled by the effective well conductivity (i.e., the flow rate within a connected well). In all scenarios tested here the effective well conductivity of the leaky well was relatively low (approx. 0.813 m/d). The impact of a higher effective well conductivity will only minimally increase the effect on the regional groundwater flow system, as bounding simulations with fully open boreholes demonstrated (see further).

Simulations with open bores (e.g. coal exploration bores) that have no restriction to groundwater flow (i.e. the effective hydraulic conductivity of the borehole is extremely large in the model) demonstrated the influence on regional scale inter-aquifer leakage is observable by comparison to the leaky well scenarios, but only in the area immediately overlying the gas extraction area. At such locations, the additional drawdown in the groundwater aquifer is at most 2 m for a 5% failure rate for an open borehole. Additional drawdowns for smaller failure rates of 1 and 2% are close to zero and 1 m, respectively. At observation points approximately 10 km away from the gas extraction area, the additional drawdown is negligible (for 1, 2, and 5% failure rate). Open bores clearly form preferential flow pathways, which when located in proximity to an active well field will have a significant impact on the groundwater response. In particular, open bores enhance the drawdown in the top aquifer by enabling water to replenish those layers depressurised by pumping. In hydrogeological systems where a vertical gradient exists between geologic layers, such open bores will have a similar impact (leakage between layers) in the absence of pumping induced drawdown.

It should be noted that the pumping rates used in this model where previously determined using a reservoir model, and are based on the necessary aquifer depressurisation to enable gas desorption and extraction. Such a system is typically dual-phase, involving both a water phase and a gas phase. When using a single phase groundwater flow model such as MODFLOW-USG (this study), the flow and pressure relationships are not representative of a dual-phase system. Because fluxes in a single phase groundwater model are driven by water pressure only, this will effectively be a

misrepresentation of a dual-phase system, and can lead to potential errors. Nevertheless, the single phase system is considered to be conservative, and will therefore not underestimate impacts.

The effect of leaky wells or open boreholes on groundwater quality was investigated using a 3D analytical solution to the convection-dispersion equation. By considering a continuous solute source positioned where the leaky well intersected an aquifer or a coal seam target formation, the spreading of a solute plume was calculated and concentrations downstream the leaky well or open borehole recorded. For the case of the leaky well the distance where a noticeable increase in solute concentration was observed was limited to 10 m downstream the well. The increase in concentration was never higher than 4% of the solute source. The largest chance for aquifer contamination is during the pre-development phase for those locations where an upward gradient exists. For the open borehole, the conclusion was similar for upward flow (from coal seam formation to aquifer). In case of down flow, an increase up to 12% of the source concentration was observed, but limited to a distance of approximately 100 m.

Finally, possible tools and technologies are discussed for monitoring well integrity failure, including an outline of a proposed experimental program for monitoring inter-aquifer leakage in a coal seam gas field. This involves non-destructive tools such as cased well logging and inspection using wireline sonic and ultrasonic tools, downhole camera and multifinger caliper. Subsequently sidewall core sampling and testing is recommended to study cement bonds, physical, mechanical and hydraulic properties. For monitoring in the post decommissioning phase, measurement of fugitive gas emissions and groundwater hydrochemistry, tracers and contaminants is proposed.

# 8 References


AMEC Geomatrix (2011). Updated trend and data analysis San Juan Basin water quality analysis project San Juan Basin, Colorado. Colorado Oil and Gas Conservation Commission Denver, Colorado Project No. 15244: 20.

APPEA (2012). CSG well construction and bore specifications. Available from: <www.appea.com.au/csg/about-csg/fact-sheets.html>. Accessed on 30/10/2012.

Arrow Energy (2011). Well Integrity: what you need to know. Retrieved June 2016. https://www.arrowenergy.com.au/__data/assets/pdf_file/0013/1273/Well-Integrity.pdf.

Azuma S, Kato H, Yamashita Y, Miyashiro K, Saito S (2013). The long-term corrosion behaviour of abandoned wells under CO2 geological storage conditions: (2) Experimental results for corrosion of casing steel. Energy Procedia 37: 5793-5803.

Bazzari J (1989). Well Casing Leaks History and Corrosion Monitoring Study, Wafra Field. Middle East Oil Show.

Bellabarba M, Bulte-Loyer H, Froelich B, Roy-Delage SL, van Kuijk R, Gulliot D, Moroni N, Pastor S, Zanchi A (2008). Ensuring Zonal Isolation Beyond the Life of the Well. Oilfield Review, 20(1): 18–31.

Burgess KA, MacDougall TD, Siegfried RW, Fields TG (2001). Wireline-conveyed through-casing formation tester preserves casing integrity. SPE 72371 presented at the SPE Eastern Regional Meeting held in Canton, Ohio, 17-19 Oct 2001.

Carey JW, Wigand M, Chipera SJ, WoldeGabriel G, Pawar R, Lichtner PC, Wehner SC, Raines MA, Guthrie GD (2007). Analysis and performance of oil well cement with 30 years of CO 2 exposure from the SACROC Unit, West Texas, USA, International Journal of Greenhouse Gas Control, 1(1): 75-85.

CDM Smith (2014). Santos Narrabri Gas Project: Groundwater modelling report. Subiaco, WA.

Commonwealth of Australia (2014). Bore integrity - Background review.

Coleman DD (1989). Geochemical fingerprinting: Identification of storage gas using chemical and isotopic analysis. In: “Underground Storage of Gas”, pp 327-338, Edited by M. R. Tek. Kluwer Academic Publishers.

Connell L, Down D, Lu M, Hay D, Heryanto D (2015). An investigation into the integrity of wellbore cement in CO2 storage wells: Core flooding experiments and simulations. International Journal of Greenhouse Gas Control, 37: 424-440.

Crow W, Carey JW, Gasda S, Brian Williams D, Celia M (2010). Wellbore integrity analysis of a natural CO2 producer, International Journal of Greenhouse Gas Control, 4(2): 186-197.

Davies RJ, Almond S, Ward RS, Jackson RB, Adams C, Worrall F, Herringshaw LG, Gluyas JG, Whitehead MA (2014). Oil and gas wells and their integrity: implications for shale and unconventional resource exploitation. Marin and Petroleum Geology 56: 239-254.

Day S, Dell’Amico M, Fry R, Javanmard Tousi H (2014). Field Measurements of Fugitive Emissions from Equipment and Well Casings in Australian Coal Seam Gas Production Facilities. CSIRO, Australia.

Darraha TH, AV Jackson RB, Warner NR, Poreda RJ (2014). Noble gases identify the mechanisms of fugitive gas contamination in drinking-water wells overlying the Marcellus and Barnett Shales. Proceedings of the National Academy of Sciences 111(39): 14076–14081.

DERM (2011) Strategic Water Information and Monitoring Plan, Queensland. Prepared for the Bureau of Meteorology.

DNRM (Department of Natural Resources and Mines) (2013). Code of practice for constructing and abandoning coal seam gas wells and associated bores in Queensland. Edition 2.0.

Doble R, McCallum J, Peeters L, Wu B, Mallants D (2018). Modelling inter-aquifer leakage associated with well integrity failure, prepared by the Commonwealth Scientific and Industrial Research Organisation (CSIRO), Canberra.

DTI (Department of Trade & Investment) (2012). Code of practice for coal seam gas well integrity. Department of Trade & Investment, Regional Infrastructures & Services, Resources & Energy, New South Wales.

Duguid A, Tombari J (2007). Technologies for Measuring Well Integrity in a CO2 Field. Sixth Annual Conference on Carbon Capture and Sequestration.

Duguid A, Butsch R, Carey JW, Celia M, Chugunov N, Gasda S, Ramakrishnan T, Stamp V, Wang J (2013). Pre-injection baseline data collection to establish existing wellbore leakage properties, Energy Procedia, 37: 5661-5672.

Dusseault M, Jackson R (2014). Seepage pathway assessment for natural gas to shallow groundwater during well stimulation, in production, and after abandonment, Environmental Geosciences, 21(3): 107-126.

Elsener B (2005). Corrosion rate of steel in concrete-Measurements beyond the Tafel law. Corrosion Science 45 (12): 3019-3033.

Esterby SR (1996). Review of methods for the detection and estimation of trends with emphasis on water quality applications. Hydrological processes 10: 127-149.

Flemisch B et al. (2011). DuMux: DUNE for multi-{phase, component, scale, physics, …} flow and transport in porous media, Advances in Water Resources, 34(9): 1102-1112.

Gasda SE, Celia MA, Wang JZ, Duguid A (2013). Wellbore permeability estimates from vertical interference testing of existing wells. Energy Procedia 37: 5376-5680.

GasFields Commission Queensland (2015). Onshore gas well integrity in Queensland, Australia. Technical Communicaition 4, July 2015.

GHD (2010). Groundwater bore deterioration: schemes to alleviate rehabilitation costs, Waterlines Report Series No 32, National Water Commission, Canberra. 243 pp. http://archive.nwc.gov.au/library/waterlines/32/groundwaterbore-deterioration-schemes-to-alleviate-rehabilitation-costs

Golding SD, Boreham CJ, Esterle JS (2013). Stable isotope geochemistry of coal bed and shale gas and related production waters: A review. International Journal of Coal Geology 120: 24-40.

Hamilton SK, Esterle JS, Golding SD (2012). Geological interpretation of gas content trends, Walloon Subgroup, eastern Surat Basin, Queensland, Australia. International Journal of Coal Geology 101: 21–35.

Hamilton SK, Golding SD, Baublys KA, Esterle JS (2014). Stable isotopic and molecular composition of desorbed coal seam gases from the Walloon Subgroup, eastern Surat Basin, Australia. International Journal of Coal Geology 122: 21-36.

Harbaugh AW (2005). MODFLOW-2005, the US Geological Survey modular ground-water model: The ground-water flow process, US Department of the Interior, US Geological Survey Reston, VA, USA.

Hawkes CD, Gardner C (2013). Pressure transient testing for assessment of wellbore integrity in the IEAGHG Weyburn–Midale CO 2 Monitoring and Storage Project, International Journal of Greenhouse Gas Control, 16: S50-S61.

Hirsch R.M., J.M. Slack, R.A. Smith (1982). Techniques of trend analysis for monthly water quality data. Water Resources Research 18(1): 107-121.

HydroGeoLogic (2006). MODHMS: A comprehensive MODFLOW-based hydrologic modeling system, Version 3.0.Rep., HydroGeoLogic Incorporated, Herndon, VA.

Jackson RB, Vengosh A, Darrah TH, Warner NR, Down A, Poreda RJ, Osborn SG, Zhao K, Karr JD (2013). Increased stray gas abundance in a subset of drinking water wells near Marcellus shale gas extraction. Proceedings of the National Academy of Sciences 110: 11250-11255. http://dx.doi.org/10.1073/pnas.1221635110.

Jackson RB (2014). The integrity of oil and gas wells. Proceedings of the National Academy of Sciences, 111(30): 10902-10903.

Kaplan IR, Galperin Y, Lu S-T, and Lee R-P (1997). Forensic Environmental Geochemistry: differentiation of fuel-types, their sources and release time. Organic Geochemistry 27(5/6): 289-317.

King GE, King DE (2013). Environmental risk arising from well construction failure: difference between barrier and well failure, and estimates of failure frequency across common well types, locations and well age. SPE 166142 presented at the SPE Annual Technical Conferenc and Exhibition held in New Orleans, Louisiana, USA, 20 Sept – 2 Oct. 2013.

Kissinger A, Helmig R, Ebigbo A, Class H, Lange T, Sauter M, Heitfeld M, Klünker J, W Jahn (2013). Hydraulic fracturing in unconventional gas reservoirs: risks in the geological system, part 2, Environmental earth sciences, 70(8): 3855-3873.

Kreis P (1991). Hydrogen evolution from corrosion of iron and steel in low/intermediate-level waste repositories. Nagra Technical Report NTB 91-21, Nagra, Wettingen, Switzerland.

Langevin CD, Thorne DT Jr, Dausman AM, Sukop MC, Weixing G (2007). SEAWAT Version 4: A Computer Program for Simulation of Multi-Species Solute and Heat Transport. Techniques and Methods Book 6, Chapter A22 U.S. Department of the Interior and U.S. Geological Survey.

Leij F, Bradford SA (1994). 3DADE: A computer program for evaluation of three-dimensional equilibrium solute transport in porous media. Research Report No. 134, US Salinity Lab, Riverside, CA.

Lewicki JL, Birkholzer J, Tsang C-F (2007). Natural and industrial analogues for leakage of CO2 from storage reservoirs: identification of features, events, and processes and lessons learned, Environmental Geology, 52(3): 457-467.

Llewellyn GT, Dorman F, Westland JL, Yoxtheimer D, Grieve P, Sowers T, Humston-Fulmer E, Brantley SL (2014). Evaluating a groundwater supply contamination incident attributed to Marcellus Shale gas development. Proceedings of the National Academy of Sciences 112(20): 6325–6330.

Lyons W, Plisga G (2004). Chapter 4, Drilling and Completions in Standard Handbook of Petroleum and Natural Gas Engineering, 2nd ed. SPE.

Mallants D, Raiber M, Davies P (2016). Decision Support System for Investigating Gas in Water Bores and Links to Coal Seam Gas Development. Project report prepared for the Department of Natural Resources and Mines, Queensland. CSIRO, Australia.

Merrick D (2015). AlgoMesh: A new software tool for building unstructured grid models, in Modflow and More 2015: Modeling a Complex World, edited, Colorado School of Mines, Golden, Colorado, USA. May 31–June 3 2015.

Moore CR, Doherty J, Howell S, Erriah L (2014). Some Challenges Posed by Coal Bed Methane Regional Assessment Modeling, Groundwater, 53(5): 737-747.

Morad K, Mireault R, Dean L (2008). Reservoir Engineering for Geologists: Coalbed Methane Fundamentals.

Moridis GJ, Freeman CM (2014). The RealGas and RealGasH2O options of the TOUGH+ code for the simulation of coupled fluid and heat flow in tight/shale gas systems, Computers & Geosciences, 65: 56-71.

Morris C, Sabbagh L, Wydrinski R, Hupp J, van Kuijk R, Froelich B (2007). Application of Enhanced Ultrasonic Measurements for Cement and Casing Evaluation, paper SPE/IADC 105648, presented at the SPE/IADC Drilling Conference, Amsterdam, February 20–22, 2007.

National Water Commission (2012). National Uniform Drillers' Licensing Committee. Minimum Construction requirements for Water Bores in Australia. Edition 3. ISBN 978-0-646-56917-8.

OGIA (2016). Hydrogeological conceptualisation report for the Surat Cumulative Management Area. Office of Groundwater Impact Assessment, DNRM, QLD.

Papendick SL, Downs KR, Vo KD, Hamilton SK, Dawson GKW, Golding SD, Gilcrease PC (2011). Biogenic methane potential for Surat Basin, Queensland coal seams. International Journal of Coal Geology 88: 123–134.

Neville CJ, MJ Tonkin (2001). Representation of multiaquifer wells in MODFLOW, paper presented at Proceedings of Modflow 2001 Conference at the International Ground Water Modeling Center, Golden, Colorado.

Nordbotten JM, Kavetski D, Celia MA, Bachu S (2009). Model for CO2 leakage including multiple geological layers and multiple leaky wells, Environmental science & technology, 43(3): 743-749.

Northey J, Pinetown K, Sander R (2014). Coal and coal seam gas resource assessment for the Namoi subregion. Product 1.2 for the Namoi subregion from the Northern Inland Catchments Bioregional Assessment. Department of the Environment, Bureau of Meteorology, CSIRO and Geoscience Australia, Australia.

Nowamooz A, Lemieux JM, Molson J, Therrien R (2015). Numerical investigation of methane and formation fluid leakage along the casing of a decommissioned shale gas well, Water Resources Research, 51(6): 4592–4622.

NSW Chief Scientist & Engineer (2014). Independent review of coal seam gas activity in NSW – information paper: abandoned wells.

Panday S, Langevin CD, Niswonger RG, Ibaraki M, Hughes JD (2013). MODFLOW–USG version 1: An unstructured grid version of MODFLOW for simulating groundwater flow and tightly coupled processes using a control volume finite-difference formulation, Report Rep. 6-A45, 78 pp, Reston, VA.

Popoola LK, Grema AS, Latinwo GK, Gutti B, Balogun AS (2013). Corrosion problems during oil and gas production and its mitigation. International Journal of Industrial Chemistry, 4(35): 1-15.

Reagan MT, Moridis GJ, Keen ND, Johnson JN (2015). Numerical simulation of the environmental impact of hydraulic fracturing of tight/shale gas reservoirs on near-surface groundwater: Background, base cases, shallow reservoirs, short-term gas, and water transport. Water Resources Research, 51(4): 2543-2573.

Satoh H, Shimoda S, Yamaguchi K, Hiroyasu K, Yamashita Y, Miyashiro K, Saito S (2013). The long-term corrosion behavior of abandoned wells under CO2 geological storage conditions: (1) experimental results for cement alternation. Energy Procedia, 37,: 5781-5792.

Schlumberger (2011). Manual for ECLIPSE Reservoir Simulation Software. Rep., Houston, Texas.

Silliman S, Higgins D (1990). An Analytical Solution for Steady-State Flow Between Aquifers Through an Open Well. Groundwater, 28(2): 184-190.

Šimůnek J, van Genuchten MT, Šejna M (2008). Development and applications of the HYDRUS and STANMOD software packages and related codes. Vadose Zone Journal, 7(2): 587-600.

Tan B, Lang M, Sheth D (2012). High-strength, low-density cement pumped on-the-fly using volumetric mixing achieves cement to surface in heavy loss coal seam gas field. SPE 158092 presented at SPE Asia Pacific Oil and Gas Conference and Exhibition held in Perth, Australia, 22-24 Oct. 2012.

Tilley BJ and Muelenbachs K (2012). Fingerprinting of gas contaminating groundwater and soil in a petroliferous region, Alberta, Canada. Published on 30 May 2012 on http://pubs.rsc.org |doi:10.1039/9781849734967-00115.

Turnadge C, Mallants D, Peeters L (2017). Sensitivity and uncertainty analysis of a regional-scale groundwater flow system stressed by coal seam gas extraction. CSIRO, Australia.

US EPA (2008). Determination of the mechanical integrity of injection wells. United States Environmental Protection Agency Region 5 – Underground Injection Control (UIC) Branch Regional Guidance # 5.

US EPA (2016a). Hydraulic Fracturing for Oil and Gas: Impacts from the Hydraulic Fracturing Watr Cycle on Drinking Water Resources in the United States. Office of Research and Development, Washington, DC. EPA/600/R-16/236Fa.

USGS (1997). Integrity of Production Wells and Confining Unit at the Naval Weapons Industrial Reserve Plant, Dallas, Texas, 1995 U.S. Geological Survey Water-Resources Investigations Report 97–4047

van Genuchten MT, Šimunek J, Leij F, Toride N, Šejna M (2012). STANMOD: Model use, calibration, and validation. Transactions of the ASABE, 55(4): 1355-1366.

Vengosh A, Jackson RB, Warner N, Darrah TH, Kondash A (2014). A critical review of the risks to water resources from unconventional shale gas development and hydraulic fracturing in the United States. Environmental science & technology, 48(15): 8334-8348.

Warner NR, Jackson RB, Darrah TH, Osborn SG, Down A, Zhao K, White A, Vengosh A (2012a). Geochemical evidence for possible natural migration of Marcellus Formation brine to shallow aquifers in Pennsylvania. Proceedings of the National Academy of Sciences, 109: 11961-11966. http://dx.doi.org/10.1073/pnas.1121181109

Warner NR, Jackson RB, Darrah TH, Osborn SG, Down A, Zhao K, White A, Vengosh A (2012b). Reply to Engelder: Potential for fluid migration from the Marcellus Formation remains possible. Proceedings of the National Academy of Sciences: 1.

Warner NR, Darrah TH, Jackson RB, Millot R, Kloppmann W, Vengosh A (2014). New Tracers Identify Hydraulic Fracturing Fluids and Accidental Releases from Oil and Gas Operations. Environmental Science and Technology, 48 (21): 12552–12560.

Watson T, Bachu S (2009). Evaluation of the potential for gas and CO2 leakage along wellbores. SPE Drilling & Completion, 115–126.

Wu B, Doble R, Turnadge C, Mallants D (2018). Bore and well induced inter-aquifer connectivity: a review of literature on failure mechanisms and conceptualisation of hydrocarbon reservoir-aquifer failure pathways. Prepared by the Commonwealth Scientific and Industrial Research Organisation CSIRO, Canberra.

Yamaguchi K, Shimoda S, Hiroyasu K, Stenhouse MJ, Zhou W, Papafotiou A, Yamashita Y, Miyashiro K, Saito S (2013). The long-term corrosion behavior of abandoned wells under CO2 geological storage conditions: (3) assessment of long-term (1,000 – year) performance of abandoned wells for geological CO2 storage. Energy Procedia, 37: 5804-5815.

CONTACT US

**t** 1300 363 400
+61 3 9545 2176
**e** enquiries@csiro.au
**w** www.csiro.au

AT CSIRO WE SHAPE THE FUTURE

We do this by using science to solve real issues. Our research makes a difference to industry, people and the planet.

As Australia's national science agency we've been pushing the edge of what's possible for over 85 years. Today we have more than 5,000 talented people working out of 50-plus centres in Australia and internationally. Our people work closely with industry and communities to leave a lasting legacy. Collectively, our innovation and excellence places us in the top ten applied research agencies in the world.

WE ASK, WE SEEK AND WE SOLVE

FOR FURTHER INFORMATION

**Land & Water**
Dirk Mallants
**t +61 8 8303 8595**
**e Dirk.Mallants@csiro.au**
**w www.csiro.au/en/Research/LWF**